

DEVELOPMENT OF A SOFTWARE FOR SEISMIC
DAMAGE ESTIMATION: CASE STUDIES

A THESIS SUBMITTED TO
THE GRADUATE SCHOOL OF NATURAL AND APPLIED SCIENCES
OF
MIDDLE EAST TECHNICAL UNIVERSITY

BY

SEZGİN KÜÇÜKÇOBAN

IN PARTIAL FULFILLMENT OF THE REQUIREMENTS FOR THE DEGREE
OF
MASTER OF SCIENCE
IN
CIVIL ENGINEERING

JULY 2004

Approval of the Graduate School of Natural and Applied Sciences

Prof. Dr. Canan Özgen
Director

I certify that this thesis satisfies all the requirements as a thesis for the degree of Master of Science.

Prof. Dr. Erdal Çokça
Head of Department

This is to certify that we have read this thesis and that in our opinion it is fully adequate, in scope and quality, as a thesis for the degree of Master of Science.

Asst. Prof. Dr. Ahmet Yakut
Supervisor

Examining Committee Members

Prof. Dr. Polat Gülkan (Chairman) (METU, CE) _____
Asst. Prof. Dr. Ahmet Yakut (METU, CE) _____
Prof. Dr. M. Semih Yücemem (METU, CE) _____
Asst. Prof. Dr. M. Altuğ Erberik (METU, CE) _____
M. S. Volkan Aydoğın (PROYA YAZILIM) _____

I hereby declare that all information in this document has been obtained and presented in accordance with academic rules and ethical conduct. I also declare that, as required by these rules and conduct, I have fully cited and referenced all material and results that are not original to this work.

Name, Last name : Sezgin KÜÇÜKÇOBAN

Signature :

ABSTRACT

DEVELOPMENT OF A SOFTWARE FOR SEISMIC DAMAGE ESTIMATION: CASE STUDIES

Küçükçoban, Sezgin

M. S. Thesis, Department of Civil Engineering

Supervisor: Asst. Prof. Dr. Ahmet Yakut

July 2004, 147 pages

The occurrence of two recent major earthquakes, 17 August 1999 $M_w = 7.4$ Izmit and 12 November 1999 $M_w = 7.1$ Düzce, in Turkey prompted seismologists and geologists to conduct studies to predict magnitude and location of a potential earthquake that can cause substantial damage in Istanbul. Many scenarios are available about the extent and size of the earthquake. Moreover, studies have recommended rough estimates of risk areas throughout the city to trigger responsible authorities to take precautions to reduce the casualties and loss for the earthquake expected.

Most of these studies, however, adopt available procedure by modifying them for the building stock peculiar to Turkey. The assumptions and modifications made are too crude and thus are believed to introduce significant deviations from the actual case. To minimize these errors and use specific damage functions and capacity curves that reflect the practice in Turkey, a study was undertaken to predict damage pattern and distribution in Istanbul for a scenario earthquake proposed by Japan International Cooperation Agency

(JICA). The success of these studies strongly depends on the quality and validity of building inventory and site property data.

Building damage functions and capacity curves developed from the studies conducted in Middle East Technical University are used. A number of proper attenuation relations are employed. The study focuses mainly on developing a software to carry out all computations and present results. The results of this study reveal a more reliable picture of the physical seismic damage distribution expected in Istanbul.

Keywords: Istanbul, earthquake, vulnerability analysis, risk assessment, damage curves, seismic damage distribution, seismic risk analysis

ÖZ

SİSMİK HASAR TAHMİNİ İÇİN BİR BİLGİSAYAR PROGRAMI GELİŞTİRİLMESİ: UYGULAMALAR

Küçükçoban, Sezgin

Yüksek Lisans Tezi, İnşaat Mühendisliği Bölümü

Tez Yöneticisi: Y. Doç. Dr. Ahmet Yakut

Temmuz 2004, 147 sayfa

Türkiye’de en son meydana gelen iki büyük deprem, 17 Ağustos 1999 $M_w = 7.4$ İzmit ve 12 Kasım 1999 $M_w = 7.1$ Düzce, deprembilim uzmanlarını ve jeologları İstanbul’da büyük hasara sebep olabilecek olası bir depremin büyüklüğünü ve yerini tahmin etmek için çalışmalar yapmaya yöneltmiştir. Depremin boyut ve büyüklüğü hakkında birçok senaryo üretilmiştir. Üstelik, çalışmalar, sorumlu yetkilileri beklenen deprem sonucundaki ölümleri ve kayıpları azaltacak önlemler almaları konusunda harekete geçirmek için, şehrin her tarafında risk alanlarının kaba tahminlerini önermektedir.

Fakat bu çalışmaların çoğu var olan prosedürleri Türkiye’ye özgü bina stoğu için değiştirerek kullanılmaktadır. Yapılan kabuller ve değişiklikler çok üstünlüktedir ve bu nedenle gerçek durumdan önemli derecede sapmalara yol açacağına inanılmaktadır. Bu hataları azaltmak ve Türkiye’deki pratiği yansıtan özel hasar fonksiyonlarını ve kapasite

eğrilerini kullanmak için, JICA tarafından önerilen bir senaryo deprem için İstanbul'daki hasar modelini ve dağılımını tahmin etmek amacıyla bir çalışma ele alınmıştır. Çalışmanın başarısı, büyük ölçüde arazi özelliği bilgilerine ve bina envanterinin kalitesine ve geçerliliğine bağlıdır.

Orta Doğu Teknik Üniversitesi'nde yürütülen çalışmalardan elde edilen bina hasar fonksiyonları ve kapasite eğrileri kullanılacak ve uygun azalım ilişkilerine yer verilecektir. Bu çalışma, esas olarak, tüm hesaplamaları gerçekleştirecek ve sonuçları sunacak bir program geliştirmeye odaklanacaktır. Çalışmanın sonuçları, İstanbul'da deprem nedeniyle beklenen fiziksel hasar dağılımının daha güvenilir bir tablosunu açığa çıkaracaktır.

Anahtar Kelimeler: İstanbul, deprem, hasar görülebilirlik analizi, risk değerlendirmesi, hasar eğrileri, sismik hasar dağılımı, sismik tehlike analizi

TO MY FAMILY...

ACKNOWLEDGMENTS

The author wishes to express his deepest gratitude to his supervisor Asst. Prof. Dr. Ahmet Yakut for the insight, guidance, advices, criticisms, encouragements, and the countless ideas that he has provided throughout this study.

My parents deserve endless appreciation for their confidence in me and for the support, love and wisdom that they have provided throughout my life.

I am thankful to all my instructors that they have played a role in my education and mental development.

My home mate Gökhan Özdemir, my office mate Serhat Bayılı, and my friend Başar Özler are highly acknowledged for their invaluable friendship and assistance throughout tense working periods.

Emre Akın, Emrah Erduran, İbrahim Erdem, Koray Sığırtmaç, Nazan Yılmaz Öztürk, Musa Yılmaz, and Seval Pınarbaşı are among the precious people who have always supported me with their beyond price friendship and love; they deserve the greatest thanks.

The author also would like to thank all faculty members and structural mechanics laboratory staff for the creative and dynamic working atmosphere that they have provided.

The research work presented in this study is supported in part by the Scientific and Research Council of Turkey (TUBITAK) under grant: YMAU-ICTAG-I574 and by NATO Scientific Affairs Division under grant: NATO SfP977231.

TABLE OF CONTENTS

PLAGIARISM.....	iii
ABSTRACT	iv
ÖZ.....	vi
DEDICATION	viii
ACKNOWLEDGMENTS	ix
TABLE OF CONTENTS.....	x
LIST OF TABLES	xiii
LIST OF FIGURES.....	xv
LIST OF SYMBOLS AND ABBREVIATIONS	xviii
CHAPTER	
1. INTRODUCTION	1
1.1 BACKGROUND	1
1.2 LITERATURE SURVEY	2
1.2.1 ATC-13 Methodology.....	4
1.2.2 FEMA/NIBS Methodology	5
1.2.3 JICA Study	7
1.2.4 KOERI Study.....	12
1.3 OBJECT AND SCOPE.....	16
2. THEORETICAL BACKGROUND	17
2.1 GENERAL	17
2.2 DISTANCE TYPE DEFINITIONS	18
2.2.1 Linear Distance.....	19

2.2.2	<i>Great Circle Distance</i>	20
2.2.3	<i>Shortest Distance of a Point to a 3D Line Segment</i>	21
2.3	ATTENUATION RELATIONSHIPS	24
2.3.1	<i>Abrahamson and Silva [20]</i>	24
2.3.2	<i>Boore et al. [12]</i>	27
2.3.3	<i>Gülkan and Kalkan [21]</i>	27
2.3.4	<i>Sadigh et al. [16]</i>	30
2.3.5	<i>Comparison of Attenuation Relationships</i>	33
2.4	COMPUTATION OF DISPLACEMENT DEMAND	43
2.4.1	<i>Capacity Spectrum Method (ATC-40 Procedure B)</i>	43
2.4.2	<i>Displacement Coefficient Method (FEMA-356)</i>	50
2.4.3	<i>Constant Ductility Procedure (Chopra and Goel)</i>	52
3.	STRUCTURE OF THE SEISMIC RISK ANALYSIS SOFTWARE	55
3.1	INTRODUCTION	55
3.2	SOFTWARE COMPONENTS	55
3.2.1	<i>Input Components</i>	58
3.2.1.1	<i>Building Inventory Data</i>	58
3.2.1.2	<i>Capacity Curve Data</i>	61
3.2.1.3	<i>Scenario Earthquake Data</i>	62
3.2.1.4	<i>Attenuation Relationship Data</i>	65
3.2.1.5	<i>Analysis Method Data</i>	65
3.2.2	<i>Calculation Components</i>	67
3.2.2.1	<i>Demand Calculation</i>	67
3.2.2.2	<i>Performance Calculation</i>	68
3.2.2.3	<i>Damage Estimation</i>	69
3.2.3	<i>Output Components</i>	71
3.2.3.1	<i>Screen Display</i>	71
3.2.3.2	<i>Report Generation</i>	72
3.2.3.3	<i>Exporting Results as Database File</i>	73

4. VERIFICATION OF SRAS	74
4.1 INTRODUCTION	74
4.2 INPUT PARAMETERS	75
4.3 DAMAGE ESTIMATION METHODOLOGY	77
4.4 RESULTS	78
4.5 DISCUSSION OF RESULTS.....	78
5. CASE STUDY: ISTANBUL.....	80
5.1 INTRODUCTION	80
5.2 DAMAGE ESTIMATION FOR ISTANBUL	81
5.2.1 <i>JICA-Check</i>	83
5.2.2 <i>JICA-New</i>	85
5.2.3 <i>IMM New</i>	86
5.3 DISCUSSION OF RESULTS.....	88
6. CONCLUSIONS AND RECOMMENDATIONS	101
6.1 SUMMARY.....	101
6.2 CONCLUSIONS.....	101
6.3 RECOMMENDATIONS FOR FUTURE STUDY	102
REFERENCES.....	104
APPENDICES	
A. SRAS MANUAL	108
B. CASE STUDY: ADAPAZARI.....	129
C. CASE STUDY: ISTANBUL.....	136

LIST OF TABLES

Table 1.1 General form of Damage Probability Matrix (ATC-13 [1])	4
Table 1.2 Building inventory employed in the analysis (JICA [11])	8
Table 1.3 Parameters of scenario earthquake models (JICA [11])	9
Table 1.4 Building damage estimates obtained by JICA [11]	12
Table 1.5 Casualties predicted by JICA [11]	12
Table 1.6 Summary of results obtained by KOERI [13]	16
Table 2.1 Coefficients for the average horizontal component [20]	26
Table 2.2 Smoothed coefficients for pseudo-acceleration response spectra (g) [12]	28
Table 2.3 Coefficients for horizontal PGA and response spectral accelerations (g) [21]	29
Table 2.4 Coefficients for rock sites with $M_w \leq 6.5$ [16]	30
Table 2.5 Coefficients for rock sites with $M_w > 6.5$ [16]	31
Table 2.6 Dispersion relationships for horizontal rock motion [16]	31
Table 2.7 Coefficients for deep soil sites [16]	32
Table 2.8 Distance definitions of attenuation relationships	34
Table 2.9 Inclusion of local site effects for each attenuation relationship	34
Table 2.10 Proposed average shear wave velocities for each attenuation relationship	35
Table 2.11 Analyses performed in order to compare spectral acceleration curves	35
Table 2.12 Structural behavior types defined by ATC-40 [8]	43
Table 2.13 Values for damping modification factor, κ (ATC-40 [8])	46
Table 2.14 Minimum allowable values for SR_A and SR_V proposed by ATC-40 [8]	47
Table 2.15 Comparison of ATC-40 Procedures	48
Table 2.16 Values for modification factor C_0	50
Table 2.17 Values of a and b coefficients	53
Table 3.1 NEHRP [27] site classification scheme	60
Table 3.2 TEC [28] site classification scheme	60
Table 4.1 Statistical distribution of buildings with respect to number of stories	76

LIST OF TABLES (CONTINUED)

Table 4.2 Vulnerability assessment criteria used in the analysis	77
Table 5.1 Comparison of analyses performed for estimating damage in Istanbul.....	81
Table 5.2 Selected maps and tables to be presented for each analysis	82
Table 5.3 Building type statistics for JICA-Check	84
Table 5.4 Damage level limits defined for JICA-Check.....	85
Table 5.5 Building type statistics for JICA-New.....	86
Table 5.6 Building type statistics for IMM-New	87
Table 5.7 Summary of results obtained for JICA-Check.....	97
Table 5.8 Summary of results obtained for JICA-New.....	98
Table 5.9 Summary of results obtained for IMM-New.....	99
Table 5.10 Summary of results obtained by JICA Study [11]	100
Table A.1 Interface differences between “Add ... File” windows	114
Table A.2 List of field types for building input file (Excel)	126
Table A.3 List of field types for building input file (Access).....	127
Table B.1 GDDA database damage statistics [30].....	129
Table B.2 Predicted damage for the GDDA dataset based on soft soil type and Gülkan and Kalkan [21] attenuation relationship.....	130

LIST OF FIGURES

Figure 1.1 Building related modules of FEMA/NIBS methodology (Kircher et al. [3])	5
Figure 1.2 Example building damage estimation process (HAZUS [10])	7
Figure 1.3 Scenarios: (a), (b), (c), (d) are Model A, B, C, D, respectively (JICA [11])	9
Figure 1.4 Set of capacity curves for two building types constructed after 1970 (JICA [11])	10
Figure 1.5 Fragility functions for RC Frame + Brick Wall constructed after 1970 (JICA [11])	10
Figure 1.6 Flowchart of the methodology used for damage estimation (JICA [11])	11
Figure 1.7 Classification of building inventory for the analysis	13
Figure 1.8 Scenario earthquake model ($M_w = 7.5$) used by KOERI [13]	14
Figure 1.9 Damage grades employed during damage estimation process	15
Figure 2.1 Seismic Risk Assessment	17
Figure 2.2 Common geometry for distance calculation procedures	19
Figure 2.3 Linear distance geometry used by the program	20
Figure 2.4 Great circle distance geometry used by the program	21
Figure 2.5 Geometry for the shortest distance to a line segment	22
Figure 2.6 Possible cases in shortest distance of a point to a line segment	22
Figure 2.7 Distance definitions proposed by attenuation relationships	33
Figure 2.8 Comparison of attenuation relationships for rock sites with $M_w = 7$	36
Figure 2.9 Comparison of attenuation relationships for soil sites with $M_w = 7$	37
Figure 2.10 Comparison of S_a values at $T=0.3s$ for $M_w = 7$. (a) rock site, (b) soil site	38
Figure 2.11 Comparison of S_a values at $T=1.0s$ for $M_w = 7$. (a) rock site, (b) soil site	39
Figure 2.12 Spectral acceleration curves for rock site with $M_w = 7$ and $d = 5$ km	40
Figure 2.13 Spectral acceleration curves for soil site with $M_w = 7$ and $d = 5$ km	41
Figure 2.14 Spectral acceleration curves for rock site with $M_w = 7$ and $d = 50$ km	42
Figure 2.15 Spectral acceleration curves for soil site with $M_w = 7$ and $d = 50$ km	42

LIST OF FIGURES (CONTINUED)

Figure 2.16 Capacity spectrum conversion.....	44
Figure 2.17 Bilinear representation of capacity spectrum	45
Figure 2.18 Spectral reduction factors, SR_A and SR_V	45
Figure 2.19 Conversion of demand spectrum	47
Figure 2.20 ATC-40 Procedure B - (a) Steps 1, 2 & 3 , (b) Step 4 , (c) Steps 5 & 6.....	49
Figure 2.21 Idealized force-displacement curve and definition for α	51
Figure 2.22 Steps 2, 3 & 4 of numerical version for the improved procedures	54
Figure 3.1 Flowchart for SRAS	57
Figure 3.2 Flowchart for site characteristics identification process.....	59
Figure 3.3 A sample set of capacity curves (numbers represent stories) (not to scale)	62
Figure 3.4 Node density effect in a fault model.....	63
Figure 3.5 Comparison of linear and meshed fault models	64
Figure 3.6 Slice number and accuracy	66
Figure 3.7 Simplified acceleration response spectrum	68
Figure 3.8 Damage estimation based on S_d limits.....	70
Figure 3.9 Damage estimation based on damage curves	71
Figure 3.10 SRAS screenshot showing results (only 7 columns are visible).....	72
Figure 4.1 Adapazarı and August 17, 1999 Izmit Earthquake fault rupture location	75
Figure 4.2 Capacity curve for mid-rise RC buildings.....	77
Figure 5.1 Ground classification map proposed by JICA Study [11].....	90
Figure 5.2 Distribution of peak ground acceleration (JICA-Check).....	91
Figure 5.3 Distribution of S_a values at the period of 0.3 sec (JICA-Check)	92
Figure 5.4 Distribution of S_a values at the period of 1.0 sec (JICA-Check)	93
Figure 5.5 Distribution of heavily damaged buildings ratio (JICA-Check).....	94
Figure 5.6 Distribution of heavily damaged buildings ratio (JICA-New)	95
Figure 5.7 Distribution of heavily damaged buildings ratio (IMM-New)	96
Figure A.1 SRAS user interface.....	109
Figure A.2 SRAS menu items.....	110
Figure A.3 New project file	112
Figure A.4 Add building inventory file window.....	113
Figure A.5 “Define S_d Limits” window	115

LIST OF FIGURES (CONTINUED)

Figure A.6 Building type frame showing damage state labels.....	116
Figure A.7 “Define Damage Curves” window	117
Figure A.8 The appearance of project file before starting the analysis	118
Figure A.9 Run window subsequent to completion of analysis.....	118
Figure A.10 “Results” frame after analysis has been completed	119
Figure A.11 Tabular view of results	120
Figure A.12 “User Details” tab in “Options” windows	121
Figure A.13 “Modification Factors” tab in “Options” menu	122
Figure A.14 “Plotting Tool for Attenuation Relationships” window	123
Figure B.1 PGA distribution obtained for different attenuation relationships.....	131
Figure B.2 Distribution of S_a values at $T = 0.3$ s and 1.0 s for two attenuation relations.	132
Figure B.3 Estimated percentage distribution of heavy damage/collapse using Gülkan and Kalkan [21] (GDDA set).....	133
Figure B.4 Estimated percentage distribution of moderate damage using Gülkan and Kalkan [21] (GDDA set).....	134
Figure B.5 Estimated damage for SU database based on soft soil using Boore et al.[12]	135
Figure C.1 A sample group of capacity curves for RC buildings	136
Figure C.2 Distribution of lightly damaged buildings ratio (JICA-Check)	137
Figure C.3 Distribution of moderately damaged buildings ratio (JICA-Check).....	138
Figure C.4 Distribution of lightly damaged buildings ratio (JICA-New).....	139
Figure C.5 Distribution of moderately damaged buildings ratio (JICA-New)	140
Figure C.6 New ground classification map proposed by this study.....	141
Figure C.7 Distribution of peak ground acceleration (IMM-New).....	142
Figure C.8 Distribution of S_a values at the period of 0.3 sec (IMM-New)	143
Figure C.9 Distribution of S_a values at the period of 1.0 sec (IMM-New)	144
Figure C.10 Distribution of lightly damaged buildings ratio (IMM-New).....	145
Figure C.11 Distribution of moderately damaged buildings ratio (IMM-New)	146
Figure C.12 Damage distribution obtained in IMM-New part (all-in-one)	147

LIST OF SYMBOLS AND ABBREVIATIONS

2D	Two-dimensional
3D	Three-dimensional
ACR	American Red Cross
ADRS	Acceleration-displacement response spectrum
a_{pi}	Spectral acceleration of trial performance point
ATC	Applied Technology Council
a_y	Yield spectral acceleration
ave	Average
BSSC	Building Seismic Safety Council
CF	Composite frame
C_m	Effective mass factor
CSM	Capacity spectrum method
D	Distance
DC	Damage curve
DF	Damage factor
d_{pi}	Spectral displacement of trial performance point
d_y	Yield spectral displacement
EFC	Earthquake Engineering Facility Classification
EN	End node of segment
F	Fault type
FEMA	Federal Emergency Management Agency
g	Acceleration of gravity
GDDA	General Directorate of Disaster Affairs
GIS	Geographical Information Systems
HW	Hanging wall site dummy variable
ID	Identification

LIST OF SYMBOLS AND ABBREVIATIONS (CONTINUED)

IMM	Istanbul Metropolitan Municipality
JICA	Japan International Cooperation Agency
KIZILAY	Turkish Red Crescent Society
KOERI	Kandilli Observatory and Earthquake Research Institute
MDF	Multi degree of freedom
MMI	Modified Mercalli Intensity
MSK	Medvedev-Sponheuer-Karnik
M_w	Moment magnitude
NEHRP	National Earthquake Hazard Reduction Program
NIBS	National Institute of Building Sciences
PF_1	Modal participation factor for the first natural mode
PGA	Peak ground acceleration
PGV	Peak ground velocity
pp	performance point
R	Ratio of elastic strength demand to the calculated yield strength coefficient
RC	Reinforced concrete
RCF	Reinforced concrete frame
r_{hypo}	Hypocentral distance
r_{jb}	Closest horizontal distance to the vertical projection of the rupture in km
r_{rup}	Closest distance to the rupture plane in km
R_y	Yield reduction factor
S	Dummy variable for the site class
S_a	Spectral acceleration
S_d	Spectral displacement
SDF	Single degree of freedom
SDL	Spectral displacement limit
SF	Steel frame
SFC	Social Function Classification

LIST OF SYMBOLS AND ABBREVIATIONS (CONTINUED)

S_m	Medium period spectral acceleration
S_{ms}	Short period spectral acceleration
SN	Start node of segment
SR_A	Spectral reduction factor
SRAS	Seismic Risk Analysis Software
SR_V	Spectral reduction factor
SU	Sakarya University
USGS	United States Geological Survey
T_e	Effective fundamental period of the building in the direction under consideration
TEC	Turkish Earthquake Code
T_n	Natural period
T_s	Characteristic period of the response spectrum
V	Base shear
V_s	Shear wave velocity
V_y	Yield strength
W	Dead weight of the building plus live loads
Y	Ground motion parameter (PGA, SA) in g
α	Ratio of post-yield stiffness to effective elastic stiffness
α_1	Modal mass coefficient for the first natural mode
β_0	Hysteretic damping
β_{eff}	Effective damping
Δ_{roof}	Roof displacement
ϕ	Longitude
$\phi_{1,roof}$	Amplitude of mode 1 at roof level
κ	Modification factor for the simulation of probable imperfections in real building hysteresis loops
λ	Latitude
μ	Ductility ratio

CHAPTER 1

INTRODUCTION

1.1 BACKGROUND

Turkey is one of the most seismically active countries in the world. This high seismic nature results in an increase in damage potential as well as some other undesirable consequences. Even if it seems impossible to estimate the outcome of future earthquakes precisely, researchers have proposed several methodologies that yield rational predictions for the adverse consequences. Some of these methodologies require detailed information about the buildings such as structural and architectural configurations, material strengths etc. whereas some others utilize only global information that can be easily obtained from a street survey. Latter methodologies are generally branded as *conventional regional assessment procedures* [30].

Conventional regional assessment procedures entail hazard assessment prior to risk or damage evaluation. Hazard assessment can be carried out in two ways: probabilistically and deterministically. Probabilistic method makes use of earthquake source zones with their defined seismicity for a specific return period. The method can be implemented with ease if a reliable earthquake database exists. It is performed to obtain maximum ground motion parameters (e.g. peak ground acceleration (PGA), spectral acceleration (S_a)) over the site with a certain probability of being exceeded in a given time interval. On the other hand, deterministic method utilizes a scenario earthquake with its defined geometry and magnitude. The method should be preferred only if a realistic and highly probable scenario fault is readily available. After completion of hazard assessment, regional vulnerability/risk assessment procedures provide rough estimates of high risk areas and damage distribution pattern for the region.

Outcome of regional assessment procedures grants access to the development of regional risk prevention/mitigation as well as disaster response planning management. And also regional loss estimation and seismic microzonation studies make use of the results generated by regional risk assessment procedures. Seismic loss estimation studies are useful tools for state, regional and local governments in planning their emergency management for future earthquakes.

Due to the recent devastating earthquakes in Turkey, administrative and public authorities have realized the significance of disaster response planning prior to an undesirable catastrophic experience. Public awareness has also forced municipalities to implement seismic microzonation studies. Considering unprecedented increase in the occurrence probability of a large magnitude earthquake in the proximity of Istanbul within 30 years, Istanbul Metropolitan Municipality (IMM) has initiated an extensive study for risk prevention/mitigation and disaster response planning. Prediction of damage distribution pattern in Istanbul was the essence of the project.

Regarding to the extremely large building database in Istanbul, the assessment could only be performed in terms of 0.005° by 0.005° (approximately 500 m by 500 m) cells where all buildings were lumped at the centers of the cells. Then, these cellular damage predictions were merged and scaled to obtain sub-district level damage pattern predictions. Conventional regional assessment procedures could not be fully employed for the buildings individually since the process necessitates numerous calculations and time-consuming database operations besides a reliable building inventory.

In this study, it is intended to develop seismic damage estimation software, which is capable of handling buildings individually, and utilize the software in predicting damage distribution in Istanbul. Thus, application of conventional regional assessment procedures to different districts for several scenario earthquakes will be faster and simpler.

1.2 LITERATURE SURVEY

In many countries, there have been several seismic loss estimation studies in district or sub-district level. Seismic loss estimation methodology consists of seismic hazard, vulnerability and loss estimation studies. Seismic hazard analysis involves compilation, preparation and analysis of earthquake catalog data, earthquake source modeling, attenuation relationship and site properties. In vulnerability analysis, building damage functions are developed to estimate building damage due to ground shaking. And

finally, the damage information obtained in vulnerability analysis part is converted to the estimates of monetary loss. Among several loss estimation methodologies, the ones that are widely accepted and implemented are discussed briefly in sections 1.2.1 and 1.2.2. These widespread methodologies are known as ATC-13 (Applied Technology Council) [1] and FEMA/NIBS (Federal Emergency Management Agency / National Institute of Building Sciences) (Whitman et al. [2]) loss estimation methodologies. Since these methodologies were developed to facilitate the estimation of earthquake induced losses for a region, they demand intense and irritating database operations to extract regional building inventory, possibly taking several months to a year to complete, prior to the analysis phase. It was the shared shortcoming of regional loss estimation methodologies and eliminated by the help of technology. Subsequent to the advances in geographical information systems (GIS), software and computer technology, regional loss estimation methodologies have become well-equipped. Nowadays, analyses are performed rapidly and results are displayed graphically in a GIS environment. Thus, regional vulnerability assessment has become handy for regional and local administrations while developing strategies to reduce risks from future earthquakes and to be prepared for emergency response and recovery.

Being one of the cultural, historical and economical centers in Turkey, Istanbul has been the focus of such research projects. Vulnerability of the existing building inventory and estimated damage distribution patterns have been investigated in a few projects that are limited with the selected district boundaries. Besides these small scale studies, two comprehensive studies were carried out for Istanbul Metropolitan Area by different research teams, namely Japan International Cooperation Agency (JICA) and Kandilli Observatory and Earthquake Research Institute (KOERI).

Since these studies cover all details of a well-organized seismic microzonation practice, a summary which is mainly focusing on building damages will be presented in sections 1.2.3 and 1.2.4 for the JICA Study [11] and KOERI Study [13], respectively. The studies were examined in depth to extract what was taken as input, how it was processed and what was computed as output. This data extraction is crucial for the determination of the reliability of assessment as well as the validity of inherent assumptions. The summaries are intentionally divided into three main parts: *Input Data*, *Analysis* and *Results*. Each part presents brief and critical information about the study. They are tried to be kept as concise as possible to facilitate rapid screening of what was done.

1.2.1 ATC-13 Methodology

The ATC-13 [1] was developed in 1985 and funded by the FEMA to develop earthquake damage evaluation data for facilities in California. The data and damage/loss estimation methodology are intended for estimating the economic consequences of a major California earthquake on regional and national basis. The methodology presents estimates of percent physical damage caused by ground shaking for the existing facilities in California. Existing facilities have been classified in two ways:

1. by Earthquake Engineering Facility Classification (EEFC) (in terms of structural system, type, size etc.)
2. by Social Function Classification (SFC) (in terms of their economic function)

The EEFC contains 78 classes of structures, 40 of which are buildings and the rest are other structure types. The SFC consists of 35 classes. The methodology is based on the utilization of damage probability matrices. Estimates of percent physical damage caused by ground shaking were developed through the estimates from more than 70 senior-level specialists in earthquake engineering. These were expressed in terms of Damage Factor (DF) versus Modified Mercalli Intensity (MMI) scale for all 78 facility classes. Damage probability matrices were developed to estimate the expected dollar loss caused by ground shaking for each facility. Table 1.1 shows general form of damage probability matrix defined in ATC-13 [1]. It is essential to note that the estimates provided are for facilities in California and based upon the subjective judgment of expert individuals.

Table 1.1 General form of Damage Probability Matrix (ATC-13 [1])

Damage State	Damage Factor Range (%)	Central Damage Factor (%)	Probability of Damage in Percent By MMI and Damage State						
			VI	VII	VIII	IX	X	XI	XII
1-NONE	0	0	95	49	30	14	3	1	0.4
2-SLIGHT	0 – 1	0.5	3	38	40	30	10	3	0.6
3-LIGHT	1 – 10	5	1.5	8	16	24	30	10	1
4-MODERATE	10 – 30	20	0.4	2	8	16	26	30	3
5-HEAVY	30 – 60	45	0.1	1.5	3	10	18	30	18
6-MAJOR	60 – 100	80	-	1	2	4	10	18	39
7-DESTROYED	100	100	-	0.5	1	2	3	8	38

1.2.2 FEMA/NIBS Methodology

Whitman et al. [2] summarized the development of a GIS based regional loss estimation methodology for the United States funded by FEMA through NIBS. This methodology was implemented in a software package (HAZUS) that operates through MapInfo and ArcView, GIS applications. Methods for estimating building losses in the FEMA/NIBS earthquake loss estimation methodology were described by Kircher et al. [3]. The flow of the methodology between the modules related to building damage and loss is shown Figure 1.1.

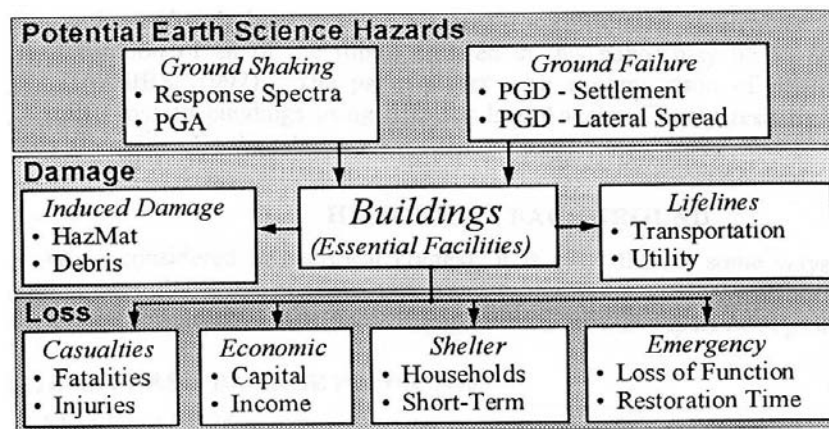


Figure 1.1 Building related modules of FEMA/NIBS methodology (Kircher et al. [3])

Thirty-six model building types are used by the methodology. These model building types are based on the classification system of FEMA 178 [4]. The methodology provides three approaches for defining an earthquake: the deterministic scenario event, the scenario event based on probabilistic seismic hazard maps and the scenario event based on user supplied ground shaking maps. Probabilistic spectral contour maps developed by the United States Geological Survey (USGS) for the National Earthquake Hazard Reduction Program (NEHRP) Provisions (Frankel et al. [5]) are employed. Attenuation equations adopted by the USGS are utilized in HAZUS. Site specific response spectra are generated by using ground motions at periods of 0.3 seconds and 1 second. Finally, ground motion demands are modified by using site amplification factors developed by the Building Seismic Safety Council for NEHRP-recommended building code standards (BSSC [6]).

In this methodology, two sets of functions or curves are used to estimate building damage due to ground shaking:

1. Capacity curves that are used with damping modified demand spectra in order to determine peak building response.
2. Fragility curves that describe the probability of reaching and exceeding different state of damage at peak building response.

Building capacity curves strongly depend on the regional construction practice in addition to regional seismicity and design code requirements. In regional vulnerability analysis or loss estimation studies, typical capacity curves are needed for a group of similar buildings rather than for a single building. In FEMA/NIBS methodology, the capacity curves of various structural systems were developed based on the concepts similar to those of FEMA 273 [7] and ATC-40 [8]. Each capacity curve is defined by two control points: yield capacity and ultimate capacity. Kircher et al. [9] presented all parameters, which are used to define yield and ultimate points, for some building types and different code design levels in the FEMA/NIBS methodology.

Fragility curves provide estimates of the cumulative probabilities of being in, or exceeding, slight, moderate, extensive and complete damage for the given level of ground shaking or peak building response. FEMA/NIBS methodology uses fragility curves that are functions of peak building response. Spectral displacement is the peak building response used for calculating structural damage and nonstructural damage to drift-sensitive components. Spectral acceleration is the peak building response used for nonstructural damage to acceleration sensitive components.

FEMA/NIBS methodology employs the Capacity Spectrum Method (CSM) of ATC-40 [8] to determine the peak building response in order to estimate losses from future earthquakes. Peak building response is estimated from the intersection of the capacity and demand curves. Probability of being or exceeding each damage state is estimated using fragility curves and peak building response parameters (S_d for structural components and drift-sensitive nonstructural components and S_a for acceleration-sensitive nonstructural components) for structural and nonstructural components, separately. Figure 1.2 illustrates the building damage estimation process.

Finally, the damage information obtained in vulnerability analysis part is converted to the estimates of monetary loss. Since details of loss estimation part are out of scope of this study, they are not presented here.

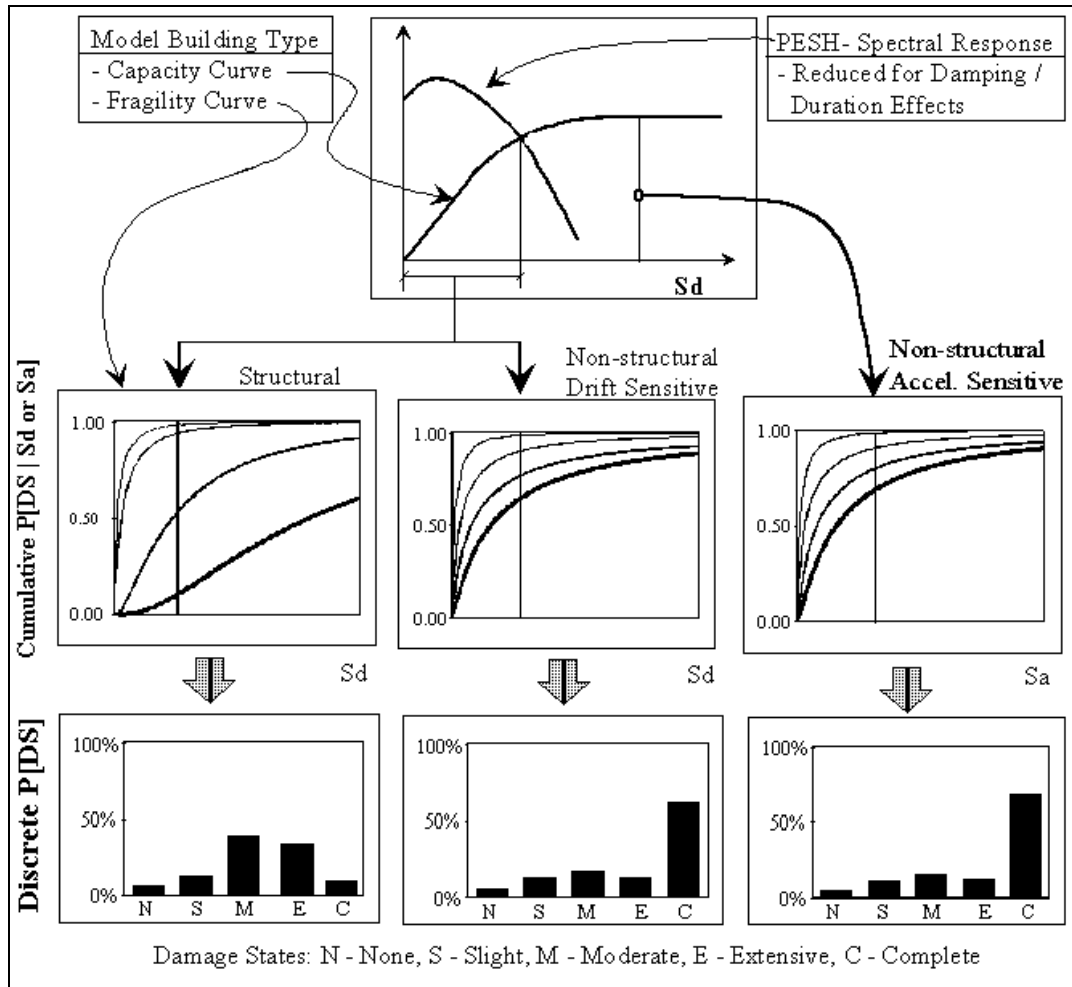


Figure 1.2 Example building damage estimation process (HAZUS [10])

1.2.3 JICA Study

The study was performed by the team organized jointly by Pacific Consultants International and OYO Corporation under the contract with JICA. It was a comprehensive study on disaster prevention and mitigation basic plan for Istanbul including seismic microzonation. The project was conducted in response to the request of the Government of the Republic of Turkey. The study intended to integrate and develop seismic microzonation studies carried out in Istanbul, recommend a city wide disaster prevention and mitigation program and advise disaster prevention considerations to be integrated with urban planning of Istanbul city.

1.2.3.1 Input Data

Total number of buildings used in the analysis was 724,623. There were 27 central districts and additional 3 districts which are Büyükçekmece, Silivri and Çatalca. The classification shown in Table 1.2 was used for the building inventory gathered by State Statistics Institute. The building inventory data were lumped at 0.005° by 0.005° geo-cells (roughly 500 m by 500 m). Total population of Istanbul used in the analysis was 8,831,766 according to the Population Census of 2000 and its population density was 96 people per hectare.

Table 1.2 Building inventory employed in the analysis (JICA [11])

Group	Structure	Floor Number	Construction Year			Total
			Pre – 1959	1960 - 1969	Post - 1970	
1	RC Frame with Brick Wall	1 - 3F	7,120	13,757	200,950	221,827
2		4 - 7F	6,280	15,449	280,231	301,961
3		8F -	481	886	18,468	19,835
4	Wood Frame	1 - 2F	4,755	697	1,583	7,035
5		3F -	3,611	222	358	4,191
6	RC Shear Wall	1 - 3F	1	0	13	13
7		4 - 7F	0	0	200	200
8		8F -	0	0	564	564
9	Masonry	1 - 2F	25,967	24,881	83,215	134,063
10		3F -	16,952	8,208	8,877	34,037
11	Prefabricated		20	12	864	896
Total			65,188	64,113	595,322	724,623

Four scenario earthquake models were determined to be used in the analysis. Parameters of each model were defined as shown in Table 1.3. Scenario fault models are presented in Figure 1.3. Model A was the most probable model and Model C was the worst case.

Capacity curves were generated for each building group using the available information obtained from recent earthquakes. An example set of capacity curves for two building types constructed after 1970 is shown in Figure 1.4. Fragility functions were

utilized to determine damage ratios. These damage ratios were used while computing the number of damaged buildings. Examples of these fragility functions for one building type constructed after 1970 are presented in Figure 1.5.

Table 1.3 Parameters of scenario earthquake models (JICA [11])

	Model A	Model B	Model C	Model D
Length (km)	119	108	174	37
Moment magnitude (Mw)	7.5	7.4	7.7	6.9
Dip angle (Degree)	90	90	90	90
Depth of upper edge (km)	0	0	0	0
Type	Strike-slip	Strike-slip	Strike-slip	Normal fault

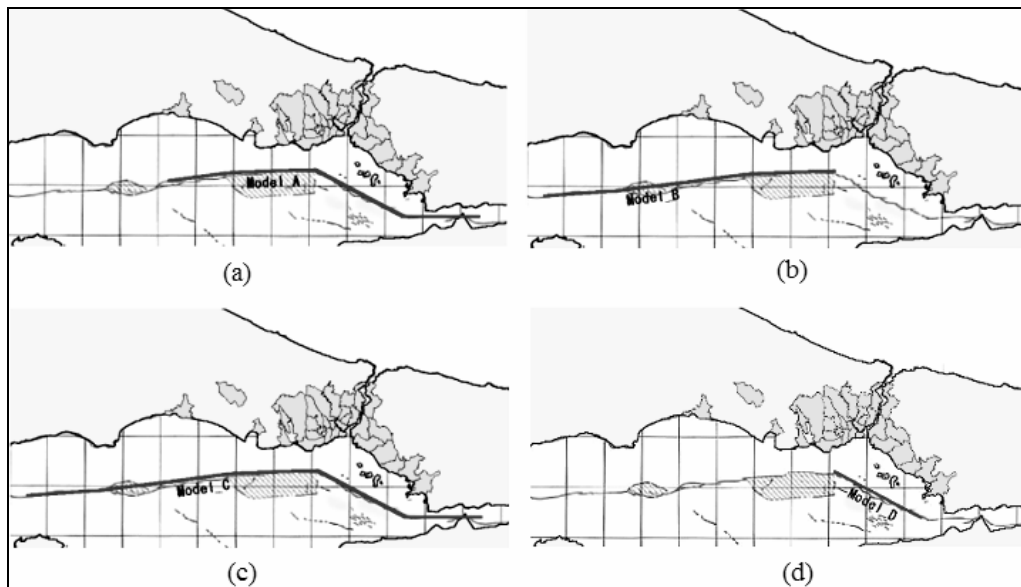


Figure 1.3 Scenarios: (a), (b), (c), (d) are Model A, B, C, D, respectively (JICA [11])

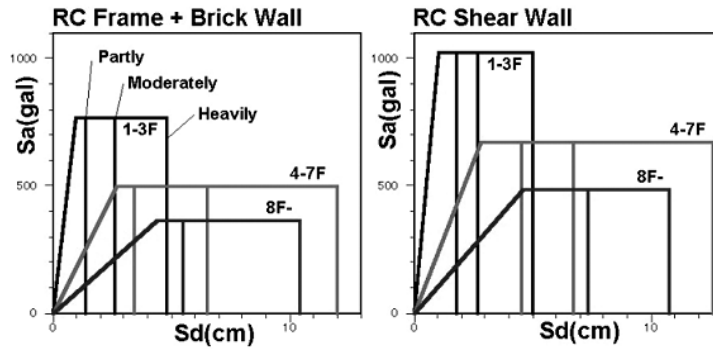


Figure 1.4 Set of capacity curves for two building types constructed after 1970
(JICA [11])

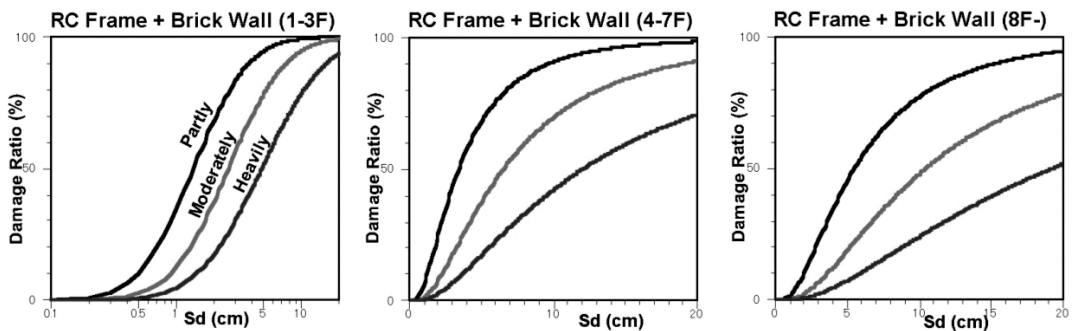


Figure 1.5 Fragility functions for RC Frame + Brick Wall constructed after 1970
(JICA [11])

1.2.3.2 Analysis

While computing peak ground acceleration (PGA) distribution for Models A, B and C, Boore et al. [12] was used. Spudich et al. [18] was selected in calculating PGA for Model D. For spectral velocity, values proposed by Campbell [17] were doubled and utilized. Since no adequate attenuation function is available for Model D, PGV could not be estimated. 5% damped acceleration response spectrum was obtained by multiplying the values estimated by Boore et al. [12] with a factor of 1.3. Site classification was performed based on NEHRP [14].

PGA, PGV and S_a values were calculated for 500 m by 500 m grid cells. Spectral acceleration values at $T = 0.2$ s and $T = 1.0$ s were taken as short-period (S_{ms}) and medium-period (S_m) spectral accelerations respectively. Standard shape of 5% damped

response spectrum provided in NEHRP [14] was approximated with S_{ms} and S_m . And also “Average Horizontal Spectral Amplification” factors specified in NEHRP [14] were utilized to modify the horizontal ground motions with respect to a nearby rock site obtained by using Boore et al. [12].

The methodology used for damage estimation is presented in Figure 1.6. Response displacement of the building (S_d) was calculated using the capacity spectrum method of ATC-40 [8]. Damage states were defined as “Heavily damaged”, “Moderately damaged” and “Partly damaged”. Fragility functions were obtained employing a probabilistic method. These functions were utilized to compute damage ratios. And finally, damage ratios were multiplied by the number of buildings that is counted in the inventory to estimate number of damaged buildings. Earthquake damage was calculated only for Model A and Model C since PGA distributions obtained for Model D and Model B resemble that of Model A and Model C, respectively.

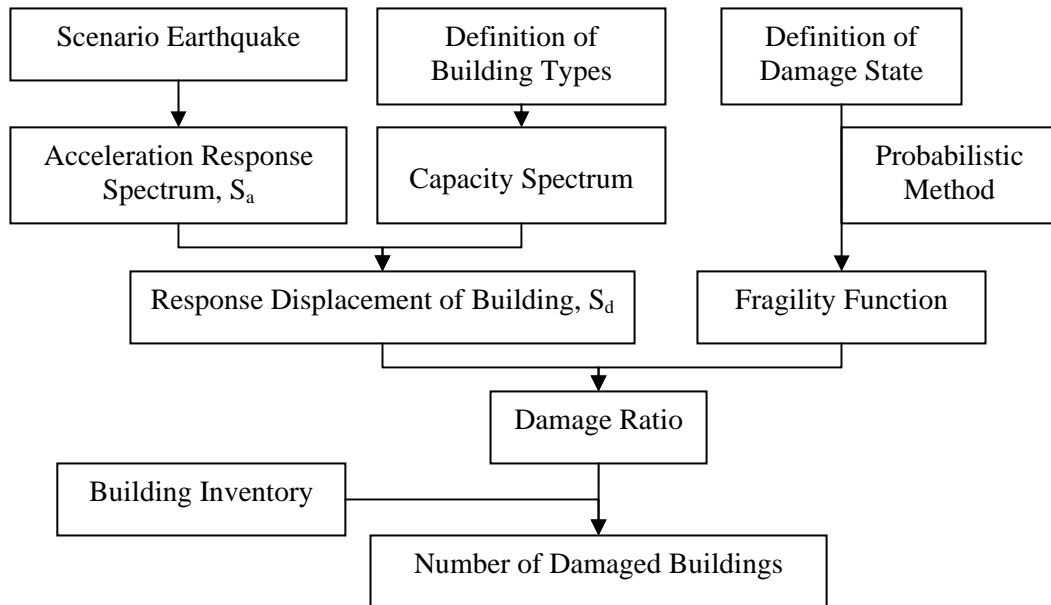


Figure 1.6 Flowchart of the methodology used for damage estimation (JICA [11])

1.2.3.3 Results

The results were obtained for each sub-district. A breakdown of the estimated building damages at district level is given in Chapter 5. Global results are summarized in

Table 1.4 and 1.5 for building damages and casualties, respectively. Other assessment results obtained for roads, bridges, lifelines, major urban facilities, hazardous facilities and port and harbors will not be presented here.

Table 1.4 Building damage estimates obtained by JICA [11]

		Heavily	Heavily + Moderately	Heavily + Moderately + Partly
Model A	Building	51,000	114,000	252,000
	Household	216,000	503,000	1,116,000
Model C	Building	59,000	128,000	300,000
	Household	268,000	601,000	1,300,000

Table 1.5 Casualties predicted by JICA [11]

	Deaths		Severely Injured	
Model A	73,000	(0.8%)	120,000	(1.4%)
Model C	87,000	(1.0%)	135,000	(1.5%)

1.2.4 KOERI Study

The study was performed by Earthquake Engineering Department of Boğaziçi University and KOERI. It was an extensive study to develop a sub-district level earthquake risk assessment for Istanbul. The project was proposed and funded by American Red Cross (ACR), in collaboration with Turkish Red Crescent Society (KIZILAY), in order to develop a basis for disaster response planning.

The ultimate objective of the study was to develop a sub-district level earthquake risk assessment for Istanbul. Since this is an extensive task and composed of several intermediate steps, two primary objectives were defined to clarify the overall process. These primary objectives are developing a risk model for Istanbul, which includes hazard assessment for a deterministic scenario earthquake ($M_w = 7.5$) and predicting building damage, casualties, damage to infrastructure and lifelines.

1.2.4.1 Input Data

Total number of buildings used in the analysis was 737,653. The geocoding was only available at sub-district level. There were 28 districts and 529 sub-districts. The classification shown in Figure 1.7 was used for the building inventory obtained from State Statistics Institute and Istanbul Metropolitan Municipality. The building inventory data were lumped at 0.005° by 0.005° geo-cells (roughly 500 m by 500 m). Day and night time populations were determined and assigned to the same geo-cells in order to calculate the casualties in Istanbul.

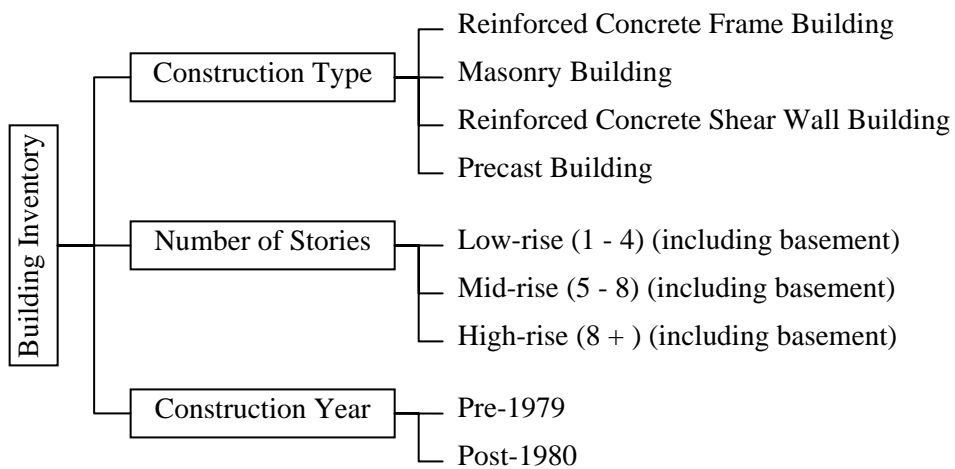


Figure 1.7 Classification of building inventory for the analysis

A scenario earthquake was determined with $M_w = 7.5$. The fault location is shown in Figure 1.8. This scenario was selected as the “credible worst case”. Displacement coefficient method proposed by FEMA 356 [19] has been employed for the computation of demand displacement.

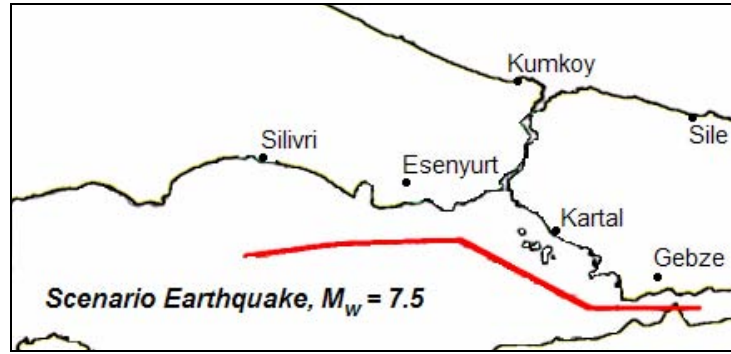


Figure 1.8 Scenario earthquake model ($M_w = 7.5$) used by KOERI [13]

1.2.4.2 Analysis

While computing PGA distribution, the average of Boore et al. [12], Sadigh et al. [16] and Campbell [17] relationships was used. For spectral acceleration values (S_a at $T = 0.2$ s and $T = 1.0$ s), the average of Boore et al. [12] and Sadigh et al. [16] was utilized. Site classification was performed based on NEHRP [14]. Spectral acceleration values at periods of 0.2 seconds and 1.0 second were taken as short-period (S_{ms}) and medium-period (S_m) spectral accelerations respectively. Standard shape of 5% damped response spectrum provided in NEHRP [14] was approximated with S_{ms} and S_m . And also “Average Horizontal Spectral Amplification” factors specified in NEHRP [14] were utilized to modify the horizontal ground motions with respect to a nearby rock site. Two separate groups of ground motion parameters were assigned to geo-cells. The first group was site dependent MSK intensities whereas the second was site dependent spectral accelerations at $T = 0.2$ s and $T = 1.0$ s. The maximum value of the parameter relating to the cell was assigned to that cell in order to be conservative.

The study employed two different methods for loss and damage estimation. First method is based on spectral displacement. It takes spectral accelerations, capacity curves for each building type and spectral displacement based vulnerabilities in order to compute building damage ratios for each type of building. On the other hand, the second method is based on MSK intensity. It takes seismic intensities and intensity based vulnerabilities while calculating building damage ratios for each building type. These damage ratios were used to estimate number of damaged buildings. And then direct economic losses and casualties were computed. Casualties were calculated for four injury severity levels as defined in HAZUS [15]. Damage grades for both methods are shown in Figure 1.9.

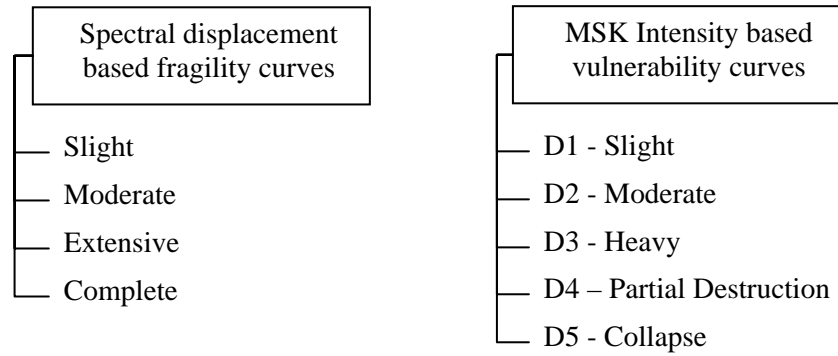


Figure 1.9 Damage grades employed during damage estimation process

Spectral displacement demand is estimated by using displacement coefficient method of FEMA-356 [19]. Building capacities were tried to be approximated by engineering judgment. The approximations made in HAZUS [15] were used directly or modified to comprise site conditions. The vulnerability functions are based on the review of existing models and the expert opinion in ATC-13 [1] supplemented by an expert technical advisory group.

1.2.4.3 Results

The results were obtained in terms of geo-cells, sub-districts and districts. Global results are summarized in Table 1.6 for building damages, number of casualties and shelter needs. District level damage estimations are discussed in Chapter 5. The monetary losses in the range of USD 11,250 million were estimated. Other results obtained for Transportation, Telecommunication, Power Transmission, Natural Gas Transmission and Sanitary Water and Waste Water Transmission Systems will not be presented here.

Table 1.6 Summary of results obtained by KOERI [13]

	Damage	Number
Intensity Based Method	Collapse (D4+D5)	40,268
	Heavy Damage (D3)	76,944
S _d Based Method	Complete (Collapse)	34,828
	Extensive	67,395
	Moderate	195,097
	Casualty Severity	Number
Intensity Based Method	Death	40,268
	Hospitalized Injury	120,804
S _d Based Method	Severity 1	109,288
	Severity 2	54,137
	Severity 3	27,840
	Severity 4	27,840
	Shelter Need	Number
Intensity Based Method	Household	608,908
S _d Based Method	Household	431,671

1.3 OBJECT AND SCOPE

Within the scope of this study, it is intended to:

1. develop a regional seismic damage prediction software
2. verify the reliability of the software by simulating the August 17, 1999 Izmit Earthquake and predicting the damage distribution in Adapazarı
3. utilize the software developed in order to predict damage distribution pattern in Istanbul resulted from a scenario earthquake (Model A proposed by JICA [11]) using two different databases.

CHAPTER 2

THEORETICAL BACKGROUND

2.1 GENERAL

Seismic risk assessment plays a crucial role in determining the undesirable consequences of future earthquakes. There are two different methods that may be followed while performing seismic risk or hazard assessments; deterministic and probabilistic (Figure 2.1). Deterministic method utilizes specific earthquake scenarios (earthquake magnitude and location are known or predicted) whereas probabilistic method considers all earthquakes with their probabilities of occurrences.

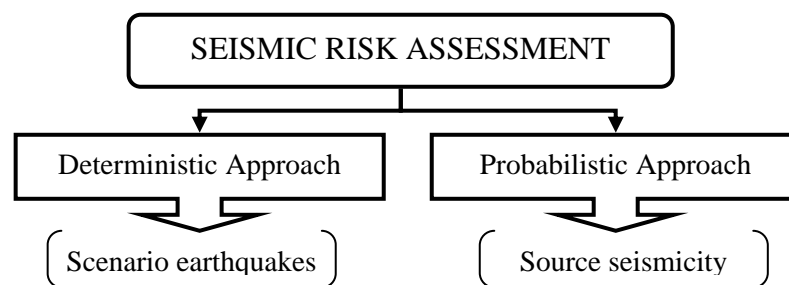


Figure 2.1 Seismic Risk Assessment

Considering the randomness inherited in earthquakes, the probabilistic framework seems to be more qualified in describing risk. But, it requires a probabilistic seismic hazard analysis which can be done only if a reliable database of earthquakes occurred in or around the region under consideration, is available.

Deterministic approach is easier and faster to implement, but it is deficient in taking into account the uncertainties and randomness. This approach is straightforward. A scenario earthquake is defined with its fault location and magnitude. Then, attenuation relations come into picture and provide expected ground motion parameters at the site. It is not necessary to have an earthquake database for the region as it is the case in probabilistic approach.

Since deterministic approach requires comparatively less data, time and effort, it is extensively used in regional seismic risk assessments. Even if it is faster to implement, the process becomes cumbersome when the number of scenario earthquakes, attenuation relations, analysis methods and buildings increases. For this reason, development of a computer program seems to be inevitable.

While developing software, basically, there are three steps that should be followed. First step is gathering and integrating the theory used in the program. Second step is generating algorithms and writing program codes. The final step is debugging process which requires running of the software for many examples and capturing the errors.

This theoretical background section is a consequence of the second step. Program makes use of well-known attenuation relationships and displacement demand computation methods. Since each of these will be declared frequently while discussing components of the software, it is better to present here the theoretical background that is required for fully understanding of the software components. Section 2.2 gives key definitions for distance types referred throughout the study. The attenuation relationships are discussed in section 2.3 whereas section 2.4 discusses methods for computation of displacement demand.

2.2 DISTANCE TYPE DEFINITIONS

The program uses latitudes and longitudes while generating fault rupture path and locating buildings. All distance calculation functions are based on the geometry and symbols shown in Figure 2.2. Both spherical and 3D Cartesian coordinates are utilized in order to obtain better distance calculation procedures.

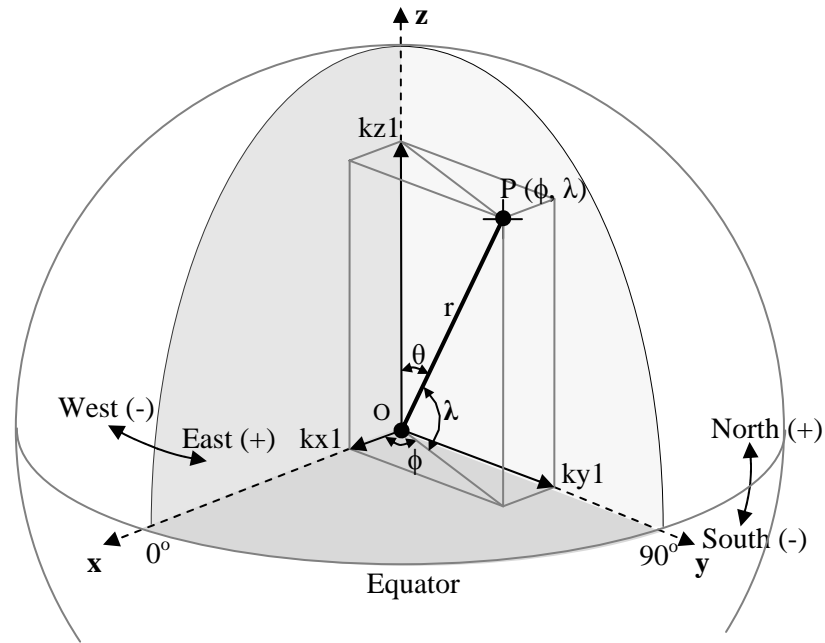


Figure 2.2 Common geometry for distance calculation procedures

East and North directions are taken as positive while West and South directions are taken as negative. It should be verified that coordinates of fault rupture path and building locations are in the same projection system. Otherwise, distance calculations may lead to errors or wrong results.

There are three different distance types used while creating a general algorithm for the shortest distance to the fault rupture. The algorithm will be better understood if one becomes skilled at these distance definitions.

2.2.1 Linear Distance

The length of a line segment combining two points on a sphere is known as linear distance. This is the shortest distance between two points. Figure 2.3 shows the geometry defined and used by the program.

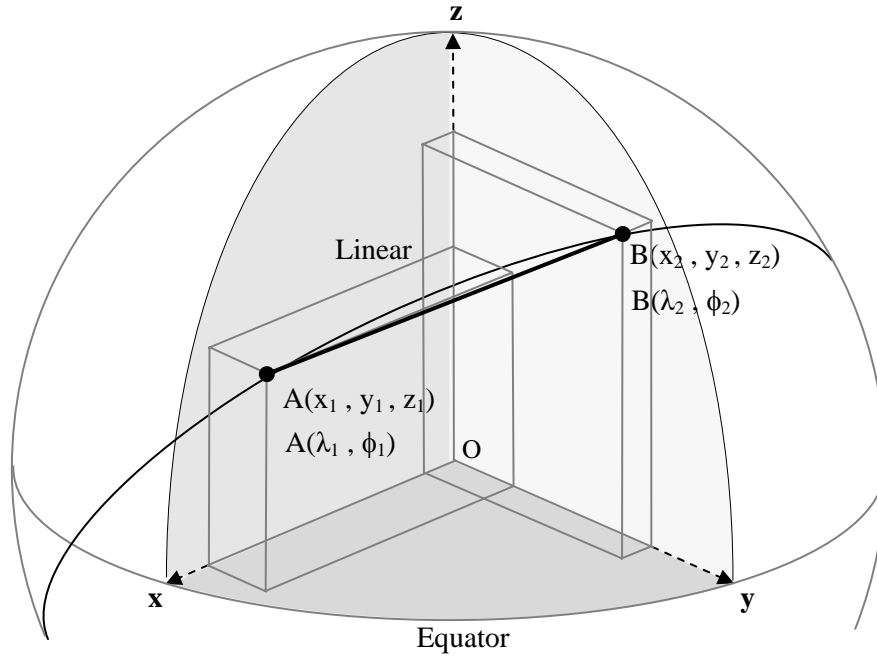


Figure 2.3 Linear distance geometry used by the program

Conversion should be performed from spherical coordinates (λ, ϕ) to 3D Cartesian coordinates (x, y, z) . This can be done using the following equation set.

$$\begin{aligned} x &= r \cdot \sin\theta \cdot \cos\phi \\ y &= r \cdot \sin\theta \cdot \sin\phi \\ z &= r \cdot \cos\theta \end{aligned} \tag{2.1}$$

where λ, ϕ : latitude, longitude

$$\theta = 90^\circ - \lambda$$

After converting spherical coordinates to 3D Cartesian coordinates, following equation yields linear distance between points $A(x_1, y_1, z_1)$ and $B(x_2, y_2, z_2)$.

$$D_{\text{linear}} = \sqrt{(x_2 - x_1)^2 + (y_2 - y_1)^2 + (z_2 - z_1)^2} \tag{2.2}$$

where x, y, z and D_{linear} are all in km.

2.2.2 Great Circle Distance

It is the shortest distance that can be traveled between any two points on the surface of a sphere. Figure 2.4 shows great circle geometry.

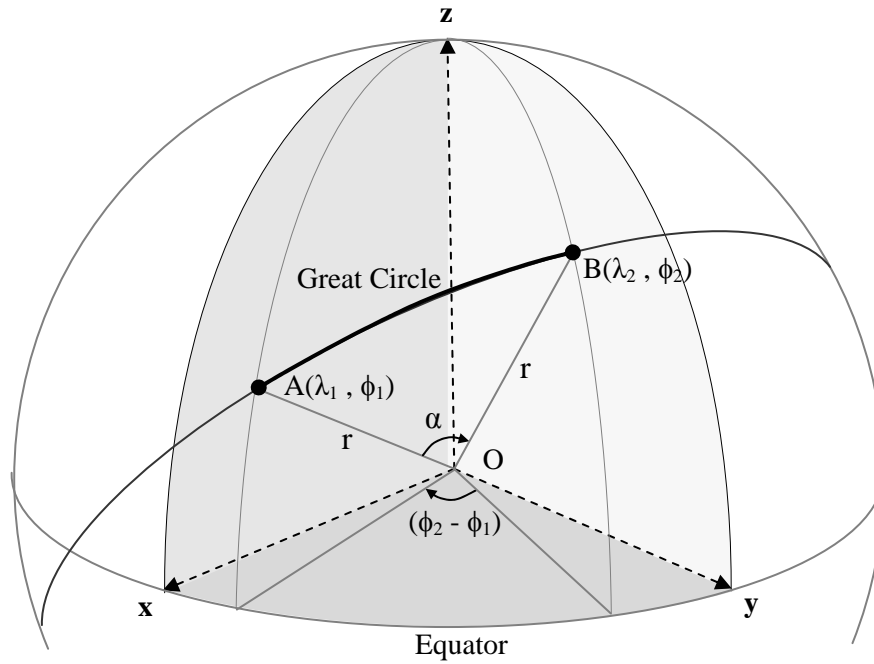


Figure 2.4 Great circle distance geometry used by the program

Great circle distance is equal to multiplication of radius by α in radians. The necessary formulation is provided below.

$$\alpha = \cos^{-1}[\sin\lambda_1 \cdot \sin\lambda_2 + \cos\lambda_1 \cdot \cos\lambda_2 \cdot \cos(\phi_2 - \phi_1)] \quad (2.3)$$

$$D_{\text{great circle}} = r \cdot \alpha \quad (2.4)$$

where λ, ϕ : latitude, longitude

α in radians, r and $D_{\text{great circle}}$ in km)

2.2.3 Shortest Distance of a Point to a 3D Line Segment

A line segment consists of all points on a line that are between two endpoints P_0 and P_1 . A point on the sphere, named as P , and a line segment form a plane that should be used for shortest distance calculations. Figure 2.5 shows the geometry.

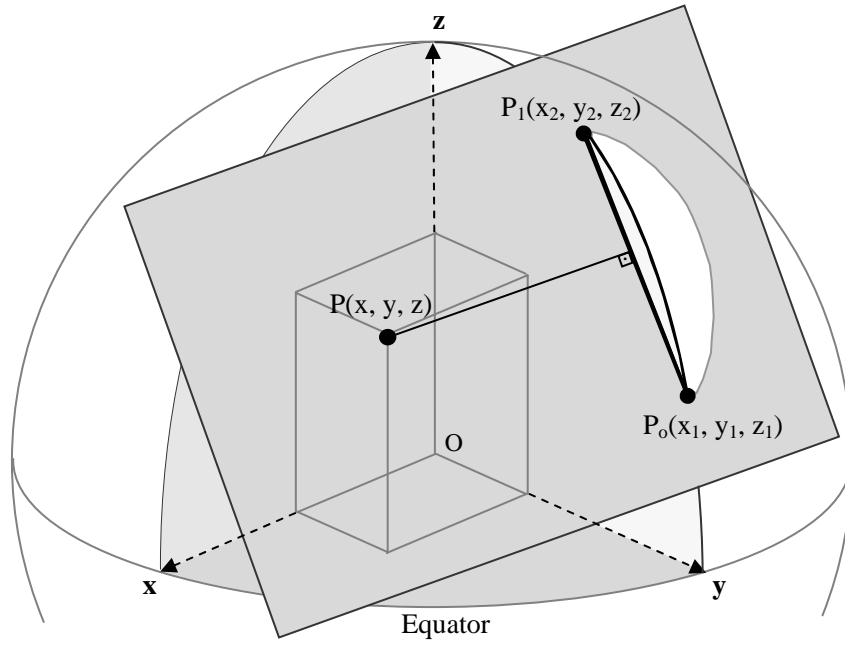


Figure 2.5 Geometry for the shortest distance to a line segment

There are three possible cases to be considered while developing a general algorithm for the calculation of shortest distance of a point to a line segment in 3D Cartesian coordinates. Figure 2.6 presents these cases.

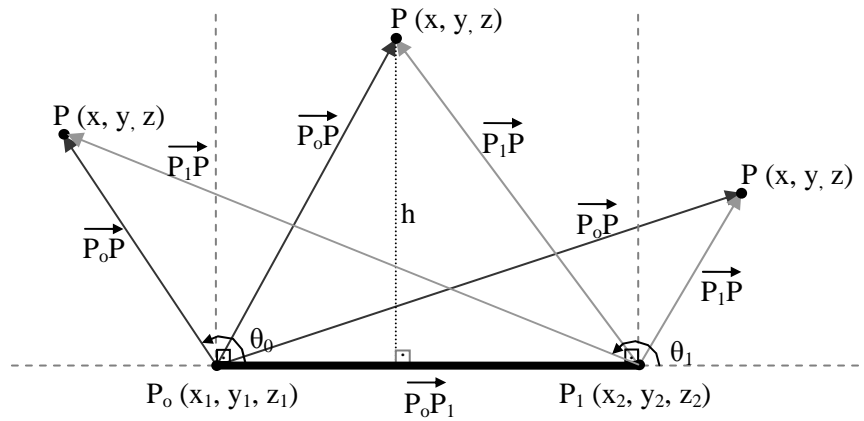


Figure 2.6 Possible cases in shortest distance of a point to a line segment

The general algorithm is provided below.

Case 1: Point P is to the left of line segment

Case 2: Point P is to the right of line segment

Case 3: Point P is within the rectangular region vertically traced by line segment

$$\begin{aligned}
 & \text{result1} = \overrightarrow{P_0P} \cdot \overrightarrow{P_0P_1} \\
 & \text{If result1} < 0 \text{ Then } (\theta_0 > 90^\circ) \\
 & \quad \text{mindist} = \|\overrightarrow{P_0P}\| \\
 & \quad \text{Exit Function} \\
 & \text{End If} \quad \left. \vphantom{\begin{aligned} & \text{result1} < 0 \text{ Then } (\theta_0 > 90^\circ) \\ & \quad \text{mindist} = \|\overrightarrow{P_0P}\| \\ & \quad \text{Exit Function} \\ & \text{End If} \end{aligned}} \right\} \text{Case 1} \\
 \\
 & \text{result2} = \overrightarrow{P_0P_1} \cdot \overrightarrow{P_0P_1} \\
 & \text{If result2} < \text{result1} \text{ Then } (\theta_1 < 90^\circ) \\
 & \quad \text{mindist} = \|\overrightarrow{P_1P}\| \\
 & \quad \text{Exit Function} \\
 & \text{End If} \quad \left. \vphantom{\begin{aligned} & \text{result2} < \text{result1} \text{ Then } (\theta_1 < 90^\circ) \\ & \quad \text{mindist} = \|\overrightarrow{P_1P}\| \\ & \quad \text{Exit Function} \\ & \text{End If} \end{aligned}} \right\} \text{Case 2} \\
 \\
 & u = (\|\overrightarrow{P_0P_1}\| + \|\overrightarrow{P_0P}\| + \|\overrightarrow{P_1P}\|)/2 \\
 & \text{area} = \sqrt{u \cdot (u - \|\overrightarrow{P_0P_1}\|)^2 \cdot (u - \|\overrightarrow{P_0P}\|)^2 \cdot (u - \|\overrightarrow{P_1P}\|)^2} \\
 & h = 2 \cdot \text{area} / \|\overrightarrow{P_0P_1}\| \\
 & \text{mindist} = h \quad \left. \vphantom{\begin{aligned} & u = (\|\overrightarrow{P_0P_1}\| + \|\overrightarrow{P_0P}\| + \|\overrightarrow{P_1P}\|)/2 \\ & \text{area} = \sqrt{u \cdot (u - \|\overrightarrow{P_0P_1}\|)^2 \cdot (u - \|\overrightarrow{P_0P}\|)^2 \cdot (u - \|\overrightarrow{P_1P}\|)^2} \\ & h = 2 \cdot \text{area} / \|\overrightarrow{P_0P_1}\| \\ & \text{mindist} = h \end{aligned}} \right\} \text{Case 3}
 \end{aligned}$$

In case 1, the sign of result1 indicates whether θ_0 is greater or less than 90° . If result1 is negative, this leads θ_0 to be obtuse and shortest distance to be length of $\overrightarrow{P_0P}$.

In case 2, the condition [result2 < result1] must be satisfied. If result2 is smaller than result1, this leads projection of $\overrightarrow{P_0P}$ on $\overrightarrow{P_0P_1}$ to be greater than $\|\overrightarrow{P_0P_1}\|$ which in turn guarantees that θ_1 is less than 90° . As a result, shortest distance is the length of $\overrightarrow{P_1P}$.

In case 3, u indicates semi-circumference of the triangle formed by three vectors. After calculating area of the triangle, h which is the shortest distance is easily obtained.

2.3 ATTENUATION RELATIONSHIPS

Independent of seismic risk assessment methodology selection, the relationship between ground motion, distance and magnitude has vital importance. Ground motion prediction relationships can be expressed as equations that estimate ground motion as a function of distance and magnitude as well as some other parameters such as type of faulting, local site classification (condition), et cetera. In this study, four attenuation relationships are used.

- Abrahamson and Silva [20]
- Boore et al. [12]
- Gülkan and Kalkan [21]
- Sadigh et al. [16]

Each attenuation relationship is summarized in the succeeding sections, mainly focusing on the limitations and input parameters of each relationship. Databases, statistical tools and numerical methods that are employed during development process of these attenuation relationships are out of the scope of this study. Interested reader may easily obtain detailed information from the reference papers.

2.3.1 Abrahamson and Silva [20]

The following attenuation relationship is proposed by N. A. Abrahamson and W. J. Silva. The equation parameters are explained briefly and coefficients are given in Table 2.1.

$$\ln Sa(g) = f_1(M, r_{rup}) + F \cdot f_3(M) + HW \cdot f_4(M, r_{rup}) + S \cdot f_5(PGA_{rock}) \quad (2.5)$$

where

Sa(g) : spectral acceleration in g

M : moment magnitude

r_{rup} : the closest distance to the rupture plane in km

F : fault type (1 for reverse, 0.5 for reverse/oblique, and 0 otherwise)

HW : hanging wall site dummy variable (1 for over the hanging wall, 0 otherwise)

S : a dummy variable for the site class (0 for rock or shallow soil, 1 for deep soil)

$$f_1(M, r_{rup}) = \begin{cases} a_1 + a_2 \cdot (M - c_1) + a_{12} \cdot (8.5 - M)^n + dd & \text{if } M \leq c_1 \\ a_1 + a_4 \cdot (M - c_1) + a_{12} \cdot (8.5 - M)^n + dd & \text{if } M > c_1 \end{cases} \quad (2.6)$$

$$dd = [a_3 + a_{13} \cdot (M - c_1)] \cdot \ln R$$

$$R = \sqrt{r_{rup}^2 + c_4^2} \quad (2.7)$$

$$f_3(M) = \begin{cases} a_5 & \text{for } M \leq 5.8 \\ a_5 + (a_6 - a_5)/(c_1 - 5.8) & \text{for } 5.8 < M < c_1 \\ a_6 & \text{for } M \geq c_1 \end{cases} \quad (2.8)$$

$$f_4(M, r_{rup}) = f_{HW}(M) \cdot f_{HW}(r_{rup}) \quad (2.9)$$

$$f_{HW}(M) = \begin{cases} 0 & \text{for } M \leq 5.5 \\ M - 5.5 & \text{for } 5.5 < M < 6.5 \\ 1 & \text{for } M \geq 6.5 \end{cases} \quad (2.10)$$

$$f_{HW}(r_{rup}) = \begin{cases} 0 & \text{for } r_{rup} < 4 \\ a_9 \cdot (r_{rup} - 4)/4 & \text{for } 4 < r_{rup} < 8 \\ a_9 & \text{for } 8 < r_{rup} < 18 \\ a_9 \cdot [1 - (r_{rup} - 18)/7] & \text{for } 18 < r_{rup} < 24 \\ 0 & \text{for } r_{rup} > 25 \end{cases} \quad (2.11)$$

$$f_5(PGA_{rock}) = a_{10} + a_{11} \cdot \ln(PGA_{rock} + c_5) \quad (2.12)$$

PGA_{rock} : the expected peak acceleration on rock in g (as predicted by the attenuation relation with $S=0$)

This relationship uses a data set which is composed of 655 recordings from 58 earthquakes with M_w between 4.5 and 7.4 including 1994 Northridge earthquake. It is appropriate for estimation of the average horizontal and vertical components for shallow earthquakes in active tectonic regions. There is one limitation to be considered while using this attenuation relationship. It should not be used to predict ground motions caused by earthquakes having a moment magnitude less than 4.5 and greater than 7.4.

Table 2.1 Coefficients for the average horizontal component [20]

Period	c_4	a_1	a_3	a_5	a_6	a_9	a_{10}	a_{11}	a_{12}
0.01	5.6	1.64	-1.145	0.61	0.26	0.37	-0.417	-0.23	0
0.02	5.6	1.64	-1.145	0.61	0.26	0.37	-0.417	-0.23	0
0.03	5.6	1.69	-1.145	0.61	0.26	0.37	-0.47	-0.23	0.0143
0.04	5.6	1.78	-1.145	0.61	0.26	0.37	-0.555	-0.251	0.0245
0.05	5.6	1.87	-1.145	0.61	0.26	0.37	-0.62	-0.267	0.028
0.06	5.6	1.94	-1.145	0.61	0.26	0.37	-0.665	-0.28	0.03
0.075	5.58	2.037	-1.145	0.61	0.26	0.37	-0.628	-0.28	0.03
0.09	5.54	2.1	-1.145	0.61	0.26	0.37	-0.609	-0.28	0.03
0.1	5.5	2.16	-1.145	0.61	0.26	0.37	-0.598	-0.28	0.028
0.12	5.39	2.272	-1.145	0.61	0.26	0.37	-0.591	-0.28	0.018
0.15	5.27	2.407	-1.145	0.61	0.26	0.37	-0.577	-0.28	0.005
0.17	5.19	2.43	-1.135	0.61	0.26	0.37	-0.522	-0.265	-0.004
0.2	5.1	2.406	-1.115	0.61	0.26	0.37	-0.445	-0.245	-0.0138
0.24	4.97	2.293	-1.079	0.61	0.232	0.37	-0.35	-0.223	-0.0238
0.3	4.8	2.114	-1.035	0.61	0.198	0.37	-0.219	-0.195	-0.036
0.36	4.62	1.955	-1.0052	0.61	0.17	0.37	-0.123	-0.173	-0.046
0.4	4.52	1.86	-0.988	0.61	0.154	0.37	-0.065	-0.16	-0.0518
0.46	4.38	1.717	-0.9652	0.592	0.132	0.37	0.02	-0.136	-0.0594
0.5	4.3	1.615	-0.9515	0.581	0.119	0.37	0.085	-0.121	-0.0635
0.6	4.12	1.428	-0.9218	0.557	0.091	0.37	0.194	-0.089	-0.074
0.75	3.9	1.16	-0.8852	0.528	0.057	0.331	0.32	-0.05	-0.0862
0.85	3.81	1.02	-0.8648	0.512	0.038	0.309	0.37	-0.028	-0.0927
1	3.7	0.828	-0.8383	0.49	0.013	0.281	0.423	0	-0.102
1.5	3.55	0.26	-0.7721	0.438	-0.049	0.21	0.6	0.04	-0.12
2	3.5	-0.15	-0.725	0.4	-0.094	0.16	0.61	0.04	-0.14
3	3.5	-0.69	-0.725	0.4	-0.156	0.089	0.63	0.04	-0.1726
4	3.5	-1.13	-0.725	0.4	-0.2	0.039	0.64	0.04	-0.1956
5	3.5	-1.46	-0.725	0.4	-0.2	0	0.664	0.04	-0.215

Note: Other coefficients $\rightarrow a_2 = 0.512, a_4 = -0.144, a_{13} = 0.17, c_1 = 6.4, c_5 = 0.03, n=2$

2.3.2 Boore et al. [12]

The following attenuation relationship is proposed by David M. Boore, William B. Joyner and Thomas E. Fumal. The equation parameters are explained briefly and coefficients are given in Table 2.2.

$$\ln Y = b_1 + b_2(M_w - 6) + b_3(M_w - 6)^2 + b_5 \ln r + b_v \ln(V_S / V_A) \quad (2.13)$$

where

$$r = \sqrt{r_{jb}^2 + h^2} \quad (2.14)$$

$$b_1 = \begin{cases} b_{ISS} & \text{for strike - slip earthquakes} \\ b_{IRS} & \text{for reverse - slip earthquakes} \\ b_{IALL} & \text{if mechanism is not specified} \end{cases} \quad (2.15)$$

Y : ground motion parameter (PGA, SA) in g

M_w : moment magnitude

r_{jb} : the closest horizontal distance to the vertical projection of the rupture in km

V_s : average shear wave velocity to 30 m, in m/sec

This relationship uses a data set which is composed of shallow earthquakes in Western North America with M_w greater than 5.0 and type of faulting equal to either strike-slip or reverse-slip. There are some limitations to be considered while using this attenuation relationship. It should not be used to predict ground motions caused by earthquakes having a moment magnitude less than 5.5 and greater than 7.0 as well as at distances greater than 80 km.

2.3.3 Gülkan and Kalkan [21]

The following attenuation relationship is proposed by Polat Gülkan and Erol Kalkan. The equation parameters are explained briefly and coefficients are given in Table 2.3.

$$\ln Y = b_1 + b_2(M_w - 6) + b_3(M_w - 6)^2 + b_5 \ln r + b_v \ln(V_S / V_A) \quad (2.16)$$

where

$$r = \sqrt{r_{jb}^2 + h^2} \quad (2.17)$$

Y : ground motion parameter (PGA, PSA) in g

M_w : moment magnitude

r_{jb} : the closest horizontal distance from the station to a site of interest in km

Table 2.2 Smoothed coefficients for pseudo-acceleration response spectra (g) [12]

Period	b_{ISS}	b_{IRV}	b_{IALL}	b_2	b_3	b_5	b_v	V_A	h	$\sigma_{ln(Y)}$
0	-0.313	-0.117	-0.242	0.527	0	-0.778	-0.371	1396	5.57	0.520
0.1	1.006	1.087	1.059	0.753	-0.226	-0.934	-0.212	1112	6.27	0.479
0.11	1.072	1.164	1.13	0.732	-0.23	-0.937	-0.211	1291	6.65	0.481
0.12	1.109	1.215	1.174	0.721	-0.233	-0.939	-0.215	1452	6.91	0.485
0.13	1.128	1.246	1.2	0.711	-0.233	-0.939	-0.221	1596	7.08	0.486
0.14	1.135	1.261	1.208	0.707	-0.23	-0.938	-0.228	1718	7.18	0.489
0.15	1.128	1.264	1.204	0.702	-0.228	-0.937	-0.238	1820	7.23	0.492
0.16	1.112	1.257	1.192	0.702	-0.226	-0.935	-0.248	1910	7.24	0.495
0.17	1.09	1.242	1.173	0.702	-0.221	-0.933	-0.258	1977	7.21	0.497
0.18	1.063	1.222	1.151	0.705	-0.216	-0.93	-0.27	2037	7.16	0.499
0.19	1.032	1.198	1.122	0.709	-0.212	-0.927	-0.281	2080	7.1	0.501
0.2	0.999	1.17	1.089	0.711	-0.207	-0.924	-0.292	2118	7.02	0.502
0.22	0.925	1.104	1.019	0.721	-0.198	-0.918	-0.315	2158	6.83	0.508
0.24	0.847	1.033	0.941	0.732	-0.189	-0.912	-0.338	2178	6.62	0.511
0.26	0.764	0.958	0.861	0.744	-0.18	-0.906	-0.36	2173	6.39	0.514
0.28	0.681	0.881	0.78	0.758	-0.168	-0.899	-0.381	2158	6.17	0.518
0.3	0.598	0.803	0.7	0.769	-0.161	-0.893	-0.401	2133	5.94	0.522
0.32	0.518	0.725	0.619	0.783	-0.152	-0.888	-0.42	2104	5.72	0.525
0.34	0.439	0.648	0.54	0.794	-0.143	-0.882	-0.438	2070	5.5	0.530
0.36	0.361	0.57	0.462	0.806	-0.136	-0.877	-0.456	2032	5.3	0.532
0.38	0.286	0.495	0.385	0.82	-0.127	-0.872	-0.472	1995	5.1	0.536
0.4	0.212	0.423	0.311	0.831	-0.12	-0.867	-0.487	1954	4.91	0.538
0.42	0.14	0.352	0.239	0.84	-0.113	-0.862	-0.502	1919	4.74	0.542
0.44	0.073	0.282	0.169	0.852	-0.108	-0.858	-0.516	1884	4.57	0.545
0.46	0.005	0.217	0.102	0.863	-0.101	-0.854	-0.529	1849	4.41	0.549
0.48	-0.058	0.151	0.036	0.873	-0.097	-0.85	-0.541	1816	4.26	0.551
0.5	-0.122	0.087	-0.025	0.884	-0.09	-0.846	-0.553	1782	4.13	0.556
0.55	-0.268	-0.063	-0.176	0.907	-0.078	-0.837	-0.579	1710	3.82	0.562
0.6	-0.401	-0.203	-0.314	0.928	-0.069	-0.83	-0.602	1644	3.57	0.569
0.65	-0.523	-0.331	-0.44	0.946	-0.06	-0.823	-0.622	1592	3.36	0.575
0.7	-0.634	-0.452	-0.555	0.962	-0.053	-0.818	-0.639	1545	3.2	0.582
0.75	-0.737	-0.562	-0.661	0.979	-0.046	-0.813	-0.653	1507	3.07	0.587
0.8	-0.829	-0.666	-0.76	0.992	-0.041	-0.809	-0.666	1476	2.98	0.593
0.85	-0.915	-0.761	-0.851	1.006	-0.037	-0.805	-0.676	1452	2.92	0.598
0.9	-0.993	-0.848	-0.933	1.018	-0.035	-0.802	-0.685	1432	2.89	0.604
0.95	-1.066	-0.932	-1.01	1.027	-0.032	-0.8	-0.692	1416	2.88	0.609
1	-1.133	-1.009	-1.08	1.036	-0.032	-0.798	-0.698	1406	2.9	0.613
1.1	-1.249	-1.145	-1.208	1.052	-0.03	-0.795	-0.706	1396	2.99	0.622
1.2	-1.345	-1.265	-1.315	1.064	-0.032	-0.794	-0.71	1400	3.14	0.629
1.3	-1.428	-1.37	-1.407	1.073	-0.035	-0.793	-0.711	1416	3.36	0.637
1.4	-1.495	-1.46	-1.483	1.08	-0.039	-0.794	-0.709	1442	3.62	0.643
1.5	-1.552	-1.538	-1.55	1.085	-0.044	-0.796	-0.704	1479	3.92	0.649
1.6	-1.598	-1.608	-1.605	1.087	-0.051	-0.798	-0.697	1524	4.26	0.654
1.7	-1.634	-1.668	-1.652	1.089	-0.058	-0.801	-0.689	1581	4.62	0.660
1.8	-1.663	-1.718	-1.689	1.087	-0.067	-0.804	-0.679	1644	5.01	0.664
1.9	-1.685	-1.763	-1.72	1.087	-0.074	-0.808	-0.667	1714	5.42	0.669
2	-1.699	-1.801	-1.743	1.085	-0.085	-0.812	-0.655	1795	5.85	0.672

Table 2.3 Coefficients for horizontal PGA and response spectral accelerations (g) [21]

Period	b_1	b_2	b_3	b_5	b_v	V_A	h	$\sigma_{ln(Y)}$
0	-0.682	0.253	0.036	-0.562	-0.297	1381	4.48	0.562
0.1	-0.139	0.2	-0.003	-0.553	-0.167	1063	3.76	0.621
0.11	0.031	0.235	-0.007	-0.573	-0.181	1413	3.89	0.618
0.12	0.123	0.228	-0.031	-0.586	-0.208	1501	4.72	0.615
0.13	0.138	0.216	-0.007	-0.59	-0.237	1591	5.46	0.634
0.14	0.1	0.186	0.014	-0.585	-0.249	1833	4.98	0.635
0.15	0.09	0.21	-0.013	-0.549	-0.196	1810	2.77	0.620
0.16	-0.128	0.214	0.007	-0.519	-0.224	2193	1.32	0.627
0.17	-0.107	0.187	0.037	-0.535	-0.243	2433	1.67	0.621
0.18	0.045	0.168	0.043	-0.556	-0.256	2041	2.44	0.599
0.19	0.053	0.18	0.063	-0.57	-0.288	2086	2.97	0.601
0.2	0.127	0.192	0.065	-0.597	-0.303	2238	3.48	0.611
0.22	-0.081	0.214	0.006	-0.532	-0.319	2198	1.98	0.584
0.24	-0.167	0.265	-0.035	-0.531	-0.382	2198	2.55	0.569
0.26	-0.129	0.345	-0.039	-0.552	-0.395	2160	3.45	0.549
0.28	0.14	0.428	-0.096	-0.616	-0.369	2179	4.95	0.530
0.3	0.296	0.471	-0.14	-0.642	-0.346	2149	6.11	0.540
0.32	0.454	0.476	-0.168	-0.653	-0.29	2144	7.38	0.555
0.34	0.422	0.471	-0.152	-0.651	-0.3	2083	8.3	0.562
0.36	0.554	0.509	-0.114	-0.692	-0.287	2043	9.18	0.563
0.38	0.254	0.499	-0.105	-0.645	-0.341	2009	9.92	0.562
0.4	0.231	0.497	-0.105	-0.647	-0.333	1968	9.92	0.604
0.42	0.12	0.518	-0.135	-0.612	-0.313	1905	9.09	0.634
0.44	0.035	0.544	-0.142	-0.583	-0.286	1899	9.25	0.627
0.46	-0.077	0.58	-0.147	-0.563	-0.285	1863	8.98	0.642
0.48	-0.154	0.611	-0.154	-0.552	-0.293	1801	8.96	0.653
0.5	-0.078	0.638	-0.161	-0.565	-0.259	1768	9.06	0.679
0.55	-0.169	0.707	-0.179	-0.539	-0.216	1724	8.29	0.710
0.6	-0.387	0.698	-0.187	-0.506	-0.259	1629	8.24	0.707
0.65	-0.583	0.689	-0.159	-0.5	-0.304	1607	7.64	0.736
0.7	-0.681	0.698	-0.143	-0.517	-0.36	1530	7.76	0.743
0.75	-0.717	0.73	-0.143	-0.516	-0.331	1492	7.12	0.740
0.8	-0.763	0.757	-0.113	-0.525	-0.302	1491	6.98	0.742
0.85	-0.778	0.81	-0.123	-0.529	-0.283	1438	6.57	0.758
0.9	-0.837	0.856	-0.13	-0.512	-0.252	1446	7.25	0.754
0.95	-0.957	0.87	-0.127	-0.472	-0.163	1384	7.24	0.752
1	-1.112	0.904	-0.169	-0.443	-0.2	1391	6.63	0.756
1.1	-1.459	0.898	-0.147	-0.414	-0.252	1380	6.21	0.792
1.2	-1.437	0.962	-0.156	-0.463	-0.267	1415	7.17	0.802
1.3	-1.321	1	-0.147	-0.517	-0.219	1429	7.66	0.796
1.4	-1.212	1	-0.088	-0.584	-0.178	1454	9.1	0.790
1.5	-1.34	0.997	-0.055	-0.582	-0.165	1490	9.86	0.788
1.6	-1.353	0.999	-0.056	-0.59	-0.135	1513	9.94	0.787
1.7	-1.42	0.996	-0.052	-0.582	-0.097	1569	9.55	0.789
1.8	-1.465	0.995	-0.053	-0.581	-0.058	1653	9.35	0.827
1.9	-1.5	0.999	-0.051	-0.592	-0.047	1707	9.49	0.864
2	-1.452	1.02	-0.079	-0.612	-0.019	1787	9.78	0.895

V_s : average shear wave velocity for the station in m/sec

This relationship uses a data set which is composed of 93 records from 47 horizontal components of 19 earthquakes occurred in Turkey between 1976 and 1999. It is appropriate for the estimation of horizontal components of peak ground acceleration as well as pseudo acceleration response spectra (5% damped). There are some limitations to be considered while using this attenuation relationship. It should not be used to predict ground motions caused by earthquakes having a moment magnitude less than 5.0 and greater than 7.5 as well as at distances greater than 150 km.

2.3.4 Sadigh et al. [16]

The following attenuation relationship is proposed by K. Sadigh, C.-Y. Chang, J.A. Egan, F. Makdisi and R.R. Youngs. The equation parameters are explained briefly and coefficients are given in Tables 2.4, 2.5, 2.6 and 2.7.

Rock Sites:

$$\ln Y = c_1 + c_2 M_w + c_3 (8.5 - M_w)^{2.5} + c_4 \ln(r_{rup} + e^{(c_5 + c_6 M_w)}) + c_7 \ln(r_{rup} + 2) \quad (2.18)$$

where

Y : ground motion parameter (PGA, SA) in g

M_w : moment magnitude

r_{rup} : the closest distance to the rupture surface in km

Note: In case of reverse/thrust faulting, the above strike-slip amplitudes are to be multiplied by 1.2 for rock sites.

Table 2.4 Coefficients for rock sites with $M_w \leq 6.5$ [16]

Period	c_1	c_2	c_3	c_4	c_5	c_6	c_7
0	-0.624	1.0	0	-2.1	1.29649	0.250	0
0.07	0.11	1.0	0.006	-2.128	1.29649	0.250	-0.082
0.1	0.275	1.0	0.006	-2.148	1.29649	0.250	-0.041
0.2	0.153	1.0	-0.004	-2.08	1.29649	0.250	0
0.3	-0.057	1.0	-0.017	-2.028	1.29649	0.250	0
0.4	-0.298	1.0	-0.028	-1.99	1.29649	0.250	0
0.5	-0.588	1.0	-0.04	-1.945	1.29649	0.250	0
0.75	-1.208	1.0	-0.05	-1.865	1.29649	0.250	0
1	-1.705	1.0	-0.055	-1.8	1.29649	0.250	0
1.5	-2.407	1.0	-0.065	-1.725	1.29649	0.250	0
2	-2.945	1.0	-0.07	-1.67	1.29649	0.250	0
3	-3.7	1.0	-0.08	-1.61	1.29649	0.250	0
4	-4.23	1.0	-0.1	-1.57	1.29649	0.250	0

Table 2.5 Coefficients for rock sites with $M_w > 6.5$ [16]

Period	c_1	c_2	c_3	c_4	c_5	c_6	c_7
0	-1.274	1.1	0	-2.1	-0.48451	0.524	0
0.07	-0.54	1.1	0.006	-2.128	-0.48451	0.524	-0.082
0.1	-0.375	1.1	0.006	-2.148	-0.48451	0.524	-0.041
0.2	-0.497	1.1	-0.004	-2.08	-0.48451	0.524	0
0.3	-0.707	1.1	-0.017	-2.028	-0.48451	0.524	0
0.4	-0.948	1.1	-0.028	-1.99	-0.48451	0.524	0
0.5	-1.238	1.1	-0.04	-1.945	-0.48451	0.524	0
0.75	-1.858	1.1	-0.05	-1.865	-0.48451	0.524	0
1	-2.355	1.1	-0.055	-1.8	-0.48451	0.524	0
1.5	-3.057	1.1	-0.065	-1.725	-0.48451	0.524	0
2	-3.595	1.1	-0.07	-1.67	-0.48451	0.524	0
3	-4.35	1.1	-0.08	-1.61	-0.48451	0.524	0
4	-4.88	1.1	-0.1	-1.57	-0.48451	0.524	0

Table 2.6 Dispersion relationships for horizontal rock motion [16]

Period	$\sigma_{ln(Y)}$
0	1.39-0.14M; 0.38 for $M > 7.21$
0.07	1.40-0.14M; 0.39 for $M > 7.21$
0.10	1.41-0.14M; 0.40 for $M > 7.21$
0.20	1.43-0.14M; 0.42 for $M > 7.21$
0.30	1.45-0.14M; 0.44 for $M > 7.21$
0.40	1.48-0.14M; 0.47 for $M > 7.21$
0.50	1.50-0.14M; 0.49 for $M > 7.21$
0.75	1.52-0.14M; 0.51 for $M > 7.21$
1.00	1.53-0.14M; 0.52 for $M > 7.21$
>1.00	1.53-0.14M; 0.52 for $M > 7.21$

Deep Soil Sites:

$$\ln Y = c_1 + c_2 M_w - c_3 \ln(r_{rup} + c_4 e^{c_5 M_w}) + c_6 + c_7 (8.5 - M_w)^{2.5} \quad (2.19)$$

where

Y : ground motion parameter (PGA, SA) in g

M_w : moment magnitude

r_{rup} : the closest distance to the rupture surface in km

$c_1 = -2.17$ for strike-slip, -1.92 for reverse and thrust earthquakes

$c_2 = 1.0$

$c_3 = 1.70$

$c_4 = 2.1863$, $c_5 = 0.32$ for $M \leq 6.5$

$c_4 = 0.3825$, $c_5 = 0.5882$ for $M > 6.5$

Table 2.7 Coefficients for deep soil sites [16]

Period	c_6 Strike-Slip	c_6 Reverse	c_7	Standard Error*
0	0	0	0	1.52-0.16M
0.075	0.4572	0.4572	0.005	1.54-0.16M
0.1	0.6395	0.6395	0.005	1.54-0.16M
0.2	0.9187	0.9187	-0.004	1.565-0.16M
0.3	0.9547	0.9547	-0.014	1.58-0.16M
0.4	0.9251	0.9005	-0.024	1.595-0.16M
0.5	0.8494	0.8285	-0.033	1.61-0.16M
0.75	0.701	0.6802	-0.051	1.635-0.16M
1	0.5665	0.5075	-0.065	1.66-0.16M
1.5	0.3235	0.2215	-0.09	1.69-0.16M
2	0.1001	-0.0526	-0.108	1.70-0.16M
3	-0.2801	-0.4905	-0.139	1.71-0.16M
4	-0.6274	-0.8907	-0.16	1.71-0.16M

* Standard error for $M > 7$ set equal to the value for $M = 7$

This relationship uses a data set which is composed of primarily California earthquakes. Geometric mean of the two horizontal components is used to represent PGA and SA. It is presented for two general site categories: rock ($V_s \approx 620$ m/s) and deep soil ($V_s \approx 310$ m/s). There are some limitations to be considered while using this attenuation relationship. It should not be used to predict ground motions caused by earthquakes having a moment magnitude less than 4.0 as well as at distances greater than 100 km.

2.3.5 Comparison of Attenuation Relationships

Attenuation relationships are compared based on three basic criteria. These are closest distance to the fault definition, site class definition and spectral acceleration curves. Comparison is performed to ease selection of proper attenuation relationship which serves best to the requirements or local conditions.

2.3.5.1 Comparison with respect to distance definitions

Shortest distance to the fault rupture plane is one of the most important parameters affecting peak ground acceleration at a site. There are different shortest distance definitions such as r_{jb} , r_{rup} and r_{hypo} proposed by different attenuation relationships. Figure 2.7 shows these shortest distance definitions where r_{jb} is the closest horizontal distance to the vertical projection of the rupture, r_{rup} is the closest distance to the rupture surface and r_{hypo} is the hypocentral distance.

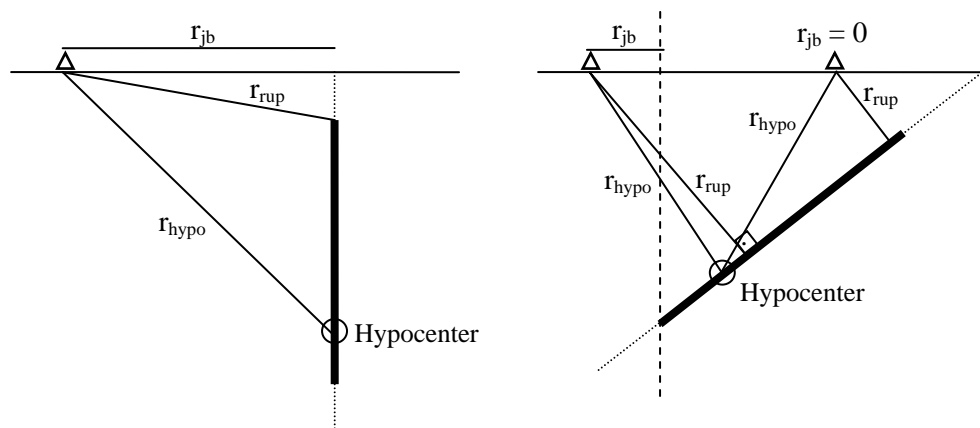


Figure 2.7 Distance definitions proposed by attenuation relationships

Each attenuation relationship uses its own definition while calculating the shortest distance to the fault. The program makes an assumption that fault rupture plane is vertical and has no depth. As a result of this assumption, fault rupture plane merges to an arc (not a line due to the curvature of earth) and different closest distance definitions gather around just one definition, r_{jb} . Table 2.8 presents distance definitions used by each attenuation relationship.

Table 2.8 Distance definitions of attenuation relationships

Attenuation relationship	Shortest distance definition	Vertical fault rupture (no depth)
Boore et al. [12]	r_{jb}	$r_{jb} \rightarrow r_{jb}$
Gülkan and Kalkan [21]	r_{jb}	$r_{jb} \rightarrow r_{jb}$
Abrahamson & Silva [20]	r_{rup}	$r_{rup} \rightarrow r_{jb}$
Sadigh et al. [16]	r_{rup}	$r_{rup} \rightarrow r_{jb}$

r_{jb} is taken as the shortest distance definition for all four attenuation relationships. r_{jb} can be expressed as the shortest distance of a point to an arc which is generated by short line segments in 3D Cartesian coordinates.

2.3.5.2 Comparison with respect to site class definitions

Local site condition is another important parameter affecting peak ground acceleration at a site. Each attenuation relationship differs in the way that they introduce local site conditions. While taking into account local site effects, Boore et al. [12] and Gülkan & Kalkan [21] relationships make use of the average shear wave velocity whereas Sadigh et al. [16] and Abrahamson & Silva [20] refer to a simplified classification: deep soil and rock. Table 2.9 summarizes the ways of introducing local site conditions for each model and Table 2.10 presents average shear wave velocities proposed by developers of each attenuation relationship.

Table 2.9 Inclusion of local site effects for each attenuation relationship

Boore et al. [12]	Gülkan and Kalkan [21]	Abrahamson and Silva [20]	Sadigh et al. [16]
<i>While introducing local site conditions,</i>			
Uses average V_s and is capable of generating spectra for all reasonable values of V_s (quantitative)	Uses average V_s and is capable of generating spectra for all reasonable values of V_s (quantitative)	Generates spectra only for Rock and Deep Soil sites (not functional for intermediate sites) (qualitative)	Generates spectra only for Rock and Deep Soil sites (not functional for intermediate sites) (qualitative)

Table 2.10 Proposed average shear wave velocities for each attenuation relationship

Boore et al. [12]	Gülkan and Kalkan [21]	Abrahamson and Silva [20]	Sadigh et al. [16]
<i>Proposed average shear wave velocities</i>			
ave $V_s = 620$ m/s (Rock)	ave $V_s = 700$ m/s (Rock)	Rock (ave $V_s = 620$ m/s)	Rock (ave $V_s = 620$ m/s)
ave $V_s = 310$ m/s (Deep Soil)	ave $V_s = 400$ m/s (Soil)		
$V_s < 180$ m/s (Soft Soil)	ave $V_s = 200$ m/s (Soft Soil)	Deep Soil (ave $V_s = 310$ m/s)	Deep Soil (ave $V_s = 310$ m/s)

2.3.5.3 Comparison with respect to spectral acceleration curves

The spectral acceleration values produced by different attenuation relationships are compared in this part. Analyses were performed for different moment magnitudes, closest distances, site conditions and attenuation relations. Table 2.11 presents combinations that were employed during analysis process. 112 runs were made but only the representative ones are selected to be presented here.

Table 2.11 Analyses performed in order to compare spectral acceleration curves

M_w	Abrahamson and Silva [20]				Boore et al. [12]				Gülkan and Kalkan [21]				Sadigh et al. [16]			
	5.5	7	5.5	7	5.5	7	5.5	7	5.5	7	5.5	7	5.5	7	5.5	7
D (km)	Rock		Soil		Rock		Soil		Rock		Soil		Rock		Soil	
1	√	√	√	√	√	√	√	√	√	√	√	√	√	√	√	√
5	√	●	√	●	√	●	√	●	√	●	√	●	√	●	√	●
10	√	√	√	√	√	√	√	√	√	√	√	√	√	√	√	√
20	√	√	√	√	√	√	√	√	√	√	√	√	√	√	√	√
30	√	√	√	√	√	√	√	√	√	√	√	√	√	√	√	√
50	√	●	√	●	√	●	√	●	√	●	√	●	√	●	√	●
100	√	√	√	√	√	√	√	√	√	√	√	√	√	√	√	√

√ : analysis performed , ● : selected to be representative for all other cases

Values obtained for moment magnitude 7 were used and the resulting graphs are presented in Figures 2.8 – 2.13. Comparison is initially performed in terms of peak ground acceleration (PGA), short-period spectral acceleration (S_a at $T = 0.3$ s) and long-period spectral acceleration (S_a at $T = 1.0$ s) variations with respect to closest distance to the fault rupture for rock and soil sites.

Considering PGA variation with respect to distance, Boore et al. [12] (B) and Gülkan & Kalkan [21] (GK) relationships attenuate more slowly as compared to Abrahamson & Silva [20] (AS) and Sadigh et al. [16] (S) relations for both rock and soil sites. Figure 2.8 shows that AS and S relations give higher PGA values at rock sites (PGA_{rock}) when compared to the values proposed by B and GK relationships. For soil sites, all attenuation relations except GK yield quite similar results whereas GK gives lower values for near field and higher values for far field.

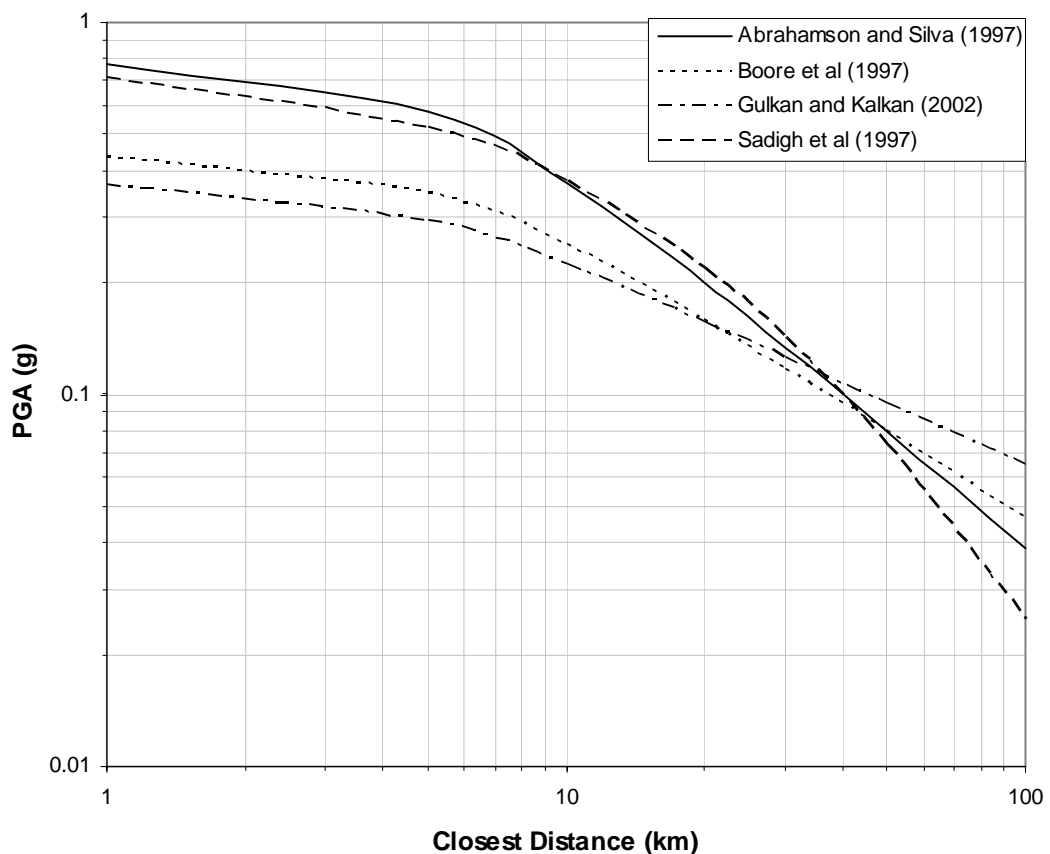


Figure 2.8 Comparison of attenuation relationships for rock sites with $M_w = 7$

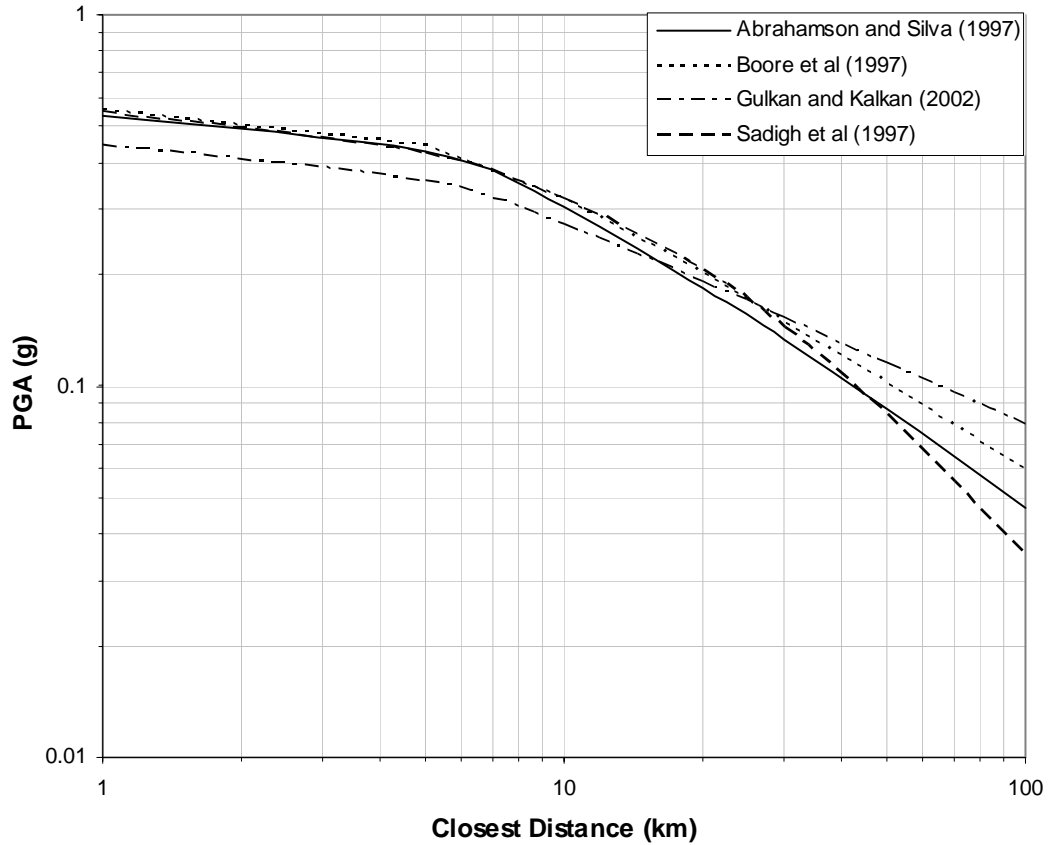
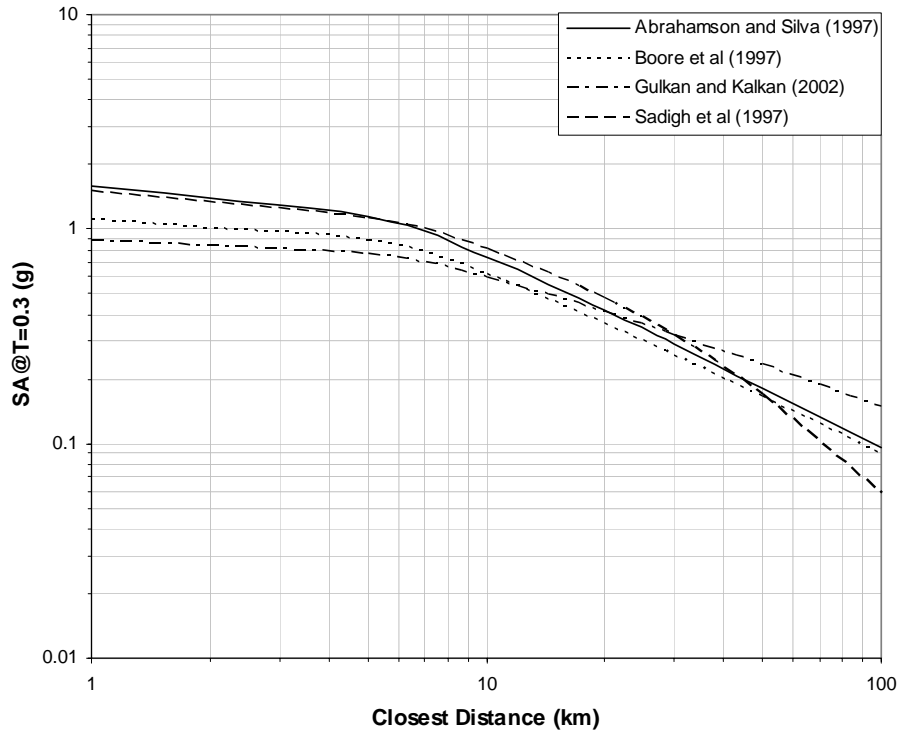


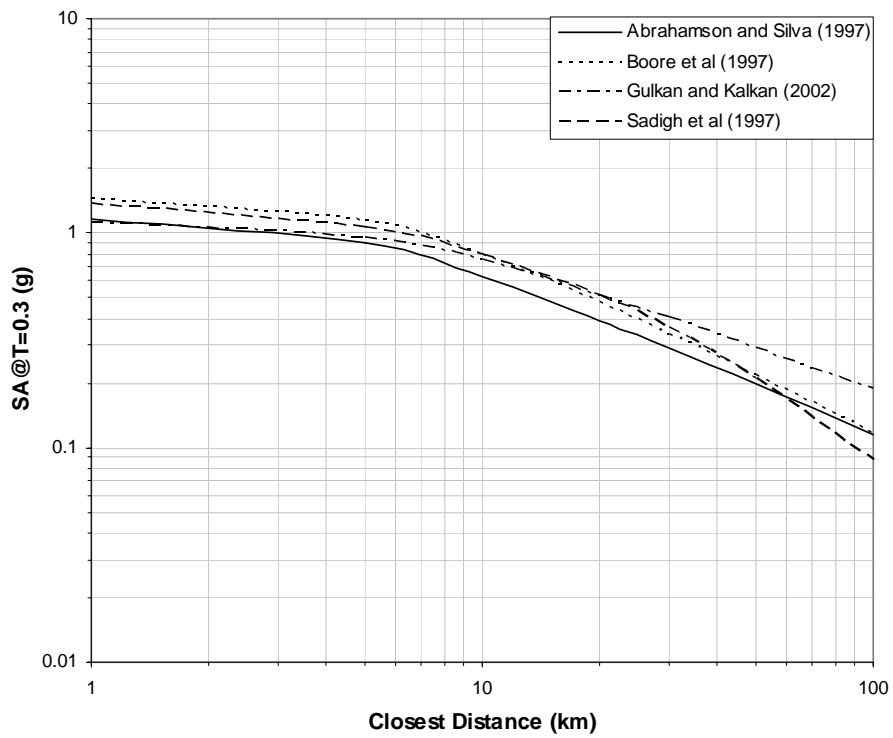
Figure 2.9 Comparison of attenuation relationships for soil sites with $M_w = 7$

Considering PGA variation with respect to site conditions, PGA values calculated by using B and GK relationships at rock sites are lower than the values found by same relations at soil sites (PGA_{soil}). In case of AS and S relations, PGA_{rock} values are higher than PGA_{soil} values and this inequality changes direction as closest distance to the fault rupture increases.

For a better understanding of each attenuation relationship, spectral acceleration values at periods of 0.3 s and 1.0 s are also plotted and presented in Figures 2.10 and 2.11. The graphs demonstrate that the variation is almost same as in the case of PGA. These spectral acceleration values at $T = 0.3$ s and $T = 1.0$ s ($Sa@T=0.3$ and $Sa@T=1.0$) are critical and they are selected as representative values of short period and long period respectively. Only these two values are required to generate a demand spectrum resembling the original curve proposed by the attenuation relationship.

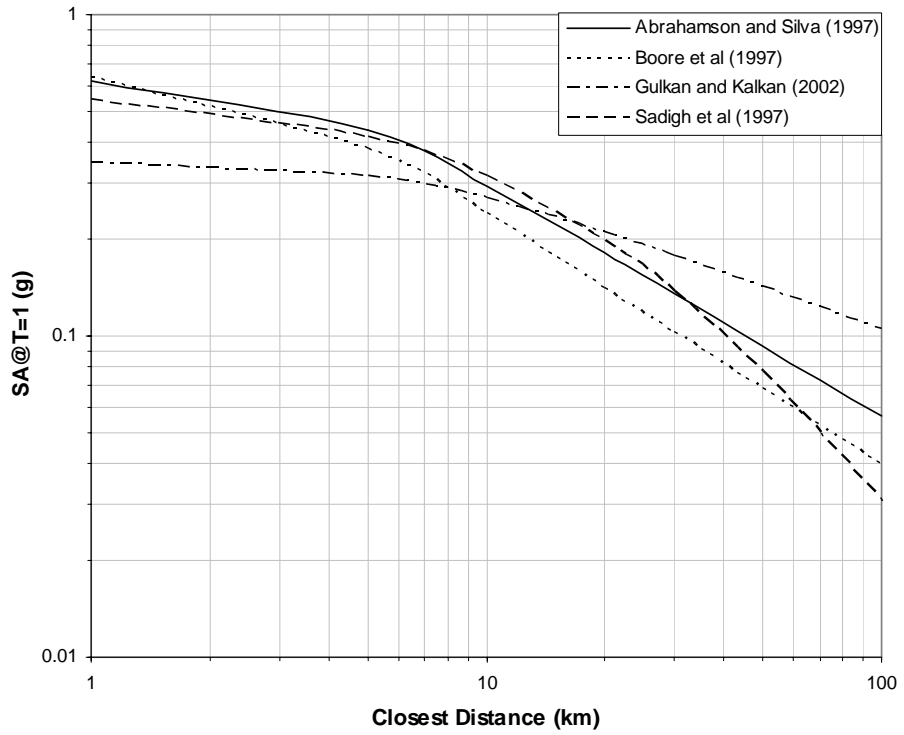


(a)

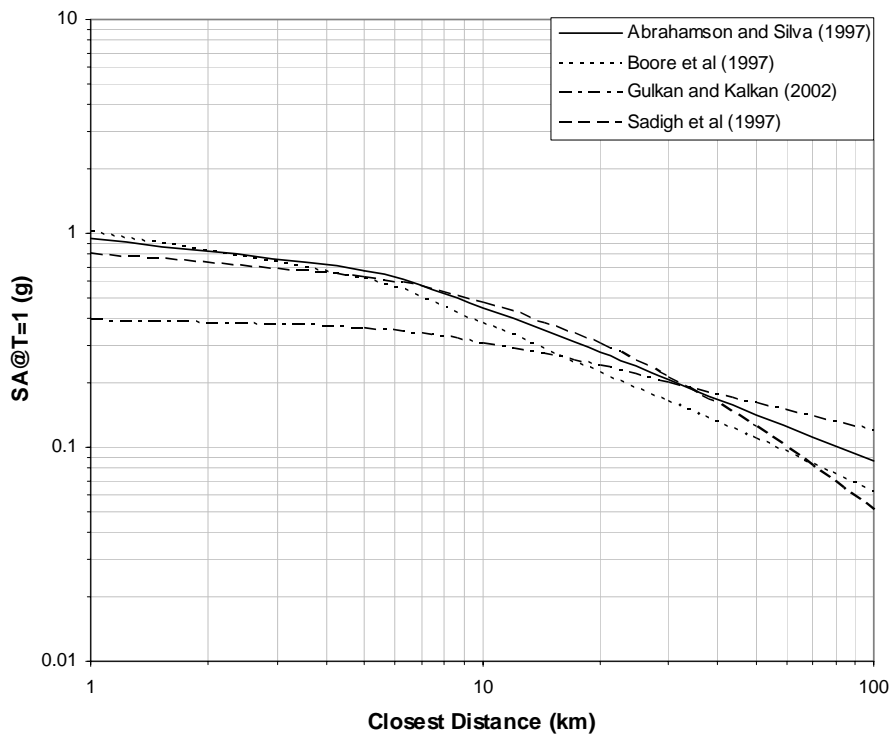


(b)

Figure 2.10 Comparison of S_a values at $T=0.3$ s for $M_w = 7$. (a) rock site, (b) soil site



(a)



(b)

Figure 2.11 Comparison of S_a values at $T=1.0s$ for $M_w = 7$. (a) rock site, (b) soil site

Secondly, another comparison is made for spectral curves obtained at distances of 5 and 50 km for rock and soil sites with an assumed moment magnitude of 7.0. Figure 2.12 shows that there is significant difference between short-period acceleration values of all four attenuation relationships when local site is rock. Long-period acceleration values follow a similar trend. AS and S relations produce almost same curves excluding the interval of 0.1 s and 0.4 s. GK relationship yields the lower bound curve whereas AS gives the upper bound.

In case of soil site (Figure 2.13), peaks of short-period acceleration values vary between 0.9g and 1.1g and long-period accelerations for all attenuation relationships are quite compatible except GK relationship which produced lower values. PGA values are between 0.35g and 0.44g. Unlike rock sites, B relationship forms the upper bound curve since AS and S relations give lower spectral acceleration values for soil sites as compared to their proposed PGA_{rock} .

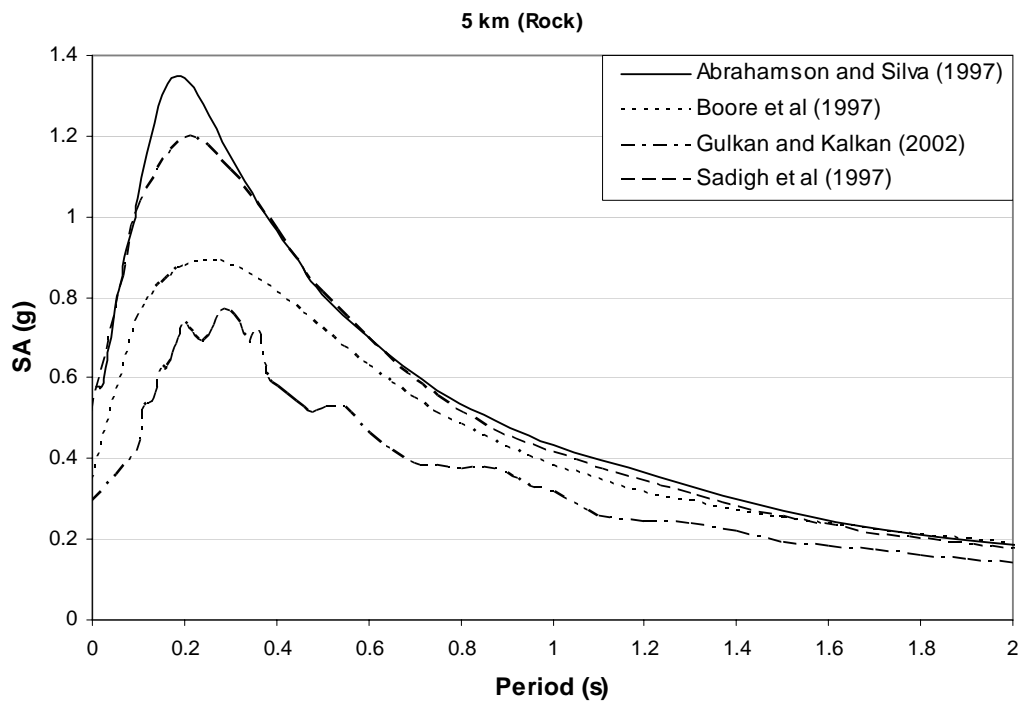


Figure 2.12 Spectral acceleration curves for rock site with $M_w = 7$ and $d = 5$ km

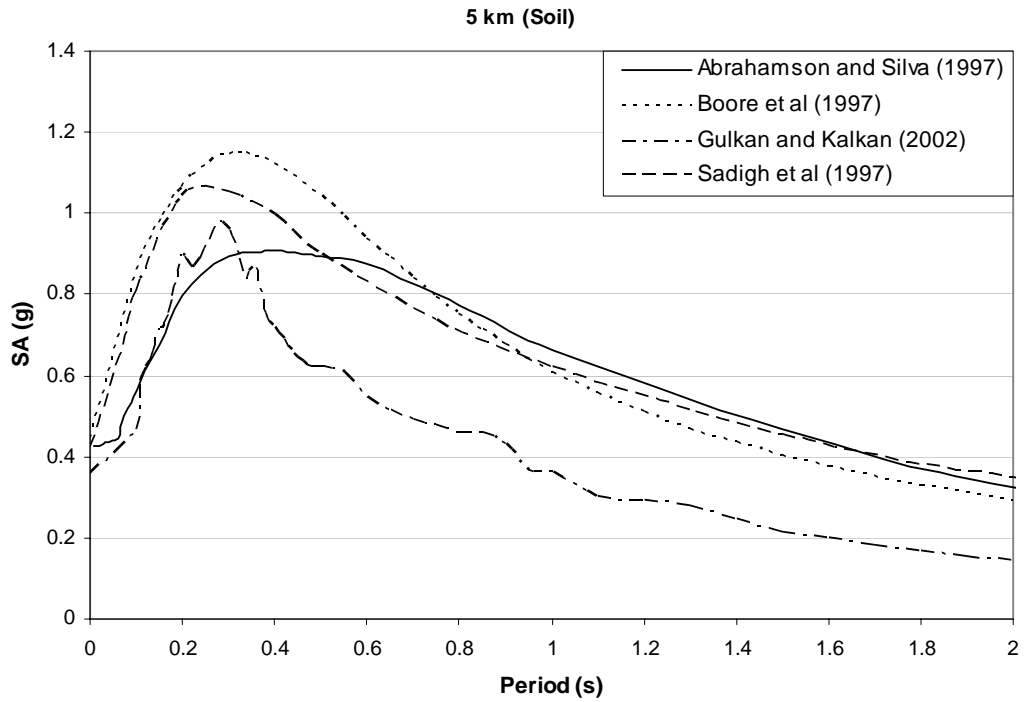


Figure 2.13 Spectral acceleration curves for soil site with $M_w = 7$ and $d = 5$ km

When closest distance to the fault rupture increases, spectral acceleration curves proposed by different attenuation relationships become similar which can be observed from Figures 2.14 and 2.15. Another observation is that GK attenuation relationship produces approximately 1.4 times larger values. This should be expected because GK relation attenuates slowly and yields larger spectral acceleration values for distant sites independent of site conditions. AS, S and B relationships are almost equivalent for rock sites and differ slightly at periods greater than 0.6 s in case of soil sites.

In summary, AS and S relations show similar behavior as it is also the case for B and GK relationships. For all cases, GK attenuation relation follows general trend but produces considerably different spectral acceleration curves since it reflects the character of earthquakes happened in Turkey. So, it might be better to employ GK attenuation relationship in order to construct spectral acceleration curves for the regions in Turkey.

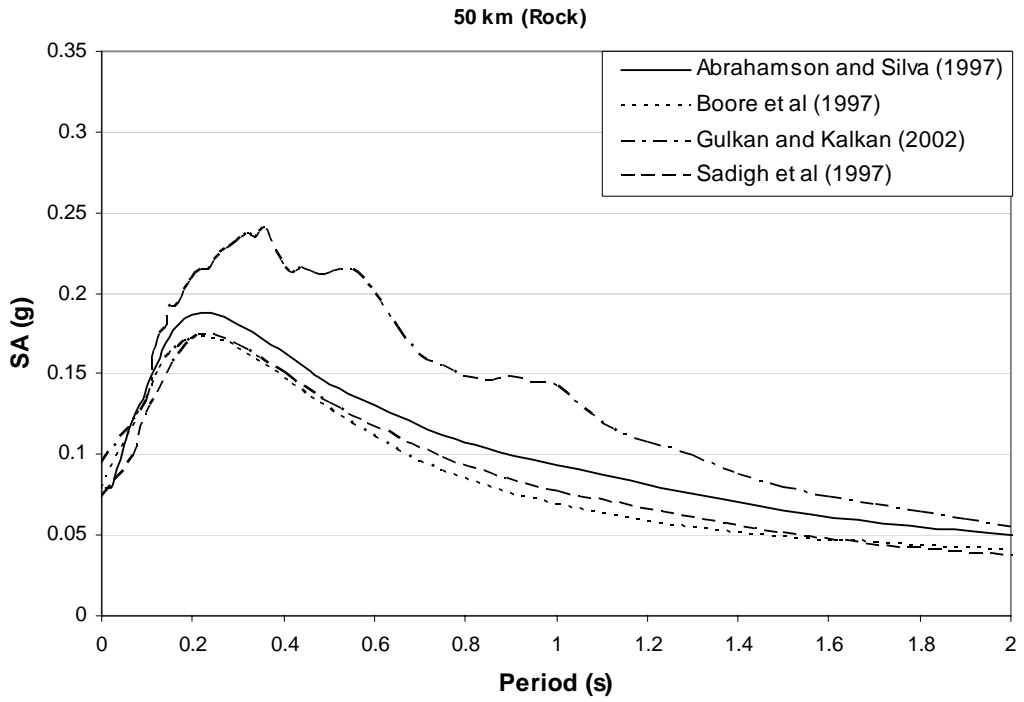


Figure 2.14 Spectral acceleration curves for rock site with $M_w = 7$ and $d = 50$ km

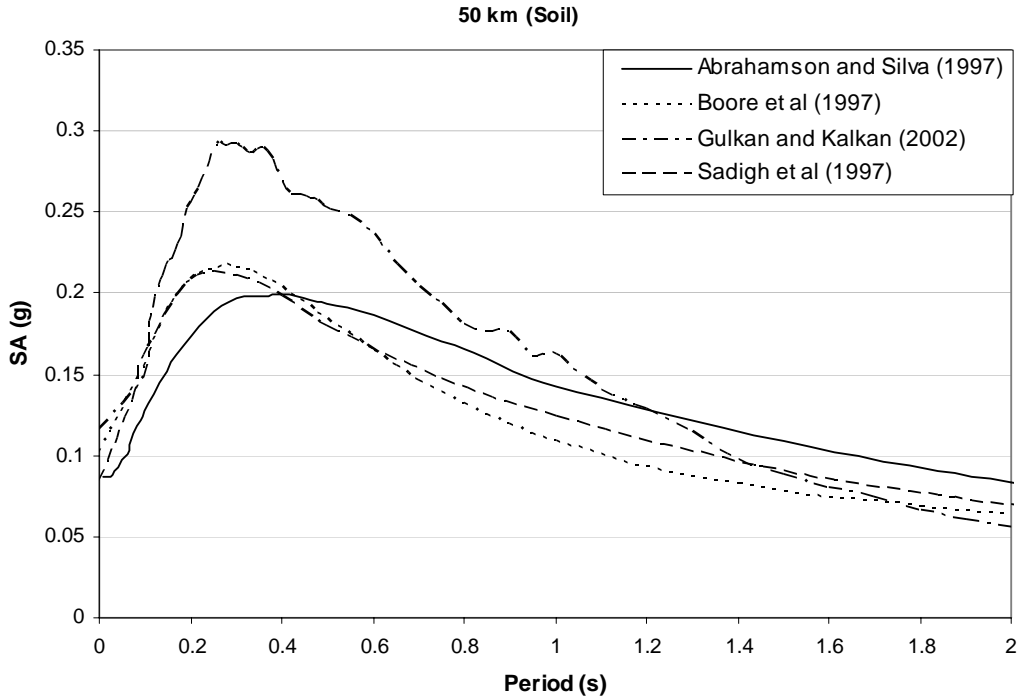


Figure 2.15 Spectral acceleration curves for soil site with $M_w = 7$ and $d = 50$ km

2.4 COMPUTATION OF DISPLACEMENT DEMAND

Seismic risk assessment methodology has another important component which is the computation of displacement demand. During this process, the displacement demand imposed by the probable or deterministic earthquakes on the structure is determined by employing different procedures each of which has its own advantages and drawbacks. The software developed uses three wide-spread methodologies. The theoretical background for each methodology is presented in the following sections. The procedures are excerpted from “Seismic Evaluation and Retrofit of Concrete Buildings (ATC-40)” [8], “Prestandard and Commentary for the Seismic Rehabilitation of Buildings (FEMA-356)” [19] and “Capacity-Demand-Diagram Methods for Estimating Seismic Deformation of Inelastic Structures: SDF Systems (Chopra & Goel)” [22] for instructive purposes. Inevitably, the tables and formulae, proposed by ATC-40, FEMA-356 and Chopra & Goel included in this study have minor differences in the way they are presented. Interested reader is referred to referenced material for further details and explanations.

2.4.1 Capacity Spectrum Method (ATC-40 Procedure B)

The analysis procedure proposed by ATC-40 [8] mainly focuses on capacity spectrum method which is one of the nonlinear static analysis procedures. In general, simplified nonlinear static analysis procedures require three components: capacity, demand and performance.

Capacity: It is the representation of the building response.

Demand: It is the representation of the seismic effect.

Performance: It is a point that represents the condition of the building to the given demand.

ATC-40 defines three different structural behavior types. Since these types will be declared frequently in the subsequent paragraphs, it should be better to present the classification scheme here.

Table 2.12 Structural behavior types defined by ATC-40 [8]

Shaking Duration	Essentially New Building	Average Existing Building	Poor Existing Building
Short	Type A	Type B	Type C
Long	Type B	Type C	Type C

A capacity curve of the overall structure should be developed by using some form of nonlinear analysis. Pushover procedure may be utilized for this purpose. It is a stepwise process in each step of which an elastic analysis is performed and necessary revisions to the model is made in order to account for reduction in resistance of yielding components. The process is repeated until the structure becomes unstable. Base shear and roof displacement values recorded in each analysis step are plotted to obtain capacity curve for that building. Then, the obtained curve should be converted into acceleration-displacement response spectrum (ADRS) format using the equations below (Figure 2.16).

$$S_a = \frac{V/W}{\alpha_1} \quad (2.20)$$

$$S_d = \frac{\Delta_{\text{roof}}}{PF_1 \cdot \phi_{1,\text{roof}}} \quad (2.21)$$

where

α_1 : modal mass coefficient for the first natural mode

W : dead weight of the building plus live loads

V : base shear

Δ_{roof} : roof displacement

PF_1 : modal participation factor for the first natural mode

$\phi_{1,\text{roof}}$: amplitude of mode 1 at roof level

S_a : spectral acceleration

S_d : spectral displacement

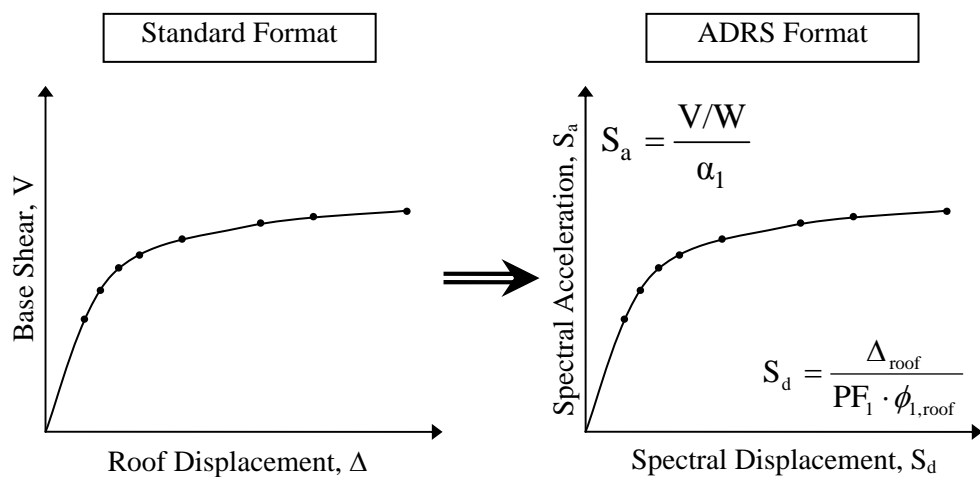


Figure 2.16 Capacity spectrum conversion

Bilinear representation of capacity spectrum is required to be used in the procedure. An example is shown in Figure 2.17 including the definitions which will be used throughout the procedure.

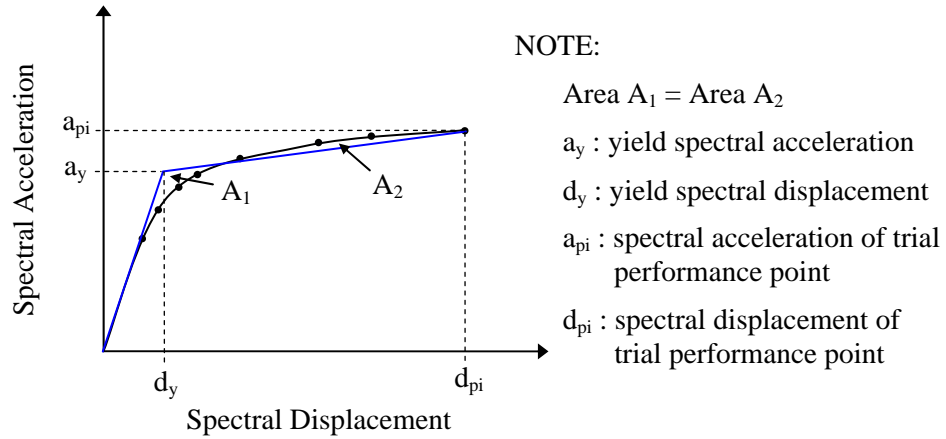


Figure 2.17 Bilinear representation of capacity spectrum

Capacity spectrum method searches for a point that is on both capacity spectrum and reduced demand spectrum. Reduced demand spectrum is used to introduce nonlinear effects. Elastic (5% damped) response spectrum is scaled by spectral reduction factors to obtain reduced demand spectrum as shown in Figure 2.18.

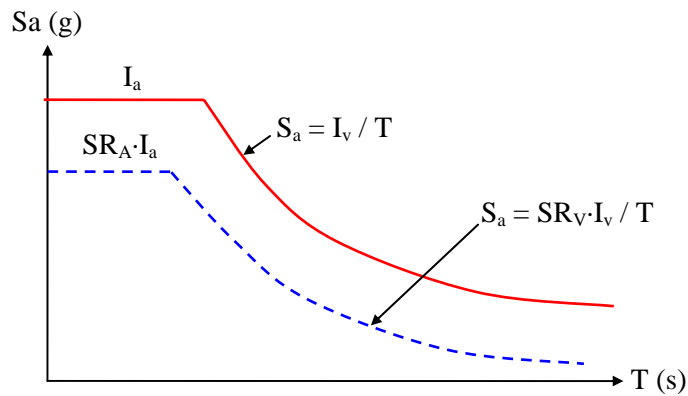


Figure 2.18 Spectral reduction factors, SR_A and SR_V

Spectral reduction factors are given in terms of effective damping. Effective damping may be calculated using the following equation.

$$\beta_{\text{eff}} = \kappa \cdot \beta_0 + 5 \quad (2.22)$$

where

β_{eff} : effective damping. This value should not be greater than 40% for Type A, 29% for Type B and 20% for Type C.

5 : viscous damping inherent in the structure (5%)

β_0 : hysteretic damping represented as equivalent viscous damping

$$\beta_0 = \frac{63.7(a_y d_{pi} - d_y a_{pi})}{a_{pi} d_{pi}} \quad (2.23)$$

κ : a modification factor for the simulation of probable imperfections in real building hysteresis loops, which may be pinching or degrading. Table 2.13 presents values for κ depending on structural behavior type and equivalent viscous damping.

Table 2.13 Values for damping modification factor, κ (ATC-40 [8])

Structural Behavior Type	β_0 (percent)	κ
Type A	≤ 16.25	1.0
	> 16.25	$1.13 - \frac{0.51(a_y d_{pi} - d_y a_{pi})}{(a_{pi} d_{pi})}$
Type B	≤ 25	0.67
	> 25	$0.845 - \frac{0.446(a_y d_{pi} - d_y a_{pi})}{(a_{pi} d_{pi})}$
Type C	Any value	0.33

Spectral reduction factors are calculated using the following equations.

$$SR_A \approx \frac{3.21 - 0.68 \cdot \ln(\beta_{\text{eff}})}{2.12} \quad (2.24)$$

$$SR_V \approx \frac{2.31 - 0.41 \cdot \ln(\beta_{\text{eff}})}{1.65} \quad (2.25)$$

Note that SR_A and SR_V values found by the above formulae should not be less than the values provided in Table 2.14.

Table 2.14 Minimum allowable values for SR_A and SR_V proposed by ATC-40 [8]

Structural Behavior Type	SR_A	SR_V
Type A	0.33	0.50
Type B	0.44	0.56
Type C	0.56	0.67

After reducing the elastic demand curve by using spectral reduction factors, it should be also converted into ADRS format. Conversion of demand curve from standard format into ADRS format is shown in Figure 2.19.

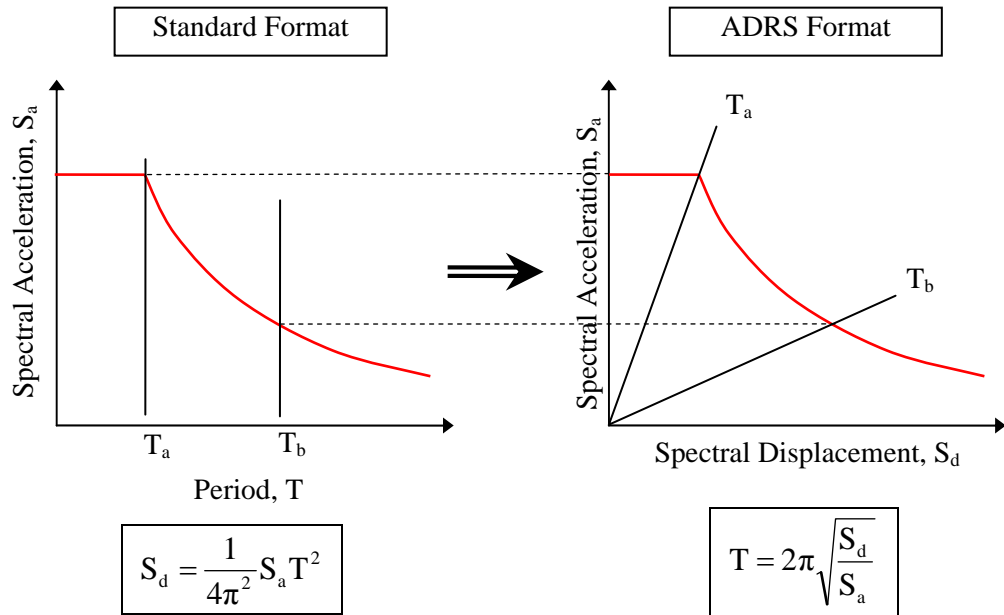


Figure 2.19 Conversion of demand spectrum

ATC-40 [8] proposes three different procedures for the capacity spectrum method. Table 2.15 summarizes the properties of each procedure. The program, developed in this study, uses Procedure B which is slightly modified while generating the algorithm.

Table 2.15 Comparison of ATC-40 Procedures

Procedure	Method	Convenience	Application	Difficulty
A	Analytical	Better for spreadsheet programming	Most transparent	Easiest to understand
B	Analytical	Best for programming	Reasonably transparent	Simpler but inherent assumptions should be fully understood
C	Graphical	Best for hand analysis	Least transparent	Easy to understand

As stated in Table 2.15, Procedure B is the most convenient procedure to be used while developing a computer program. The handiness of procedure comes from a basic assumption. The initial slope, the yield point (a_y , d_y) and the post-yield slope remains constant. In other words, once a bilinear representation of capacity spectrum is obtained, no modification will be done in each iteration step. The following step-by-step procedure and Figure 2.20 go over the main points of ATC-40 Procedure B [8].

1. Develop 5% damped (elastic) response spectrum in ADRS format.
2. Plot a family of reduced spectra on the same chart. (Preferably for values of β_{eff} starting from 5% up to 30% with increments of 5%. Note β_{eff} limits recommended for each type of structural behavior.)
3. Transform capacity curve into a capacity spectrum. Develop a bilinear model of the capacity spectrum considering a balance between the areas under original and bilinear capacity spectra.
4. For a range of displacement values around the point a^* , d^* which is determined using equal displacement rule, calculate effective damping, β_{eff} .
5. Plot obtained d_{pi} , β_{eff} points on the same chart.
6. Draw a line passing through the points produced in step 5. The performance point is located at the intersection of this line with the capacity spectrum.

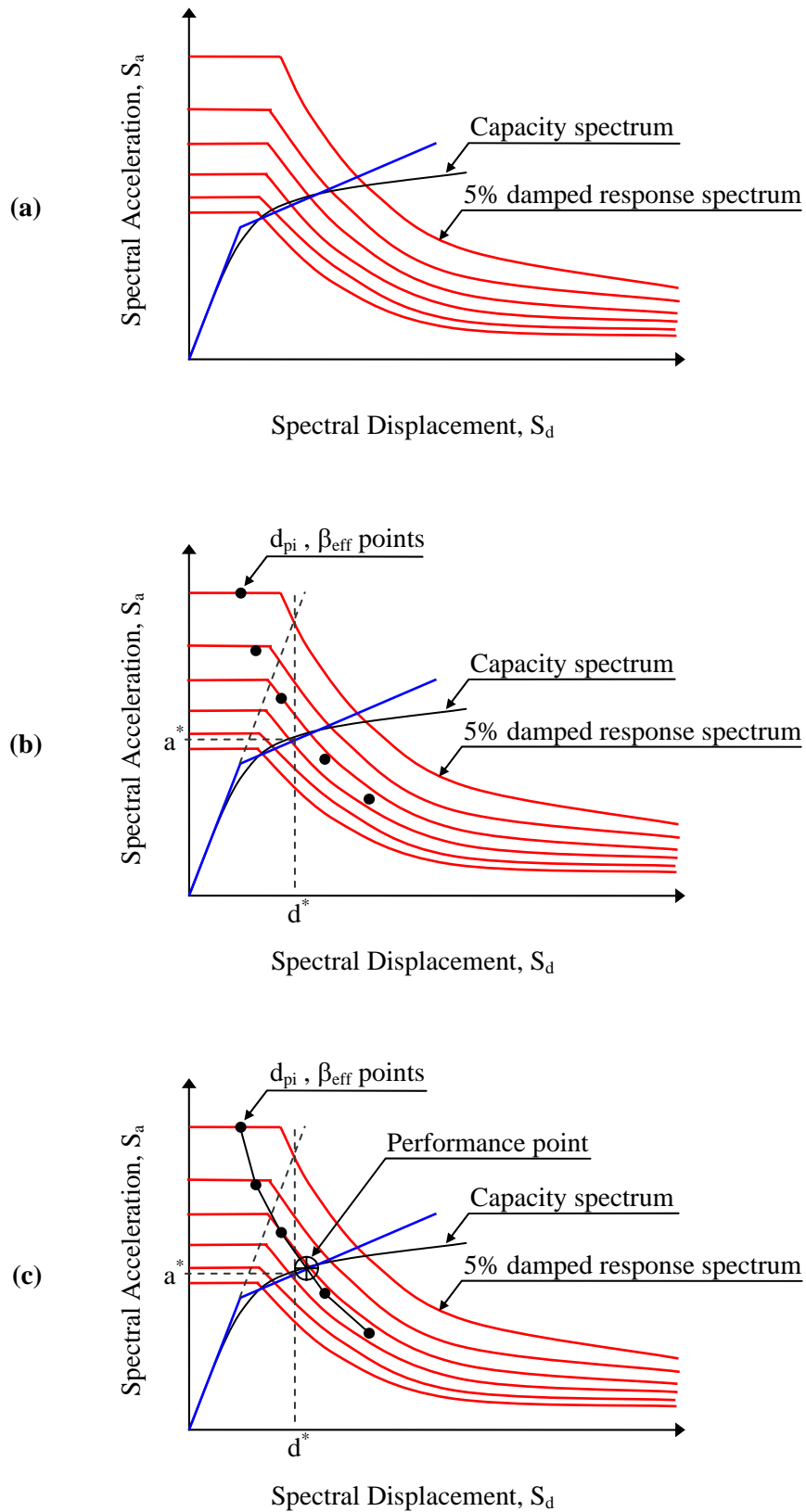


Figure 2.20 ATC-40 Procedure B - (a) Steps 1, 2 & 3 , (b) Step 4 , (c) Steps 5 & 6

2.4.2 Displacement Coefficient Method (FEMA-356)

The analysis procedure proposed by FEMA-356 [19] mainly focuses on obtaining a target displacement from the elastic displacement by means of some modification factors which are explained briefly in the following paragraphs. Inelastic displacement demand, δ_t , can be calculated using equation 2.26. The equation and its parameters are taken from FEMA-356 and some parts are slightly modified for better interpretation.

$$\delta_t = C_0 C_1 C_2 C_3 S_a \frac{T_e^2}{4\pi^2} g \quad (2.26)$$

where

C_0 : a modification factor that relates spectral displacement of an equivalent SDF system to the roof displacement of the structure (MDF). C_0 values, proposed by FEMA, are presented in Table 2.16. Linear interpolation shall be used to calculate intermediate values.

Table 2.16 Values for modification factor C_0

Number of Stories	Any Load Pattern
1	1.0
2	1.2
3	1.3
5	1.4
10+	1.5

C_1 : a modification factor that relates expected maximum inelastic displacement to the calculated linear elastic response displacement (C_1 must always be ≥ 1.0 and ≤ 1.5)

$$C_1 \begin{cases} = 1.0 & \text{for } T_e \geq T_s \\ = [1.0 + (R - 1)T_s/T_e]/R & \text{for } T_e < T_s \\ \leq 1.5 & \text{for } T_e < 0.10 \text{ sec} \end{cases} \quad (2.27)$$

T_e : the effective fundamental period of the building in the direction under consideration

T_s : characteristic period of the response spectrum

R : ratio of elastic strength demand to the calculated yield strength coefficient

$$R = \frac{S_a}{V_y/W} \cdot C_m \quad (2.28)$$

S_a : response spectrum acceleration at T_e and damping ratio of the building, in terms of g

g : acceleration of gravity

V_y : yield strength

W : effective seismic weight

C_m : effective mass factor (It is taken as 1.0 in the program. This assumption is conservative in all cases)

C_2 : a modification factor representing effect of pinching and degradation in stiffness/strength (It is taken as 1.0 in the program)

C_3 : a modification factor representing P- Δ effects

$$C_3 = \begin{cases} 1.0 & \text{for } \alpha \geq 0 \\ 1.0 + [|\alpha| (R - 1)^{3/2}] / T_e & \text{for } \alpha < 0 \end{cases} \quad (2.29)$$

α : ratio of post-yield stiffness to effective elastic stiffness as shown in Figure 2.21.

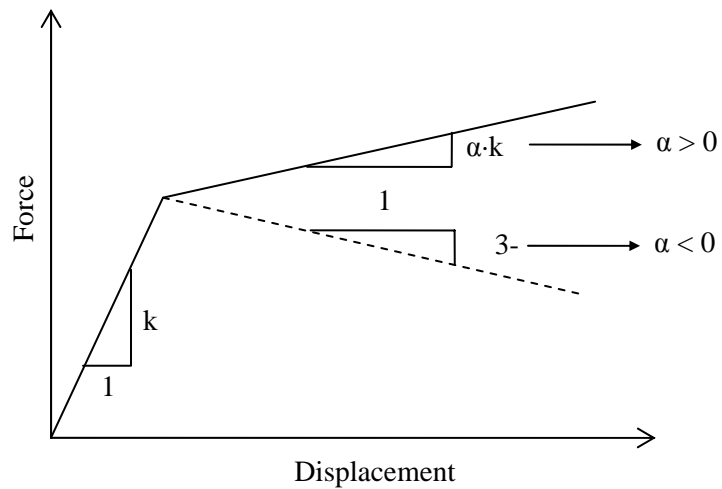


Figure 2.21 Idealized force-displacement curve and definition for α

2.4.3 Constant Ductility Procedure (Chopra and Goel)

An improvement to the ATC-40 [8] procedures is proposed by Chopra and Goel. This improved method utilizes well-known constant ductility design spectrum that is why it is declared as ‘constant ductility procedure’ throughout this study. The main difference between ATC-40 procedures and the improved ones is the way in which the demand is calculated. ATC-40 procedures employ equivalent linear systems whereas the improved ones enable to analyze an inelastic system.

There are three versions of improved procedures; Procedure A, B and Numerical. Procedures A and B are very similar to ATC-40 procedures A and B. They reduce the errors in the ATC-40 procedures by keeping hold of graphical attractiveness of both methods [22]. The numerical version is a reworked copy of the improved procedures and facilitates programmable algorithm generation. Since it is better for programming, it is preferred while developing the software.

The numerical version requires usage of $R_y - \mu - T_n$ equations. There are three different sets of equations proposed by the following researchers:

- Newmark-Hall [23]
- Krawinkler and Nassar [24]
- Vidic, Fajfar and Fischinger [25]

For the sake of completeness, each equation set is explained briefly in the subsequent paragraphs.

Newmark-Hall [23] developed $R_y - \mu - T_n$ equations based on elastoplastic systems. The reversed equations, giving μ as a function of R_y , are (Chopra [26]):

$$\mu = \begin{cases} \text{Undefined} & T_n < T_a \\ (1 + R_y^{2/\beta}) / 2 & T_a < T_n < T_b \\ (1 + R_y^2) / 2 & T_b < T_n < T_c \\ \frac{T_c}{T_n} R_y & T_c < T_n < T_c \\ R_y & T_n > T_c \end{cases} \quad (2.30)$$

where

$$\beta = \ln(T_n/T_a)/\ln(T_b/T_a) \quad (2.31)$$

Krawinkler and Nassar [24] developed $R_y - \mu - T_n$ equations based on earthquake response of bilinear systems. The equations, giving μ as a function of R_y , are:

$$\mu = 1 + \frac{1}{c} (R_y^c - 1) \quad (2.32)$$

where

$$c(T_n, \alpha) = \frac{T_n^a}{1 + T_n^a} + \frac{b}{T_n} \quad (2.33)$$

α : the coefficient representing slope of the yielding branch (αk) in terms of initial stiffness, k (presented previously in Figure 2.21)

a and b coefficients depend on value of α . Table 2.17 presents a and b coefficients corresponding to different α values.

Table 2.17 Values of a and b coefficients

α	a	b
0	1	0.42
0.02	1	0.37
0.10	0.8	0.29

Vidic, Fajfar and Fischinger [25] developed $R_y - \mu - T_n$ equations based on earthquake response of bilinear systems. The equations, giving μ as a function of R_y , are:

$$\mu = \begin{cases} 1 + \left[0.74(R_y - 1) \frac{T_0}{T_n} \right]^{1.053} & T_n \leq T_0 \\ 1 + [0.74(R_y - 1)]^{1.053} & T_n > T_0 \end{cases} \quad (2.34)$$

where

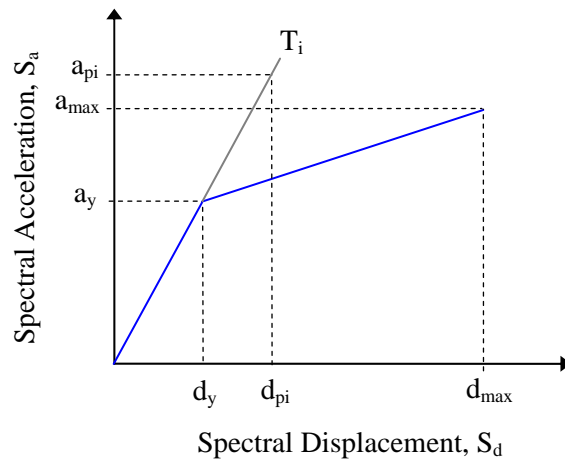
$$T_0 = 0.75\mu^{0.2} T_c \leq T_c \quad (2.35)$$

Since T_0 also depends on ductility, the procedure requires an iterative solution. A simplifying assumption of $T_0 = T_c$ may be used for non-iterative solution.

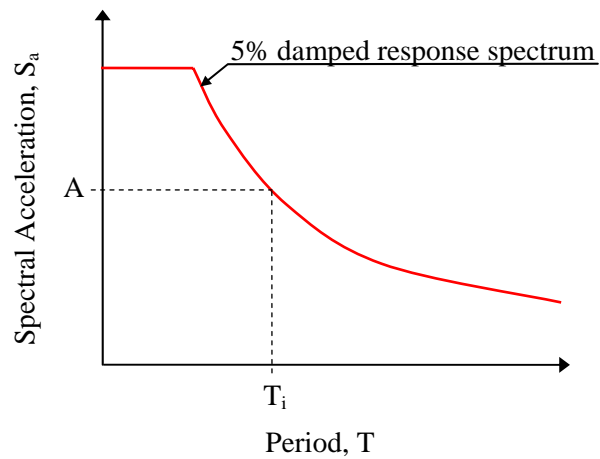
Numerical version of the improved methods is composed of the following steps. Figure 2.22 also describes some steps graphically.

1. Develop 5% damped (elastic) response spectrum in standard format.
2. Transform capacity curve into a capacity spectrum. Develop a bilinear model of the capacity spectrum considering a balance between the areas under original and bilinear capacity spectra.

3. Calculate T_i from $2\pi(d_y / a_y)^{0.5}$
4. Using 5% damped response spectrum, find spectral acceleration A for period T_i .
5. Calculate R_y using the equation $R_y = A / a_y$.
6. Select the set of $R_y - \mu - T_n$ equations to be used in the analysis and compute μ using the selected equation set.
7. Calculate S_{di} using the equation ($S_{di} = d_y \cdot \mu$) $\rightarrow S_{di}$ is the performance point.



Step 2 & 3



Step 4

Figure 2.22 Steps 2, 3 & 4 of numerical version for the improved procedures

CHAPTER 3

STRUCTURE OF THE SEISMIC RISK ANALYSIS SOFTWARE

3.1 INTRODUCTION

This study mainly focuses on developing seismic risk analysis software. The software developed uses the deterministic approach to predict the probable damage distribution for a specified region caused by a deterministic earthquake. Fault locations and building stock layouts are entered in terms of latitudes and longitudes. Results are also provided in latitudes and longitudes which makes mapping of results simpler and faster. It is capable of handling four attenuation relationships and three displacement demand computation methods. These relationships and methods are explained in Chapter 2.

Development of the software is basically performed by dividing the overall process into smaller sub-processes. Each sub-process, namely component, has made programming and debugging processes simpler and more efficient. Since the source codes of each component as well as the software itself reflect only programming details, it would be a vain attempt to include these codes. As a replacement for source codes, the step-by-step algorithms are provided to demonstrate and understand what the software does behind the nice-looking interface. Structure of the software with its components is discussed in depth in section 3.2.

3.2 SOFTWARE COMPONENTS

The name “Seismic Risk Analysis Software” is given to the software developed. From now on, it will be frequently denoted by the initial capitals as “SRAS”. SRAS has a modular structure that is deliberately chosen to ease error handling process and constitute

a well-built base for further modifications and upgrades. These partitions or components provide an open structure to the software by making it clearer and easier to use. Since SRAS has been developed just for educational purposes, it may give the impression of being much more instructive than necessary for experienced users.

Just as a reminder, SRAS is a computer program and all well-known facts about commercial software are also valid for SRAS. What is given as an input will be returned as an output of same quality. In other words, if *garbage* enters, *garbage* will be out. So, it is the user responsibility to verify the reliability of the results produced by SRAS.

Flowchart of the software is presented in Figure 3.1. SRAS is basically composed of three major modules that are common to all computer programs. These are input, calculation and output components. Each component has different numbers of sub-categories. This section is devoted to explaining these major components including their subdivisions.

As an overview, the software entails five data sets to start analysis. Building inventory data, attenuation relationship data, scenario earthquake data, capacity curves for each building type and analysis method data are the fundamental inputs to SRAS. Reliable building inventory data is a must to obtain realistic results for the defined scenario earthquakes assuming that the attenuation relationships and analysis methods yield dependable results.

After completion of input data, the calculation phase starts. This phase is composed of three parts, which are demand calculation, performance calculation and damage estimation. Demand calculation part, initially, finds the shortest distance between each building in the region and the scenario earthquake fault and then generates smoothed acceleration response spectrum expected under each building. Subsequently, performance calculation module computes performance point using the generated demand curve and provided capacity curve for each building. Finally, damage estimation module predicts the performance of each building under the scenario earthquake induced forces. Results obtained from the analysis are exported to a database file or displayed on the screen. And also, a report is created which includes the site based distribution of damage and all input data.

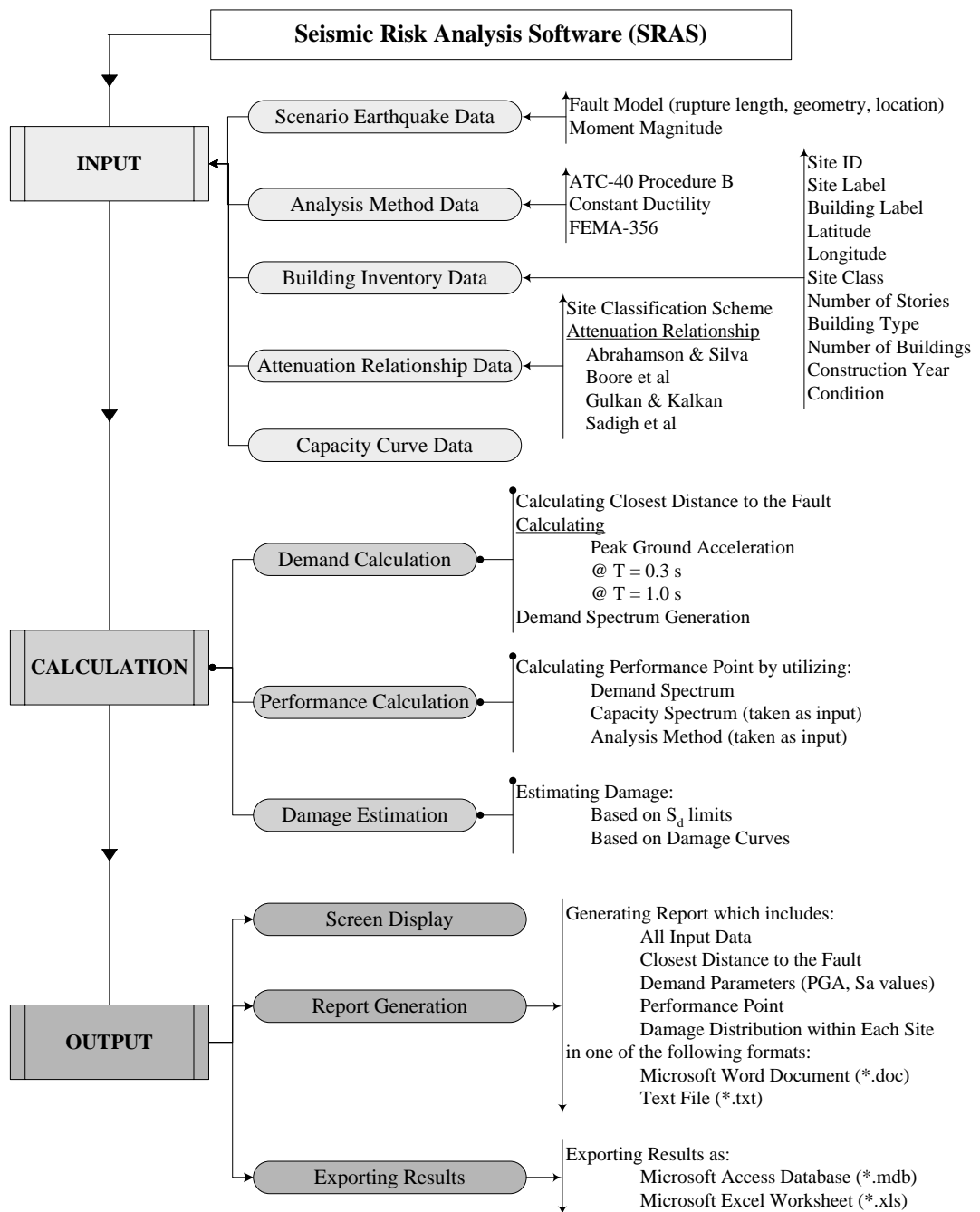


Figure 3.1 Flowchart for SRAS

3.2.1 Input Components

SRAS needs five major input components in order to be able to start analysis. These input components are building inventory, capacity curves, scenario earthquake, attenuation relationship and analysis method. Each of these components has vital importance in predicting a realistic damage distribution for the region under consideration. In the following paragraphs, these components will be covered in details to ensure proper input to SRAS.

3.2.1.1 Building Inventory Data

Seismic risk analysis software requires building stock information which is the fundamental input for risk analysis. Accuracy of analysis results depend on not only the methods or attenuation relationships used but also the reliability of the building database. Using reliable sources in collecting regional building data is crucial to obtain realistic and dependable results. This data gathering process may not be a serious problem in developed countries which probably have completed digitization of the entire country including transportation, power and water supply distribution and communication networks. These high resolution digital maps give all detailed information about the region under consideration. In the case of undeveloped or developing countries, the process seems quite challenging. Aside from detailed regional digital maps, it is even impossible to obtain a sketchy digital map only showing the district boundaries. After overcoming the difficulties in obtaining building inventory information, a preliminary screening is required to prepare this raw data as an input for SRAS. Building inventory input file should include the characteristics of buildings in the region. Building characteristics refer to the properties of each building that are going to be utilized during the analysis. There are 12 properties required for each building:

- | | |
|--------------------------------|------------------------|
| 1. Site ID | 7. Number of Stories |
| 2. Site Label | 8. Building Type |
| 3. Building Label | 9. Number of Buildings |
| 4. Latitude | 10. Construction Year |
| 5. Longitude | 11. Apparent Condition |
| 6. Site Class or Average V_s | 12. Information |

Site ID is numerical representation of Site Label. Site Label is the name of the sub-district or district depending on the resolution of digital map and building inventory.

Building Label is used to assign a name for each building, especially for hospitals, schools and other public buildings. Latitude and longitude define the spatial location of building in terms of geographical coordinate system. SRAS recognizes two different formats while introducing site characteristics: Site Class or Average V_s . A site classification scheme should be selected in order to let the program interpret the site class or shear wave velocity entered for each building. The corresponding numbers for the selected classification scheme classes or average shear wave velocities are written to the input file. SRAS uses average shear wave velocity corresponding to the selected site class or available average shear wave velocity. It is the users' responsibility to select site classes properly for each building. The flowchart for soil type identification is shown in Figure 3.2.

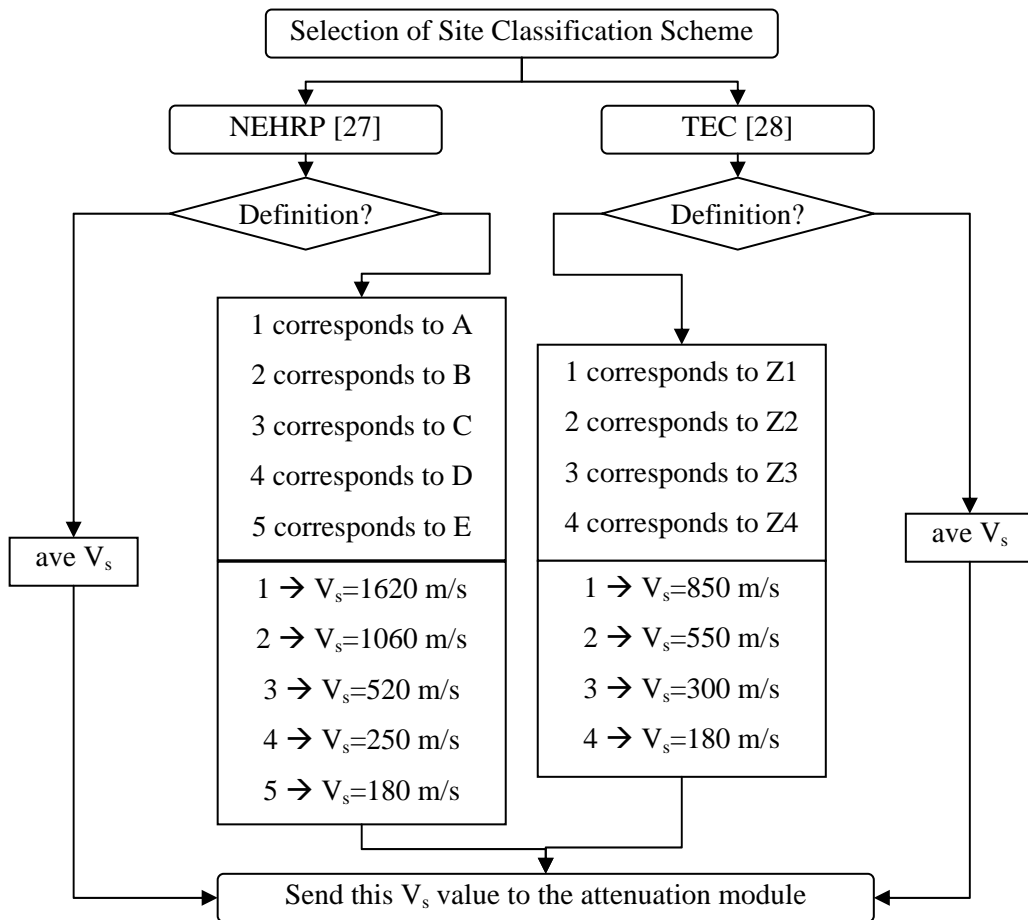


Figure 3.2 Flowchart for site characteristics identification process

There are two site classification schemes used in the program: NEHRP [27] and TEC [28]. Each of these site classification schemes has its own qualitative and quantitative definitions as shown in Tables 3.1 and 3.2.

Table 3.1 NEHRP [27] site classification scheme

Class Name	General Description	Mean V_s (m/s)		
		Min.	Ave.	Max.
A	HARD ROCK (e.g. metamorphic rocks with very widely spaced fractures)	1500	1620	-
B	ROCK (e.g. granites, igneous rocks, conglomerates, sandstones, and shales with close to widely spaced fractures)	760	1060	1500
C	VERY DENSE SOIL and SOFT ROCK (e.g. soft igneous sedimentary rocks, sandstones, and shales, gravels, and soils with >20% gravel)	360	520	760
D	STIFF SOIL (e.g. loose to very dense sands, silt loams and sandy clays, and medium stiff to hard clays and silty clays (15 < N < 50 blows/ft))	180	250	360
E	SOFT SOILS (e.g. loose submerged fills and very soft to soft (N < 15 blows/ft) clays and silty clays > 3m (10 ft) thick)	-	140	180

Table 3.2 TEC [28] site classification scheme

Class Name	General Description	Mean V_s (m/s)		
		Min.	Ave.	Max.
Z1	FIRM to HARD ROCKS (e.g. rock, very stiff clay, very dense sands)	700	850	-
Z2	GRAVELLY SOILS and SOFT to FIRM ROCKS (e.g. tuffs, agglomerate, stiff clays, dense sands)	400	550	700
Z3	STIFF CLAYS and SANDY SOILS (e.g. soft deposits, medium dense sand, stiff clay and silt)	200	300	400
Z4	SOFT SOILS (e.g. high water table + alluvial deposits, loose and, soft clay and silt)	-	180	200

Number of stories is another important parameter required for both statistical distribution of buildings and computation of demand displacement. Building Type represents construction type and is entered as a string with maximum 15 characters. It is necessary to decide how many different building types will be included in the analysis and to define each type clearly. Then for each building in the stock, a decision on the type should be made by selecting one of these pre-determined types. For instance, if three building types are defined such as “Reinforced Concrete Frame - RCF”, “Steel Frame - SF” and “Composite Frame - CF”, then each building in the stock should be given a type from these three types and corresponding abbreviation for that type should be written as Building Type while preparing the input file.

Number of Buildings is used to reduce the input file size in the case of district based performance analysis in which all buildings within the district are assumed to be located at the center of that district. Thus, buildings having same properties and district can be modeled as just one building by defining the number of buildings in the group. If it is left blank, it will be assumed that entered properties belong to only one building. Construction Year provides information about the age of building and design code available at that time. Apparent Condition is a visual impression on the building which can be “Very Poor”, “Poor”, “Moderate” and “Good”. These apparent conditions are entered as numbers 1, 2, 3 and 4 respectively. If it is left blank, it will be assumed as “Moderate”. Finally, an additional space is provided for further information which may be used for special remarks or notes.

After completion of screening and revising processes, the building inventory input file should have 12 columns. Further details about creating an input file are provided in the program manual that is made available in Appendix - A.

3.2.1.2 Capacity Curve Data

Another important parameter, which is given as a separate file, is the capacity curve data for each building type. These curves are defined for each building type and for different intervals of number of stories using “Capacity Curve Wizard”. The curves are in ADRS format which means that they are plotted in S_a versus S_d environment. Each building type has its own capacity curve plotted for various intervals of number of stories. As an instance, if there are five different building types in the building inventory, then there should be five capacity curve groups. Each group should have curves plotted for different number of stories. Figure 3.3 demonstrates this definition process.

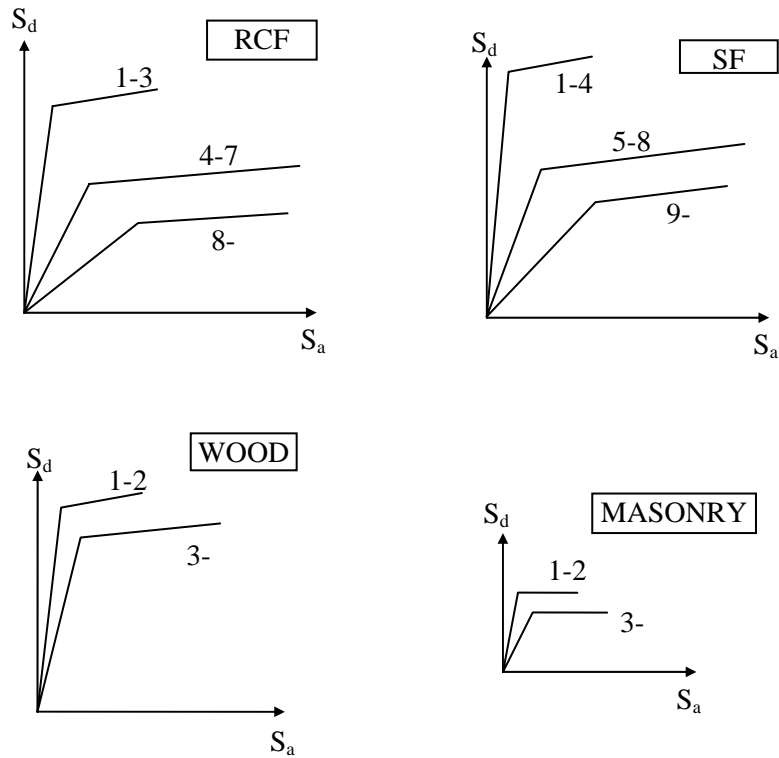


Figure 3.3 A sample set of capacity curves (numbers represent stories) (not to scale)

The program reads the type and number of stories for each building from the building input file and decides which capacity curve is going to be used for that building. This separation of capacity curves from building input files enables to define a general capacity curve database for a country considering the current practice and to use these capacity curves in performing risk assessments for various regions. Details of capacity curve data file generation is provided in the program manual which is included in Appendix - A.

3.2.1.3 Scenario Earthquake Data

It is the major component of SRAS that is simulating the scenario earthquake. This component is attached to the main code as “Fault Modeling Wizard”. The wizard creates fault models by using the information about their spatial location. A fault model is created by defining nodes in terms of latitudes and longitudes. Program combines these nodes by lines and generates a fault model which is composed of linear segments. Magnitude of the scenario earthquake is also defined while generating the fault. Once a

fault model is created, it can be utilized in other scenario analyses for different regions around that fault.

SRAS uses two fault models; linear and meshed. These models are different from well-known fault types. Fault type defines major characteristics of a fault whereas fault model is a representation of real fault rupture in simulated analysis environment. Both models assume that fault rupture path is composed of segments which are defined manually by entering nodal point data. The segments are linear between two nodal points and thus they do not follow the curvature of the Earth unless nodes are closely spaced.

Linear Fault Model: If the nodes defined on the fault rupture path are in close proximity of each other, or in other words the nodes are closely spaced, the curvature of earth may be ignored in between two nodes and the assumption of linear fault segment will be valid. Figure 3.4 illustrates the importance of node density while generating a fault model.

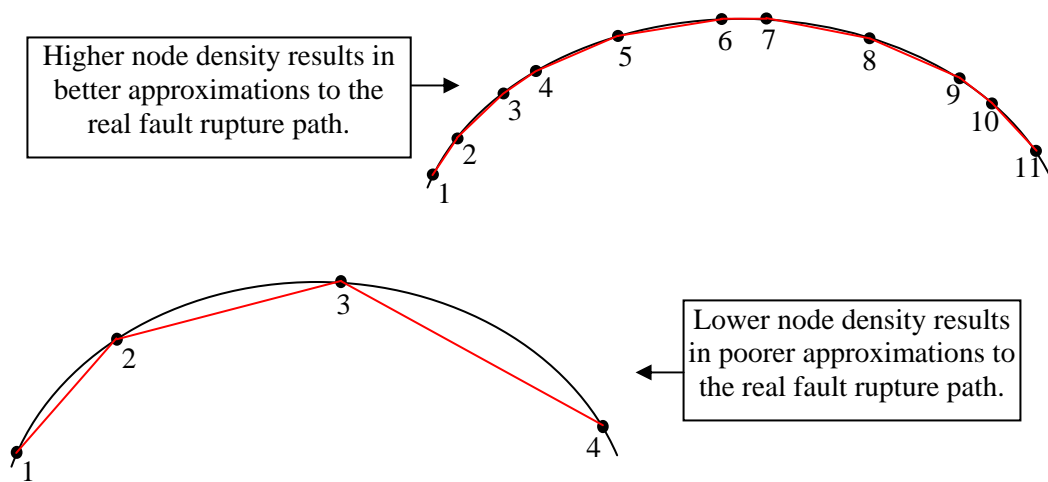


Figure 3.4 Node density effect in a fault model

Meshed Fault Model: If the nodes are located noticeably apart from each other, then some additional nodes should be inserted in between two distant nodes to keep segment lengths as smaller as possible. This objective can be achieved by defining a meshed fault model. It enables user to generate new intermediate nodes for each segment considering different mesh sizes provided by the user. If large mesh sizes (50 is sufficient most of the times) are defined, then the fault rupture path seems to duplicate the curved

real path (or great circle distance between starting and ending nodes) as shown in Figure 3.5.

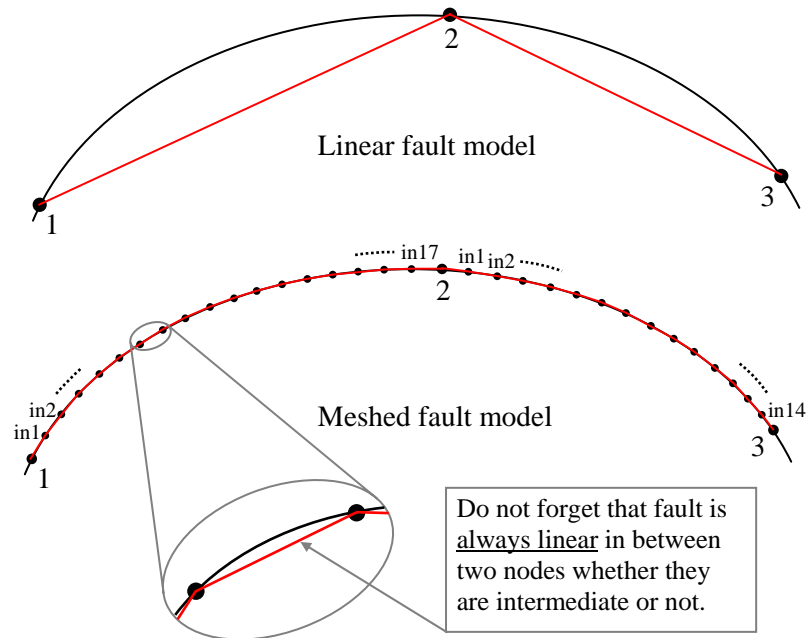


Figure 3.5 Comparison of linear and meshed fault models

Mesh Generator Function: This sub-function generates a meshed fault model by calculating intermediate node coordinates and writing them to a file in order to be used in the subsequent analysis steps. The algorithm is provided below. (EN: end node of segment, SN: start node of segment, meshsize: number of divisions for a segment)

For Each fault segment

$$\Delta_{\text{latitude}} = (\text{EN}_{\text{latitude}} - \text{SN}_{\text{latitude}}) / \text{meshsize}$$

$$\Delta_{\text{longitude}} = (\text{EN}_{\text{longitude}} - \text{SN}_{\text{longitude}}) / \text{meshsize}$$

For i=0 to meshsize-1

$$\text{New_node_lat} = \text{SN}_{\text{latitude}} + i \cdot \Delta_{\text{latitude}}$$

$$\text{New_node_long} = \text{SN}_{\text{longitude}} + i \cdot \Delta_{\text{longitude}}$$

Print to file

Next i

Next fault segment

Fault characteristics: Every fault model has common properties which are number of nodes, number of segments, node and segment data matrices. Total number of nodes and coordinates of each node with its node number are entered manually or read from a text file. Then program creates segment data matrix automatically. The segment data matrix includes curved length, linear length and mesh size for each segment. Curved length is the great circle distance between two end points of the line segment whereas linear length is the well-known linear distance. Mesh size defines the number of sub-segments for each segment. Expected moment magnitude of the earthquake is another fault characteristic. Details of fault model generation are available in the program manual attached in Appendix - A.

3.2.1.4 Attenuation Relationship Data

Local site conditions have considerable effects on response of buildings under earthquake loads. This is not only related with the soil type under the site, but it has also something to do with characteristics of the motion path that seismic waves followed while reaching the site. Attenuation relationships try to compensate those site effects. SRAS is capable of handling four different attenuation relationships, which are presented in section 2.3. These attenuation relationships are Gülkan and Kalkan [21], Abrahamson and Silva [20], Sadigh et al. [16] and Boore et al. [12]. Each attenuation relationship is programmed as a sub-function and inserted into the main attenuation module. This sub-functioning makes it handy for further updates and modifications as well as addition of new attenuation relationships.

The software has an attenuation wizard that enables the user to select the attenuation model visually. This gives the opportunity to review the limitations of each relationship and select the most appropriate model for the region under consideration. It is the users' responsibility to verify the proper attenuation relationship selection. The wizard modifies its graphical user interface depending on the selected attenuation relationship to make the collection of input parameters more straightforward.

3.2.1.5 Analysis Method Data

Analysis method refers to the procedure followed while computing the displacement demand. The software is capable of handling three well-known procedures. These are capacity spectrum method, constant ductility method and displacement

coefficient method. Each of these methods was discussed in section 2.4 in a detailed manner.

SRAS takes analysis method as an input which includes some other parameters related to the selected procedure. ATC-40 procedure requires slice number, error percentage and structural behavior type of buildings. Slice number and error percentage are used for the convergence and accuracy of the iterative methodology. Figure 3.6 shows the definitions for slice number and error percentage. Structural behavior type is selected for all structures in the inventory as “A”, “B” or “C” which were defined in Table 2.12.

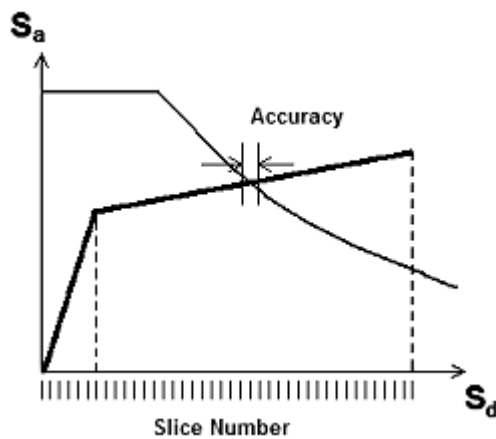


Figure 3.6 Slice number and accuracy

Constant Ductility procedure requires slice number, error percentage and $R_y-\mu-T_n$ relationship. Slice number and error percentage are same as in the case of ATC-40 procedure (Figure 3.6). $R_y-\mu-T_n$ relationship is selected from the available three relations, named as “Newmark – Hall”, “Krawinkler - Nassar” and “Vidic – Fajhar – Fischinger”. Details of these relations were covered in section 2.4.3. Displacement coefficient method does not require any parameters since it is not an iterative procedure.

After selecting one of the available procedures using “Analysis Method Wizard”, an analysis method file is created in order to be used in the analysis. The file may also be utilized for other analysis since it does not include project or scenario specific parameters. Details of analysis method file generation are available in the program manual presented in Appendix - A.

3.2.2 Calculation Components

SRAS uses three calculation components. These components are demand calculation, performance calculation and damage estimation. Initially, demand calculation module runs and computes the closest distance between each building and fault rupture as well as spectral acceleration values required to construct a demand curve. Secondly, performance calculation module starts analysis and computes the demand displacement for each building. Finally, damage estimation module predicts damage level of each building. Each of these modules is composed of several sub-routines and functions. The following paragraphs give details of each component.

3.2.2.1 Demand Calculation

It is the key component of SRAS that is utilizing the attenuation relationships to generate spectral acceleration curves and attached to the main code as a separate module. This module is composed of functions that calculate the closest distance to the fault, compute the spectral acceleration values for each attenuation relationship defined in section 2.3 and generate demand spectrum.

By using the spatial coordinates of buildings and scenario fault model, the closest distance between each building and fault is computed which is, in fact, nothing but the distance of a point to a line segment. This topic is covered in section 2.2. Then, required parameters for the attenuation relationships become complete. Depending on the selected attenuation relationship, the spectral acceleration values that are PGA, S_a at $T=0.3$ sec and S_a at $T=1.0$ sec are calculated. Finally, demand calculation module generates a smooth design-like response curve to be used in the subsequent steps of the analysis. Increasing fraction of the spectrum is not modeled and it is taken as constant within the interval $0 < T < T_{\text{intersect}}$. This simplifying assumption makes it easier to develop an algorithm for finding the intersection point of capacity and demand spectra. The programming algorithm is summarized in the following steps.

1. Calculate the closest distance to the fault
2. Check which site classification scheme is selected (NEHRP [27] / TEC [28]).
3. Check which attenuation relationship is utilized.
4. Interpret the selected site class on the basis of classification scheme and attenuation relationship. If Boore et al. [12] or Gülkan & Kalkan [21] attenuation relation is selected, use average shear wave velocity for the selected site class to

obtain acceleration response spectrum. For the other two attenuation models use “Rock” if average shear wave velocity is greater than 550 m/s and use “Soil/Deep Soil” if average V_s is less than 550 m/s in order to obtain acceleration response spectrum.

5. Take S_a values at $T=0.3$ sec and $T=1.0$ sec as I_a and I_v respectively and construct simplified acceleration response curve as shown in Figure 3.7. Use this curve as demand curve in the following steps of analysis.

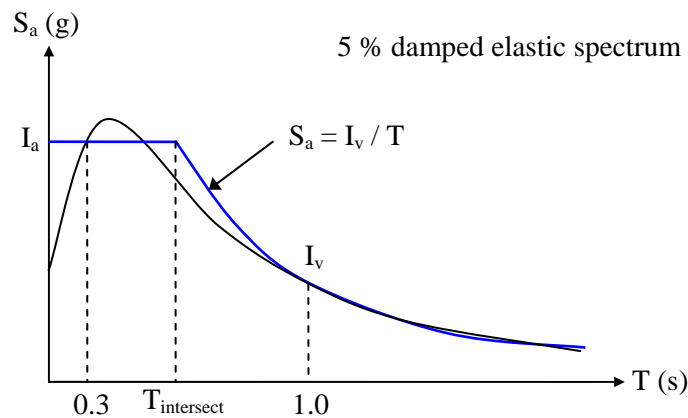


Figure 3.7 Simplified acceleration response spectrum

3.2.2.2 Performance Calculation

Performance of each building is computed by this module. SRAS is capable of computing the demand displacement using three different methodologies. These well-known analysis methods were discussed in section 2.4 including all necessary details. While developing the software, no additional assumptions were made in addition to the ones inherited in the methodologies. SRAS is a tool just to perform analyses faster. It does not recommend new methods or techniques. Considering this aspect, the computed demand displacements are not more reliable than the method chosen for analysis.

SRAS uses the selected analysis method, which was initially provided as an input, to calculate demand displacement. Each analysis method is developed as a separate function within performance calculation module. Each function takes necessary demand

and capacity parameters and yields performance point. Performance point is a term used to represent demand displacement. Computed performance point is returned to the main program as a matrix which has the values of spectral displacement, spectral acceleration and period. If the performance point can not be found, function returns “-1” for those values. This is observed when ATC-40 [8] or Constant Ductility [22] procedure was selected and no intersection is found between capacity curve and reduced demand curve. In this case, the structure may probably collapse, since demand is much higher than the available capacity.

3.2.2.3 *Damage Estimation*

SRAS utilizes two methods for performing damage estimation. The first method is based on S_d limits (referred as *SDL Method* from now on) whereas the second method utilizes damage curves (referred as *DC Method* from now on). SRAS has default definitions for both methods and the user may modify the limits or curves depending on the available building inventory information.

SDL Method: *SDL* method uses capacity curve in ADRS format to define damage level intervals. The user may define maximum 9 damage levels and label them accordingly for each building type. An example is shown in Figure 3.8 for a building type having three damage levels labeled as “Light”, “Moderate” and “Heavy”. Every building type has its own damage level definition which means different damage level definitions can be done for different building types. For instance, if “STEEL” frame structures have three damage levels, it is possible to assign two or five damage levels to “RC” frame structures. It is also possible to employ same damage levels for all building types.

The damage level definition process mostly depends on the building types and the project requirements. While estimating damage, the procedure below is repeated for each building in the stock.

1. Read type of building and number of stories from the input file and select appropriate capacity curve for the building.
2. Using damage level definitions, calculate numerical limits for each damage level interval.
3. Check which interval contains performance point and select that damage level as estimated building damage.

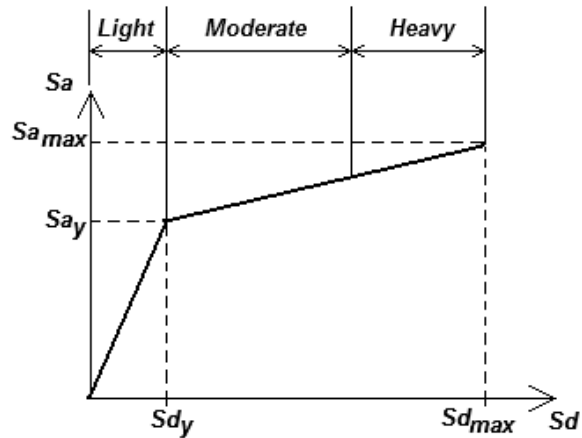


Figure 3.8 Damage estimation based on S_d limits

DC Method: DC method uses damage curves to define percentage damage. For each building type, the user may define damage curves representing an interval of number of stories. An example is shown in Figure 3.9 for a building type having three damage curves representing different intervals of number of stories. Every building type has its own damage curves, indicating that different intervals of number of stories can be used for different building types. For instance, if “STEEL” frame structures have three damage curves, it is possible to assign two or five damage curves to “RC” frame structures. And it is also possible to employ same number of damage curves for all building types. This is the case when all type of buildings are classified as “Low-rise (1-3)”, “Mid-rise (4-7)” and “High-rise (8+)”

In general, the percentage damage estimation may be utilized to obtain smooth transitions and variations between buildings. While estimating damage, the procedure below is repeated for each building in the stock.

1. Read type of building and number of stories from the input file and select appropriate damage curve for the building.
2. Using selected damage curve, read or linearly interpolate percentage damage value corresponding to the performance point spectral displacement.
3. Assign that percentage damage to estimate building damage.

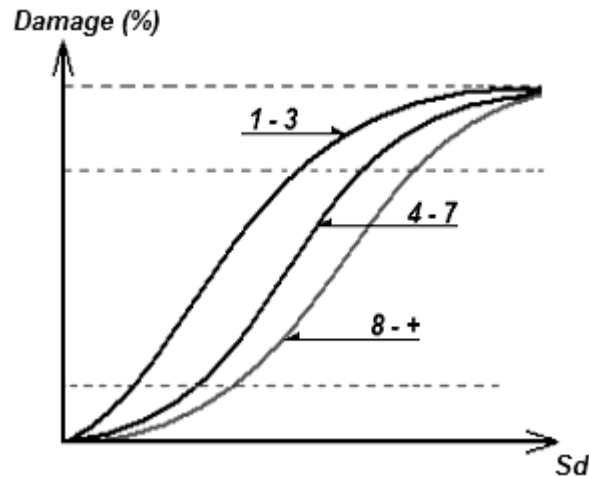


Figure 3.9 Damage estimation based on damage curves

3.2.3 Output Components

Every program has a special way of displaying or presenting the results. This is expected since each program is developed for an individual purpose. Output components refer to sub-routines and graphical interfaces used for conveying results to the user. The most widespread output components are screen display, report generation and data storage.

Since the ultimate objective in this study is to develop a user friendly seismic risk analysis software, tabular results are preferably better than other formats. Almost all well-known GIS applications, such as ArcGIS and MapInfo, make use of tabular data while generating maps or geo-databases. Considering this aspect, SRAS is developed to present the results in both tabular and text file format. The following paragraphs provide detailed information about each component.

3.2.3.1 Screen Display

Screen display is very practical to check the results for obvious inconsistencies and critical deviations. If the results are found to be unsatisfactory, then the analysis is repeated by eliminating the errors in input data until the abnormality disappears. SRAS presents the results in a table where computed values are appended next to the columns of building input data. Thus, the number of columns on the output table becomes twenty five.

appropriate way. Engineering reports are the best ways of conveying the outcome of a study to the authorities concerned. Regarding to this aspect, SRAS is equipped with a report generation module. This module prepares a preliminary report for the project including input data, methodology and results.

The report is composed of several pages. There is a cover page showing the project title, information about the person who made the study and report generation date and time. Secondly, building inventory statistics are given instead of writing all building data. Then, nodal and segmental data of the scenario earthquake fault model is added to the report. Next, attenuation relationship, analysis method and capacity curve data are provided. Finally, the estimated damage distribution within the district for each building type is printed and report generation is finalized. Details of report generation process are explained in program manuals that are provided in Appendix - A.

3.2.3.3 Exporting Results as Database File

After completing initial screening of the results, it is necessary to export results. The results are exported as database files since tabulated results will ease post-processing. Two database formats are supported by SRAS. These are Microsoft Excel Worksheet (*.xls) and Access Database (*.mdb). While generating digital maps or geodatabases, these file formats are quite handy and practical. The created output file includes all data shown on screen as aforementioned in section 3.2.3.1. No additional information is given regarding to the methodology used. Details for exporting results are available in program manuals appended as Appendix - A.

CHAPTER 4

VERIFICATION OF SRAS

4.1 INTRODUCTION

Every computer program should be checked for the inconsistencies and errors after development process. This phase is called as *debugging*. The best way of software debugging is to use it for benchmark problems and compare the outputs with benchmark results. If the results are same or very similar, the software proves to be reliable. But in the case of risk analysis and damage distribution, the situation is not that simple. Observed regional damage distribution reported after an earthquake may show significant variations depending on the selected assessment methodology and even on the assessment team employed. For instance, two separate teams may present different damage distribution maps that follow the same trend but have dissimilar quantitative results for the same region. So, this makes it quite difficult to define a quantitative benchmark case in risk analysis problems. Since no quantitative benchmark results are available, the best thing to do is trying to catch the general trend in regional damage distribution and to predict the number of collapsed buildings satisfactorily for the region experiencing an earthquake. By means of spot checks of intermediate steps, the modules of the software can be debugged as well.

SRAS has been verified by using it for the estimation of damage distribution in Adapazari due to August 17, 1999 Izmit Earthquake. Although it is known prior to the verification that the damage pattern in Adapazari was too multifaceted to be predicted by conventional regional assessment procedures, it is aimed to check SRAS outcome for the consistency of results rather than the precise correspondence with the observed damage statistics by General Directorate of Disaster Affairs (GDDA). The verification process will

be explained in four sections. First section describes the input parameters used in the analysis. Second part gives details of damage estimation methodology. Third section presents the results and the last part discusses reliability of the results as well as SRAS.

4.2 INPUT PARAMETERS

Adapazari district and fault rupture generated by the August 17, 1999 Izmit Earthquake are mapped and presented in Figure 4.1. Required input parameters for the assessment are building inventory data, scenario earthquake fault data, attenuation relationship data, capacity curve data and analysis method data. These input parameters will be explained in the following paragraphs to demonstrate clearly what was provided to SRAS as input. Since building inventory database is quite large, it will be a vain attempt to present all buildings as tables. Instead, only statistical information is provided here regarding to the building inventory. Data files are appended to the attached disk.

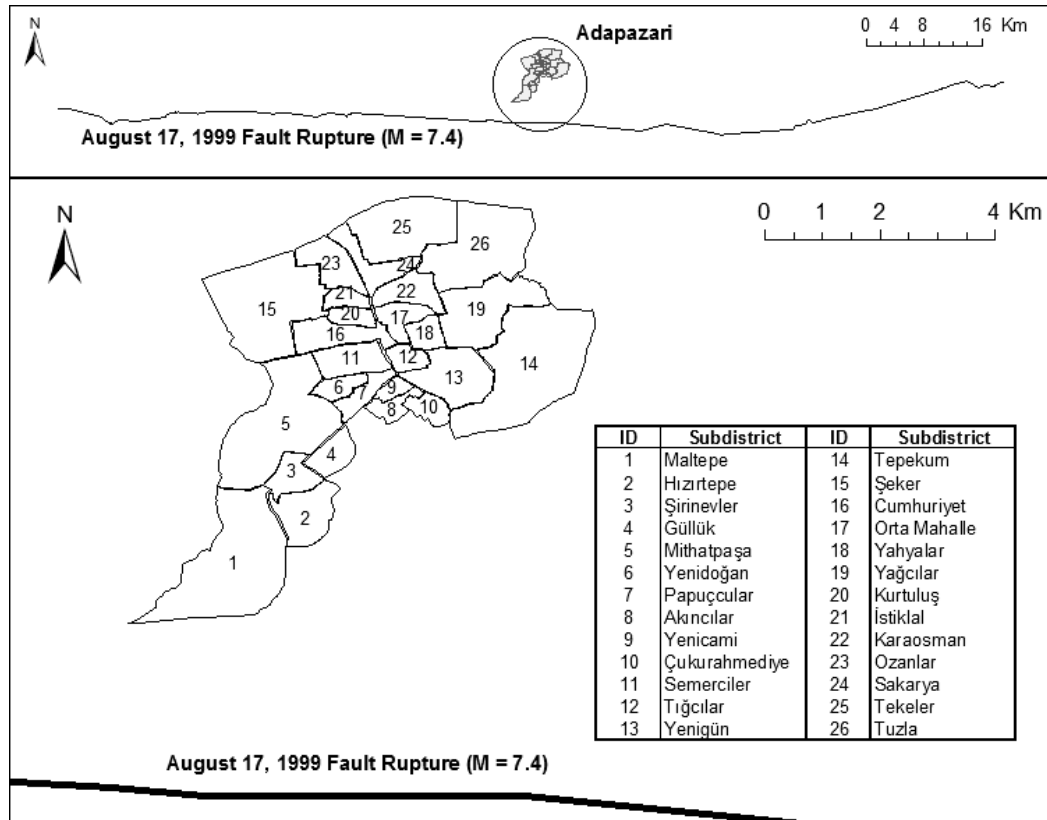


Figure 4.1 Adapazari and August 17, 1999 Izmit Earthquake fault rupture location

Two sets of building inventory data were employed in the study. One of the sets was composed of 2747 buildings lumped at the centers of sub-districts. This data set was obtained from the GDDA database and lacked spatial locations of buildings. The other set was Sakarya University (SU) database of 241 collapsed buildings including spatial locations and detailed information on the structural and architectural features. All buildings in the sets were reinforced concrete with moment resisting frame. The statistical information about the building inventory data sets is provided in Table 4.1.

Table 4.1 Statistical distribution of buildings with respect to number of stories

Set-1 (2747 Buildings)			Set-2 (241 Buildings)		
# of Stories	# of Buildings	%	# of Stories	# of Buildings	%
4	1192	43.4	3	9	3.7
5	1404	51.1	4	31	12.9
6	148	5.4	5	116	48.1
7	1	0.0	6	76	31.5
8	1	0.0	7	9	3.7
9	1	0.0			

The fault rupture of August 17, 1999 Izmit Earthquake was used as the scenario earthquake fault model (Figure 4.1). The model was generated by defining 148 nodes in latitudes and longitudes. A moment magnitude of 7.4 was selected to simulate the earthquake.

Four attenuation relationships were utilized to observe the variations in peak ground acceleration and spectral acceleration values. These attenuation relations are Abrahamson and Silva [20], Boore et al. [12], Gülkan and Kalkan [21] and Sadigh et al. [16]. Calculations were performed for two different site conditions, rock and soft soil. Each site class was assumed to be uniform throughout the district.

Three analysis methods were implemented to compute inelastic displacement demands of the buildings in the region. These are capacity spectrum method of ATC-40 [8], displacement coefficient method of FEMA-356 [19] and constant ductility method proposed by Chopra and Goel [22].

Building capacity curves were developed separately depending on the database used. For the GDDA database, all buildings were represented by a single capacity curve since they are all mid-rise (4-7 stories) reinforced concrete buildings. Figure 4.2 illustrates this capacity curve in acceleration-displacement response spectra format. Employing the recommendations given in Yakut et al. [29], individual capacity curves were obtained for the buildings in SU database.

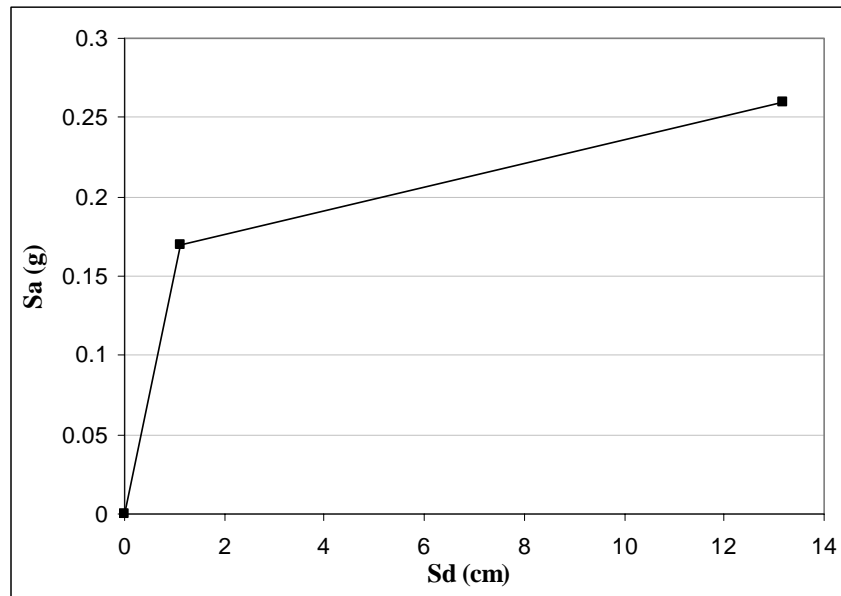


Figure 4.2 Capacity curve for mid-rise RC buildings

4.3 DAMAGE ESTIMATION METHODOLOGY

SRAS was employed for the analysis. Using four attenuation relationships and three analysis methods, analyses were performed for each site condition and building inventory geodatabase. All modification factors have been taken as 1.0 in the analysis. SDL method, covered in section 3.2.2.3, was employed as damage estimation methodology. The assessment criteria, defined in Table 4.2, were used to determine the expected damage level for each building in the inventory. S_d , S_{dy} and S_{dmax} are the computed, yield and ultimate spectral displacement values, respectively.

Table 4.2 Vulnerability assessment criteria used in the analysis

Damage Level	Criterion
None / Light	$S_d \leq S_{dy}$
Moderate	$S_{dy} < S_d \leq \frac{(S_{dy} + S_{dmax})}{2}$
Heavy / Collapsed	$\frac{(S_{dy} + S_{dmax})}{2} < S_d$

4.4 RESULTS

48 analyses were carried out to check the reliability of the software. The results of all analyses are available in the attached disk inside the folder named as “Adapazari_Case_Study”. Since it is impractical to generate maps for all results, only representative ones were selected to be mapped. Figures B.1 and B.2 show the regional distribution pattern of PGA, S_a at $T = 0.3$ s and $T = 1.0$ sec, respectively. Damage distribution patterns obtained by using Gülkan and Kalkan [21] attenuation relationship for soil sites and GDDA geodatabase are presented as Figures B.3 and B.4. The outcome of analyses performed by using SU database was mapped to observe the variations between three analysis methods. Figure B.5 illustrates three assessment procedures with damage estimations based on soft soil using Boore et al. [12].

The results were also tabulated for a comparison between the damage statistics of GDDA and the predicted damage by SRAS. Table B.1 presents the damage statistics for GDDA database whereas Table B.2 shows the results obtained by SRAS using Gülkan and Kalkan [21] attenuation relationship and uniform soft soil type.

4.5 DISCUSSION OF RESULTS

Dependability of damage estimates obtained for Adapazari is open to discussion not because of SRAS but for the involved site effects and structural attributes experienced in Adapazari. Evidently, discrepancies between observed and predicted damages for the GDDA buildings are apparent in Tables B.1 and B.2. For this reason, SRAS outcome was examined thoroughly for every step of analysis prior to damage estimation process. Computed closest distance values were well-matched with the ones separately generated

using the commercial software ArcView 8.3. Thus, distance calculation module proves its reliability. Calculated demand parameters were also verified by manual execution of attenuation relationship equations. Unsurprisingly, PGA and S_a values were decreasing as getting away from the fault. So, demand calculation module proves to be consistent and dependable. Computed inelastic displacement demands were compared with the ones calculated separately by hand and they were almost same ignoring insignificant rounding errors. Finally, damage estimation module was checked for its dependability. This was the easiest part because even rapid screening of results was sufficient to justify damage level assignments made by SRAS. In summary, SRAS has proved to be a reliable tool for performing lengthy calculations of conventional regional assessment procedures.

CHAPTER 5

CASE STUDY: ISTANBUL

5.1 INTRODUCTION

The 17 August 1999 $M_w = 7.4$ Izmit and 12 November 1999 $M_w = 7.1$ Düzce earthquakes prompted seismologists and geologists to conduct studies to predict magnitude and location of a potential earthquake that can cause substantial damage in Istanbul. One of these studies was Parsons et al. [31] and the striking outcome of the study was summarized as follows: (Parsons et al. [31])

We find a $62 \pm 15\%$ probability of strong shaking ($MMI \sim > VIII$; equivalent to a peak ground acceleration of 0.34-0.65g (Wald et al., 1999) in greater Istanbul over the next 30 yr (May 2000-2030), $50 \pm 13\%$ over the next 22 yr, and $32 \pm 12\%$ over the next 10 yr. Inclusion of renewal doubles the time-averaged probability; interaction further increases the probability by a factor of 1.3.

These extremely high probabilities of occurrence have triggered responsible authorities to take precautions to reduce the casualties and the losses from the expected earthquake. Among several studies carried out, as discussed previously, JICA has performed an extensive study (referred as *JICA Study* [11] from now on) that covers a large study area and building inventory (referred as *JICA database* from now on). All data including building inventory, scenario faults, site classes, damage estimation results etc. were made public for researchers. As an application of the software developed in this study, it was intended to re-calculate the probable damage distribution in Istanbul using the JICA database by employing newly developed capacity curves that are peculiar to construction practice in Turkey.

Considering this aspect, SRAS has been utilized for the estimation of probable damage distribution in Istanbul due to a scenario earthquake (model A of JICA Study [11]) of moment magnitude 7.5. Three separate analyses were performed to be able to make comparisons. These analyses will be referred as *JICA-Check*, *JICA-New*, and *IMM-New*.

All data used for the analyses were recorded to the attached disk as a zipped folder named as “Istanbul_Case_Study”. A “Read Me” file was put into the same folder to explain directory mapping. The interested reader may perform several analyses; prepare maps or tables of interest by using the available data on the attached disk. Each analysis carried out in this study is explained separately in Section 5.2. The results obtained from the analyses are compared and discussed in Section 5.3.

5.2 DAMAGE ESTIMATION FOR ISTANBUL

Three analyses, namely *JICA-Check*, *JICA-New* and *IMM-New*, were carried out. The similarities and differences between the analyses are presented in the following table.

Table 5.1 Comparison of analyses performed for estimating damage in Istanbul

	JICA-Check	JICA-New	IMM-New
Building Inventory	The ratios for building types and heights in JICA database were converted to number of buildings. This rough conversion inherits certain assumptions.	The building inventory obtained from IMM was intersected with the JICA Study area and those falling within the study area were selected for the analysis.	The building inventory obtained from IMM was used.
Site Classification Map	Site classification map proposed in JICA Study was utilized to assign the site classes.	Site classification map proposed in JICA Study was utilized to assign the site classes.	A new site classification map was utilized.
Capacity Curves	Newly developed capacity curves were used.	Newly developed capacity curves were used.	Newly developed capacity curves were used.

Although results of regional damage estimation process require lots of maps and tables, in this study it is believed to be more effective to display representative maps and tabulate damage estimation results in district level. For this purpose, maps and tables, presented in Table 5.2, were prepared for each analysis.

Table 5.2 Selected maps and tables to be presented for each analysis

	MAPS	TABLES
JICA-Check	Ground Classification (JICA) Distribution of PGA Distribution of S_a at $T = 0.3$ s Distribution of S_a at $T = 1.0$ s Distribution of Heavily DB* Distribution of Moderately DB** Distribution of Lightly DB**	Summary of damage estimation results in district level
JICA-New	Distribution of Heavily DB Distribution of Moderately DB** Distribution of Lightly DB**	Summary of damage estimation results in district level
IMM-New	Ground Classification (New)** Distribution of PGA** Distribution of S_a at $T = 0.3$ s** Distribution of S_a at $T = 1.0$ s** Distribution of Heavily DB Distribution of Moderately DB** Distribution of Lightly DB**	Summary of damage estimation results in district level

*DB**: Damaged Buildings, ****: presented in Appendix C

While generating maps for heavily/moderately/lightly damaged buildings, the ratio of damaged buildings to the total number of buildings for each district was utilized since these ratios provide valuable information for the comparison between different analyses. Number of damaged buildings in the districts of a province may show drastic variations whereas the ratios show gradual changes. In view of this, the ratios were employed while generating damage distribution maps.

As a technical reminder, building inventory database for Istanbul was extremely large and each analysis took almost an hour using a Pentium-4 computer having 1 GHz RAM. It would probably take longer time on another computer depending on the memory and processor units. Although the processing time seems quite long, it is comparable to other GIS based damage estimation programs that perform analysis on the basis of buildings rather than grids. Using grids decreases the processing time but causes loss of accuracy.

In the subsequent sections 5.2.1, 5.2.2 and 5.2.3, the analyses are explained under three subtitles: *Input data*, *Analysis* and *Results*. Each part was made as concise as possible to prevent any confusions or misinterpretations. The input parameters used in the analysis were described in input data part. Analysis part gives details of damage estimation methodology and the last part presents the results. An overall comparison for these analyses and the other studies is provided in section 5.3.

5.2.1 JICA-Check

Input data: Required input parameters for the assessment are building inventory data, scenario earthquake fault data, attenuation relationship data, capacity curve data and analysis method data.

Building inventory data set (JICA database) was composed of 724,561 buildings lumped at the centers of 0.005° by 0.005° grids. This data set was obtained from the JICA Study [11] and converted into a new format in order to make it ready for use in SRAS. The original data set (JICA database) contained the number of buildings and their corresponding ratios defined for each building type, building height and the construction year. Unfortunately, no additional information was available to show a relationship between the ratios provided for different characteristics. It was almost impossible to calculate the number of buildings for a specified building type, height and construction year. Due to these limitations it was assumed that the percentage of each building type for a district is also valid for the distribution within each building height interval. This assumption has eliminated the difficulty in relating building type to building height. The construction year could not be used due to lack of reliable data. Converted building inventory data were overlaid on ground classification map of JICA Study [11] and associated NEHRP site classes were obtained for each building group lumped at the centers of grids. Building inventory summary based on building type is shown in Table 5.3.

Table 5.3 Building type statistics for JICA-Check

Building Type	Number of Buildings	Percentage (%)
RC	545,697	75.31
WOOD	10,944	1.51
MASONRY	165,249	22.81
RC Shear Wall	761	0.11
PREFABRIC	873	0.12
STEEL	1,037	0.14
<i>Total</i>	724,561	100.00

Scenario earthquake fault model A, proposed in the JICA Study [11], was employed for the analysis. This model was the most probable model and the assigned moment magnitude was 7.5. Attenuation relationship of Boore et al. [12] was utilized since it was also selected to be used in the JICA Study [11].

Capacity curves for reinforced concrete frame structures were obtained from Yakut et al. [29]. These curves were scaled with the relativity coefficients to generate capacity curves for other building types. These coefficients are obtained from the ratio of capacity curve values (proposed in HAZUS) for reinforced concrete structures to the values for other building types. Thus, capacity curves for each building type were produced and they are peculiar to the practice in Turkey. Capacity spectrum method of ATC-40 [8] was selected for the computation of demand displacements.

Analysis: Using the input data mentioned above, the analysis was carried out to estimate damage level of each building. The SDL method was used in damage estimation. Three damage levels were introduced as “Lightly damaged”, “Moderately damaged” and “Heavily damaged”. Another damage level, labeled as “Collapse/No Intersection”, was created automatically by SRAS for those buildings having no intersection between their capacity and demand curves. They were added to the “Heavily damaged” building class. The damage level limits used in the study are given in Table 5.4.

Table 5.4 Damage level limits defined for JICA-Check

Damage Level	Criterion
Light	$S_d \leq S_{dy}$
Moderate	$S_{dy} < S_d \leq \frac{(S_{dy} + S_{dmax})}{2}$
Heavy / Collapsed	$\frac{(S_{dy} + S_{dmax})}{2} < S_d$

Results: The results including all data files and ArcView 8.3 map files are available in the attached disk inside the folder named as “JICA-Check”. Since it is impractical to generate maps for all results, only representative ones were selected to be mapped. Figure 5.1 demonstrates ground classification map used by JICA Study [11]. Figures 5.2, 5.3 and 5.4 show the regional distribution patterns of PGA, S_a at $T = 0.3$ s and $T = 1.0$ sec, respectively. Maps for the distribution of lightly, moderately and heavily damaged buildings are given in Figures C.2, C.3 and 5.5, respectively.

The results were also tabulated for a comparison between the three analyses and previous studies. Table 5.7 presents the damage estimation results for Istanbul obtained by SRAS using Boore et al. [12] attenuation relationship.

5.2.2 JICA-New

Input data: Required input parameters for the assessment are building inventory data, scenario earthquake fault data, attenuation relationship data, capacity curve data and analysis method data. Scenario earthquake fault model, attenuation relationship, capacity curves and analysis method were selected the same as the ones used in the JICA-Check.

Building inventory data set (IMM database) was composed of 1,409,487 buildings having their spatial coordinates. This data set was obtained from the IMM and projected into a new coordinate system in order to obtain the coordinates in latitudes and longitudes. Then by using ArcView 8.3, these buildings were overlaid on ground classification map of JICA Study [11] and associated NEHRP site classes were obtained for the ones falling in the study area of JICA. The buildings lacking ground class information were removed from the database. Based on building type and number of stories, a second elimination was performed to delete buildings missing that information. Finally, 1,195,711 buildings were made ready for the use in SRAS. Unfortunately, no additional information was

available regarding to the construction years and apparent conditions of the buildings. Building inventory summary based on building type is shown in Table 5.5.

Table 5.5 Building type statistics for JICA-New

Building Type	Number of Buildings	Percentage (%)
RC	1,038,641	86.86
MASONRY	144,214	12.06
STEEL	904	0.08
WOOD	6,486	0.54
TUNNEL	2	0.00
OTHERS	5,461	0.46
PREFABRIC	3	0.00
<i>Total</i>	1,195,711	100.00

Analysis: Using the input data mentioned above, the analysis was carried out to estimate damage level of each building. The SDL method was used in damage estimation. The damage levels and limits that were introduced in the JICA-Check part were also utilized while performing analysis for this part.

Results: The results including all data files and ArcView 8.3 map files are available in the attached disk inside the folder named as “JICA-New”. Only representative results were selected to be mapped. Since ground classification map of JICA Study [11] was used, distribution of PGA and spectral acceleration values will be the same with those maps (Figures 5.1, 5.2, 5.3 and 5.4) presented for JICA-Check part. The maps for the distribution of lightly, moderately and heavily damaged buildings are given in Figures C.4, C.5 and 5.6, respectively.

The results were also tabulated for a comparison between the three analyses and previous studies. Table 5.8 presents the damage estimation results for Istanbul obtained by SRAS using Boore et al. [12] attenuation relationship.

5.2.3 IMM-New

Input data: Required input parameters for the assessment are building inventory data, scenario earthquake fault data, attenuation relationship data, capacity curve data and analysis method data.

Similar to the case JICA-New IMM database was used. By using ArcView 8.3, these buildings were overlaid on ground classification map proposed in this study and associated NEHRP site classes were obtained for the ones falling in the ground classification map area. The buildings lacking ground class information were removed from the database. Based on building type and number of stories, a second elimination was performed to delete buildings missing that information. Finally, 1,313,327 buildings were made ready for the use in SRAS. Unfortunately, no additional information was available regarding to construction years and apparent conditions of the buildings. Building inventory summary based on building type is shown in Table 5.6. Scenario earthquake fault model, attenuation relationship, capacity curves and analysis method were selected as the ones used in the JICA-Check.

Table 5.6 Building type statistics for IMM-New

Building Type	Number of Buildings	Percentage (%)
RC	1,140,695	86.86
MASONRY	159,523	12.15
STEEL	907	0.07
WOOD	6,728	0.51
TUNNEL	2	0.00
OTHERS	5,469	0.42
PREFABRIC	3	0.00
<i>Total</i>	1,313,327	100.00

Analysis: Using the input data mentioned above, the analysis was carried out to estimate damage level of each building. The SDL method was used in damage estimation. The damage levels and limits that were introduced in the JICA-Check part were also utilized for this part.

Results: The results including all data files and ArcView 8.3 map files are available in the attached disk inside the folder named as “IMM-New”. Figure C.6 demonstrates ground classification map proposed by this study. Figures C.7, C.8 and C.9 show the regional distribution patterns of PGA, S_a at $T = 0.3$ s and $T = 1.0$ s, respectively. Maps for the distribution of lightly, moderately and heavily damaged buildings are given in Figures C.10, C.11 and 5.7, respectively. An additional map showing all damage levels at once was also provided as Figure C.12.

The results were tabulated for a comparison between the three analyses and previous studies. Table 5.9 presents the damage estimation results for Istanbul obtained by SRAS using Boore et al. [12] attenuation relationship.

5.3 DISCUSSION OF RESULTS

Damage estimates obtained for Istanbul using different building inventories and ground classification maps prove once again that reliability of regional damage estimation strongly depends on the quality and accuracy of the data at hand. Discrepancies between the results of three analyses and JICA Study [11] were expected since all of them have special deficiencies in different steps of the process. For instance, JICA Study [11] uses capacity curves that do not reflect the real practice in Turkey. JICA-Check database is not so dependable since it inherits considerable assumptions. JICA-New employs ground classification map proposed by JICA. IMM-New utilizes a new but rough ground classification map that is generated from surface geology maps of Istanbul. So, it should be better to discuss the effects of each parameter; building inventory, ground classification map and capacity curve, separately.

Two databases: JICA and IMM differ significantly in the number of buildings that they contain. The number of buildings in the IMM database almost doubles the number of buildings in the JICA database. The IMM database seems more reliable than JICA database considering the information about number of stories, but it may be misleading for building type information. On the other hand JICA database is a secret box that shields what is inside. In view of these, building inventory effect can not be investigated in a detailed manner with the available databases. Assumptions made in JICA-Check part while trying to extract building inventory data gave rise to unrealistic results. As can be easily observed from Tables 5.7, JICA-Check predicted no heavily damaged buildings for the districts: Besiktas, Beykoz, Gaziosmanpasa, Kagithane, Sariyer, Sisli, Tuzla and Uskudar. This mainly results from high percentage of low-rise buildings for those districts. Although it is not common to have high-rise masonry or wood buildings, JICA-Check database contains many of those unrealistic buildings coming from conversion of the ratios to number of buildings depending on the percentage of building type. So, the districts having high percentages of high and mid-rise buildings had high percentages of heavily damaged buildings since most of them came out to be masonry. But JICA-Check

was just a preliminary study in order to find and debug errors in SRAS prior to the IMM-New part.

Ground classification map affects the results significantly. The maps of JICA and this study basically differ for the European side of Istanbul. There are minor differences for the Anatolian side. Besides this, there are some districts such as Zeytinburnu where two maps hold opposing views. JICA map proposes NEHRP site class “D” for Zeytinburnu whereas NEHRP site class “B” was proposed by the new map. Districts should be divided into two in order to figure out the effects of site class variation. First group districts are those that are fully or partially assigned to stiffer ground classes in the new map. These districts are Avcilar, Bagecilar, Bahcelievler, Bakirkoy, Bayrampasa, Besiktas, Beyoglu, Eminonu, Esenler, Eyup, Fatih, Gungoren, Kagithane, Kucukcekmece and Zeytinburnu. For these districts, the IMM-New results for heavily damaged building ratios are lower than the ones calculated in JICA-New. Second group districts are those that are fully or partially assigned to softer ground classes in the new map. These districts are Adalar, Beykoz, Gaziosmanpasa, Kadikoy, Kartal, Maltepe, Pendik, Sariyer, Sisli, Tuzla, Umraniye and Uskudar. For these districts, the IMM-New results for heavily damaged building ratios are higher than the ones calculated in JICA-New. Therefore, site effects verify their importance in damage estimation process.

Capacity curves were the most critical part of the analysis. A sample group of capacity curves for reinforced concrete frame structures used by JICA and this study is presented in Figure C.1. As can be directly observed from Figure C.1, the capacity curves used in this study have lower capacity but higher ductility as compared to the ones used by JICA. This is responsible for the high percentages of moderately and heavily damaged buildings. Because when yield capacity is low and ductility is high, demand spectrum generally intersects with the capacity spectrum between the yield and ultimate capacity points.

In summary, the results obtained from the analyses and the JICA results do require further detailed investigation in order to discover the shielded factors affecting results. Although there are some discrepancies, the results of IMM-New and JICA seem to be quite compatible. Supplementary analyses may be carried out easily by using SRAS and utilizing updated ground classification maps, capacity curves, attenuation relationships and building inventory data. Since these analyses have been performed as a case study, broad examination of results is out of the scope of this study. All building input files for SRAS, maps and ArcView 8.3 files are provided in the attached disk.

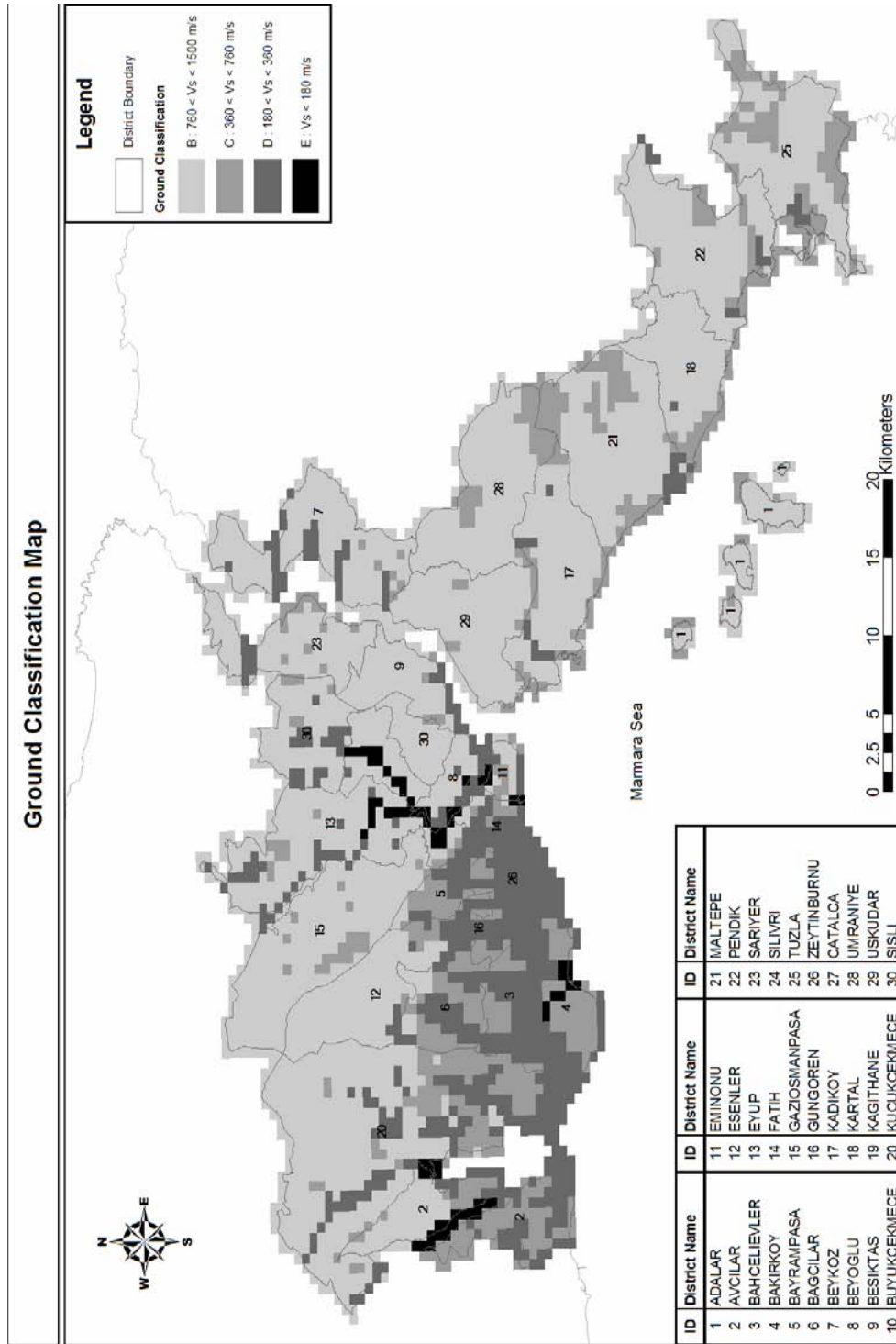


Figure 5.1 Ground classification map proposed by JICA Study [11]

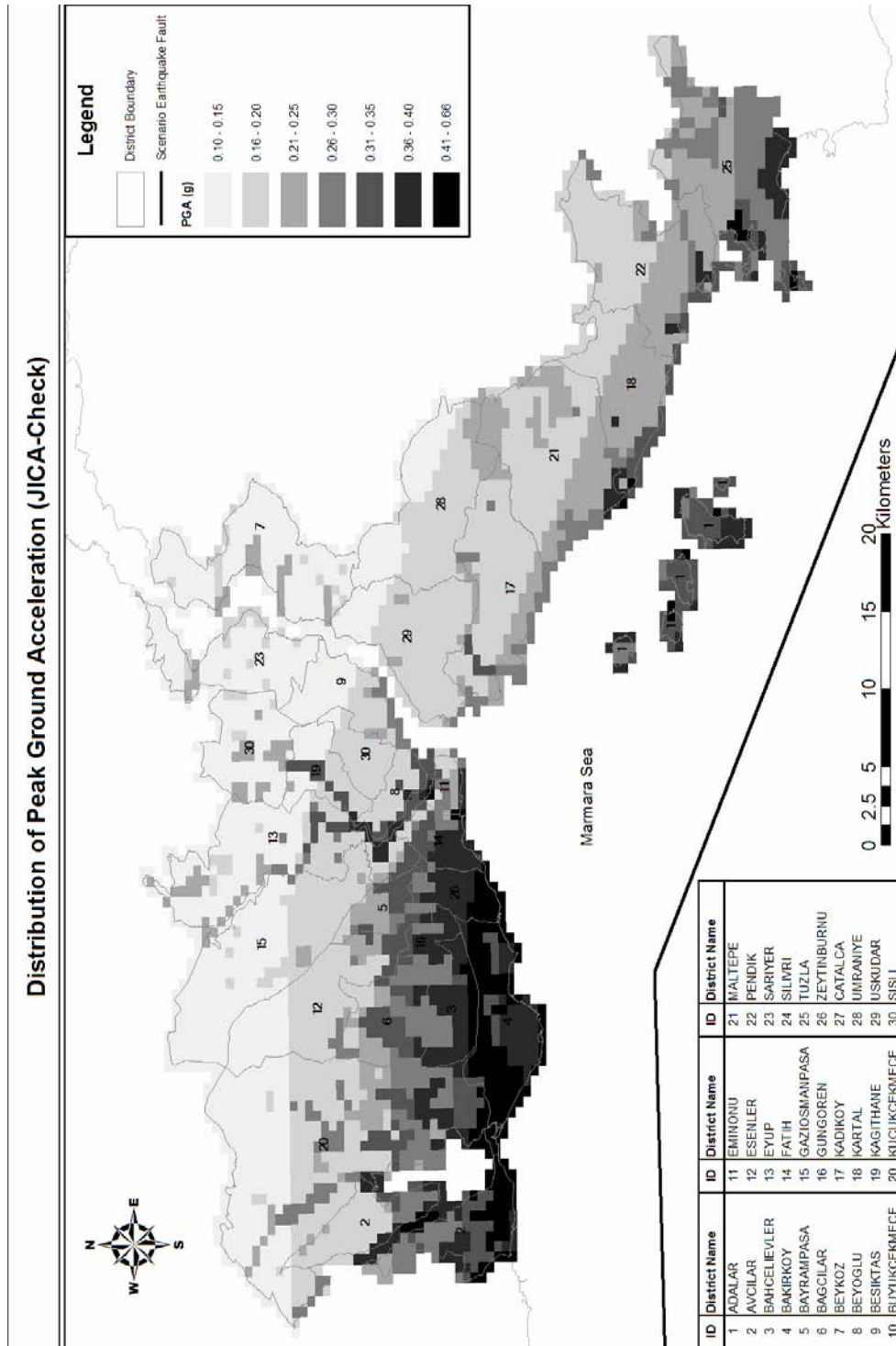


Figure 5.2 Distribution of peak ground acceleration (JICA-Check)

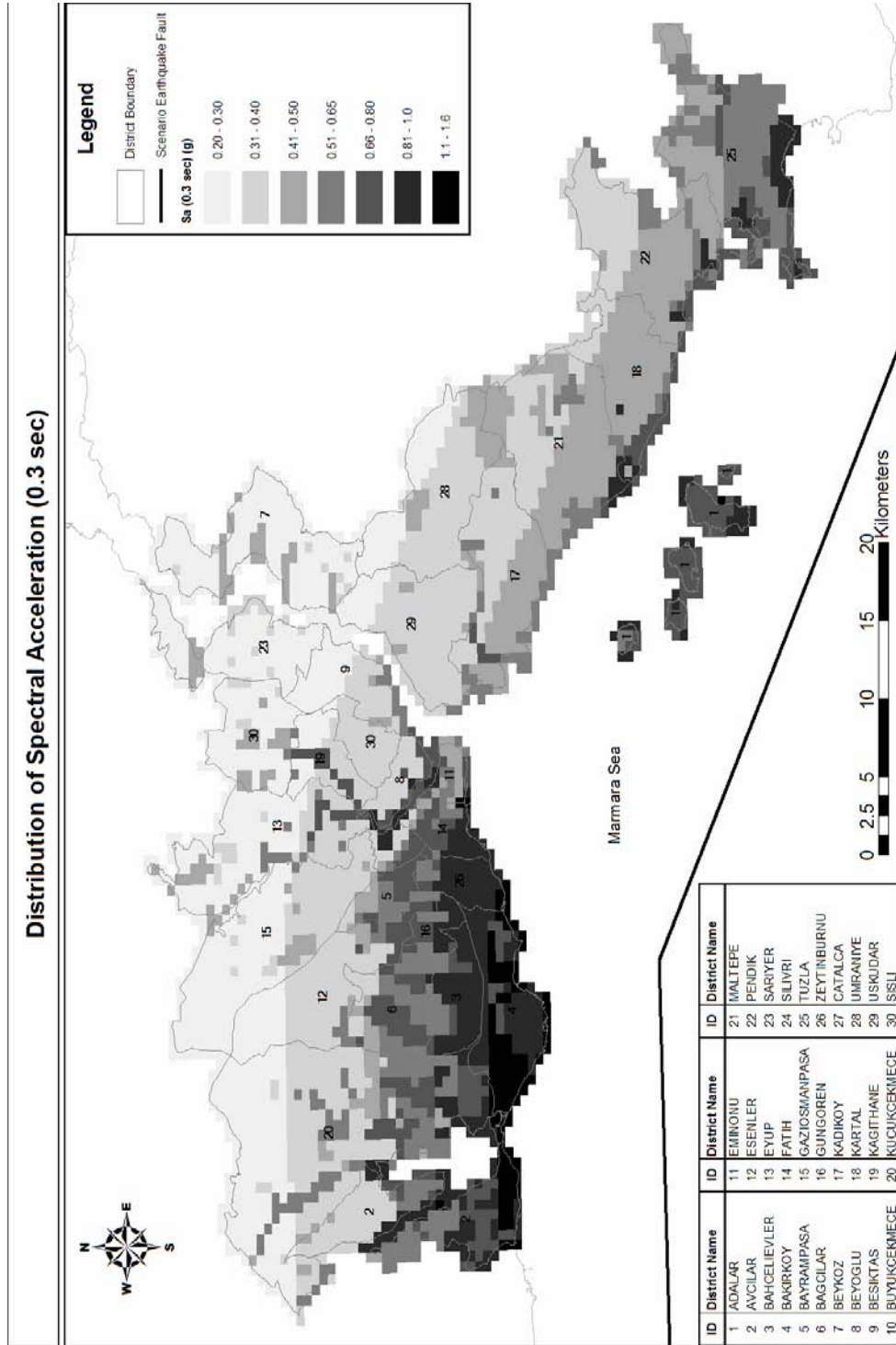


Figure 5.3 Distribution of S_a values at the period of 0.3 sec (JICA-Check)

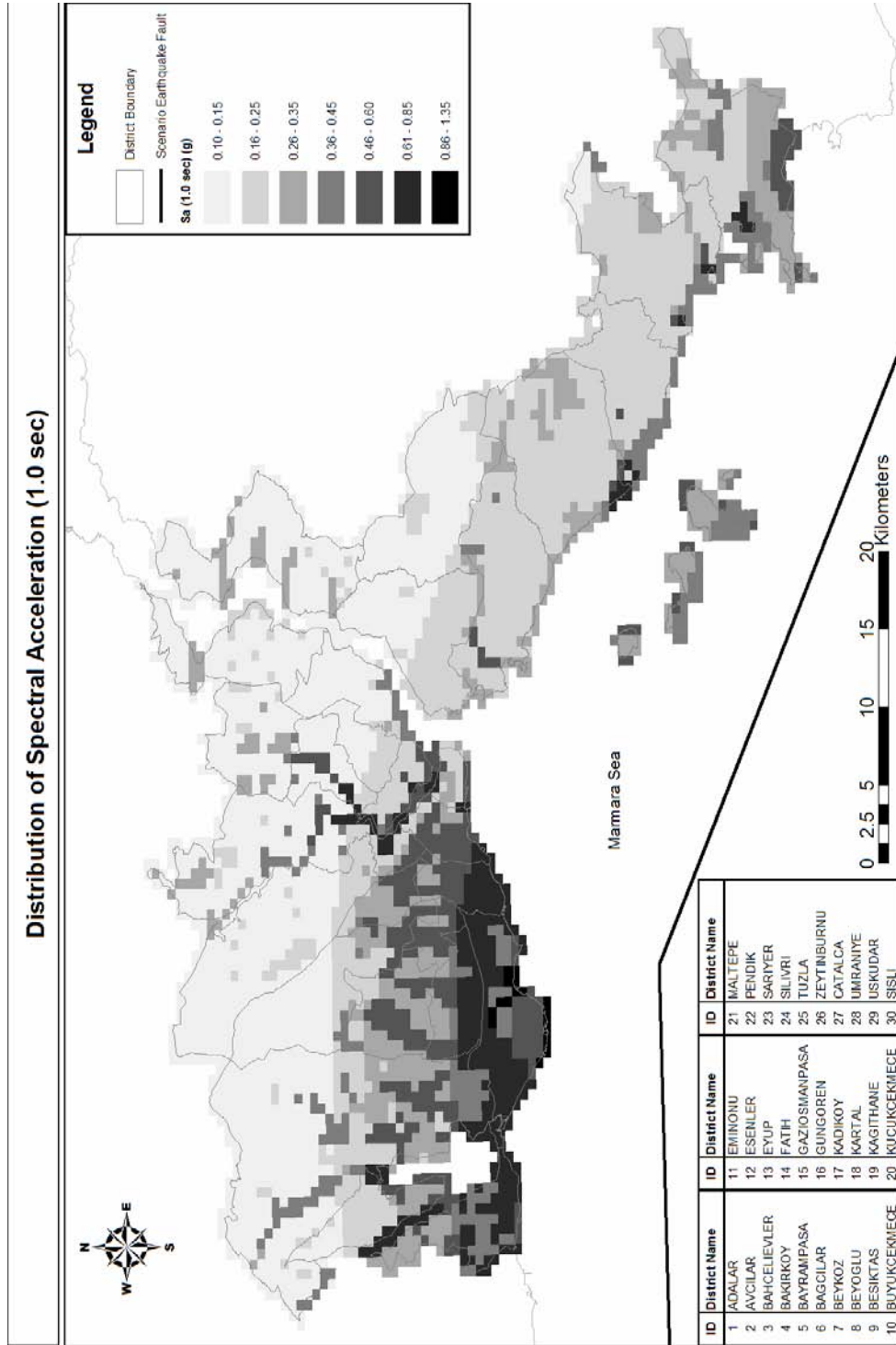


Figure 5.4 Distribution of S_a values at the period of 1.0 sec (JICA-Check)

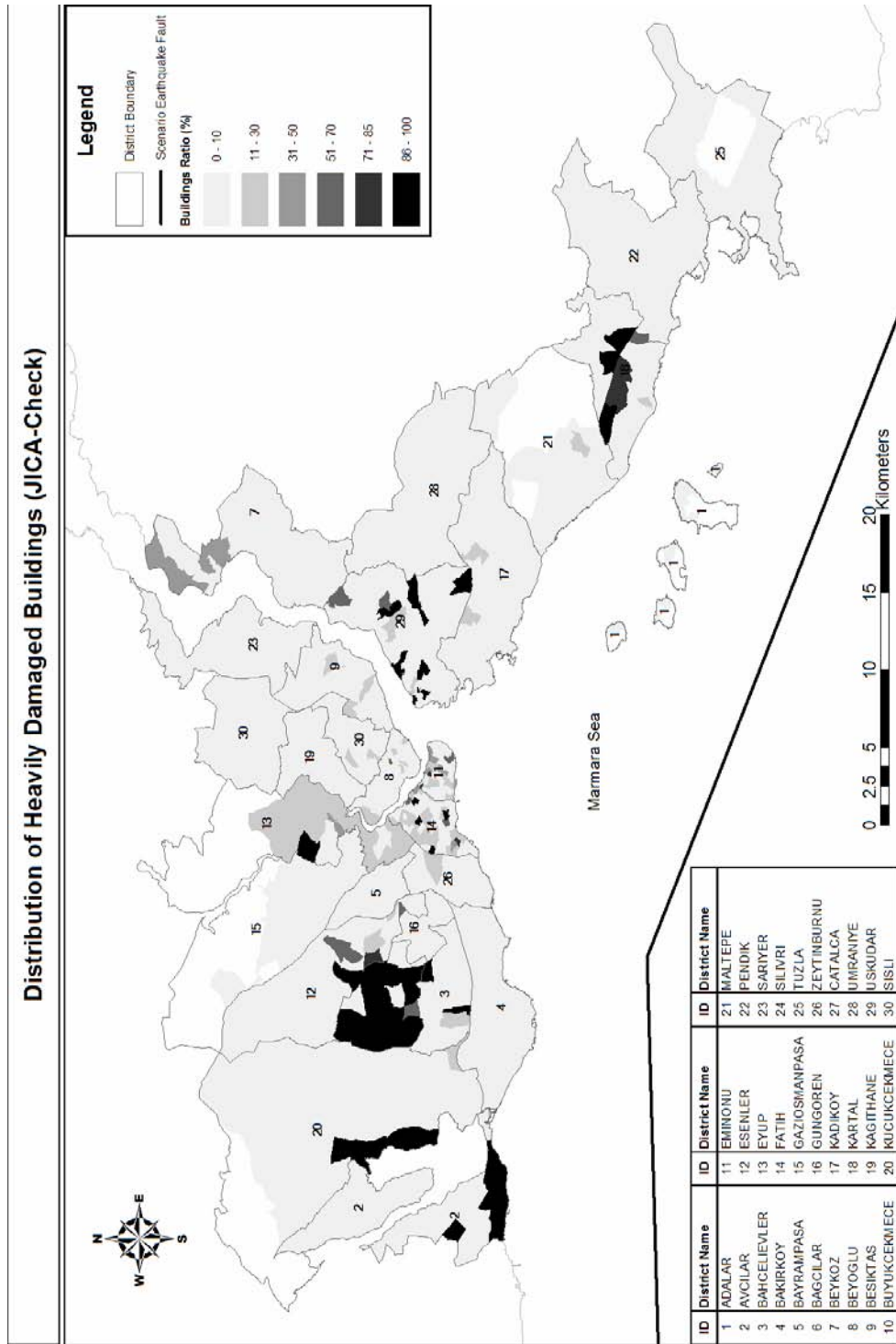


Figure 5.5 Distribution of heavily damaged buildings ratio (JICA-Check)

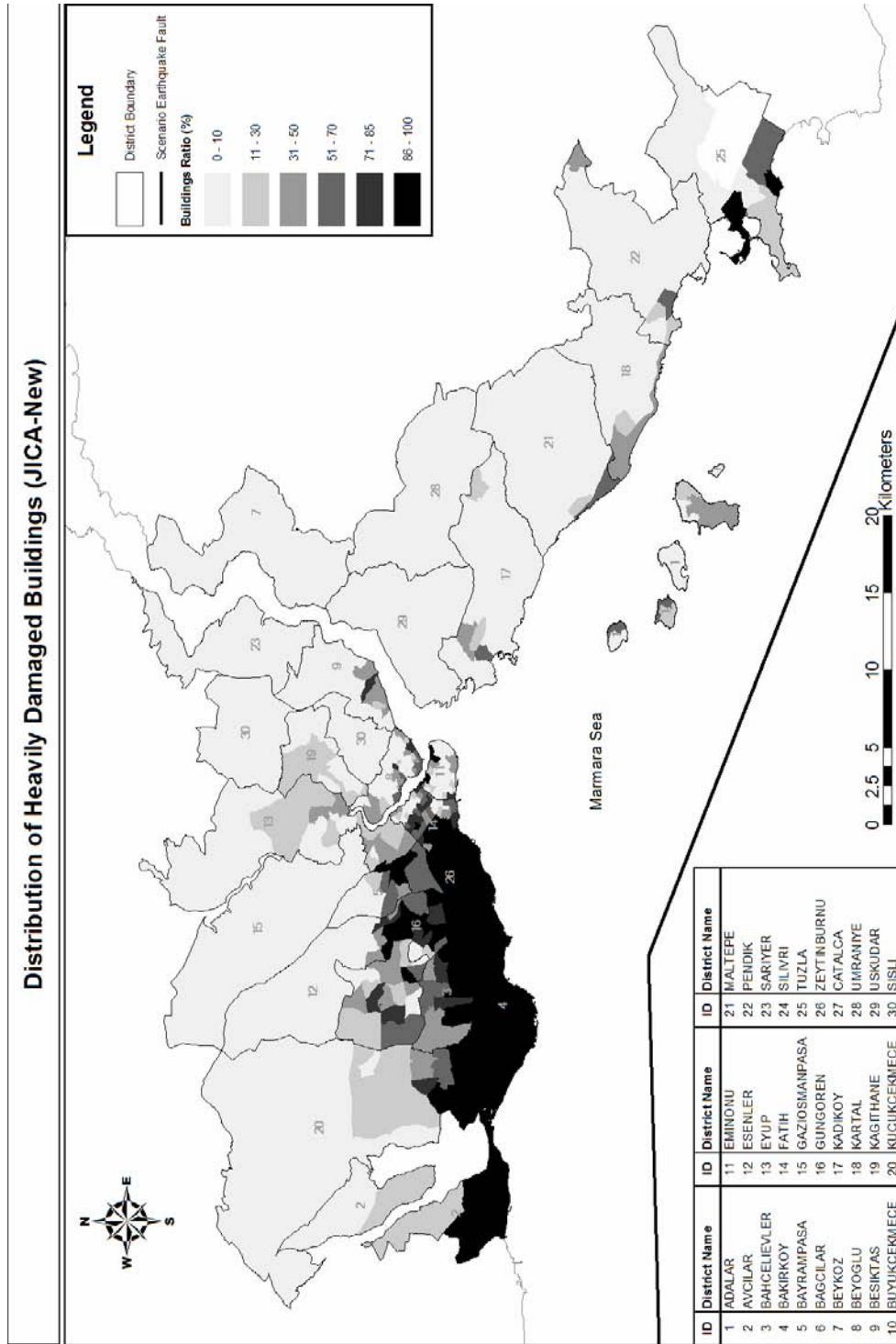


Figure 5.6 Distribution of heavily damaged buildings ratio (JICA-New)

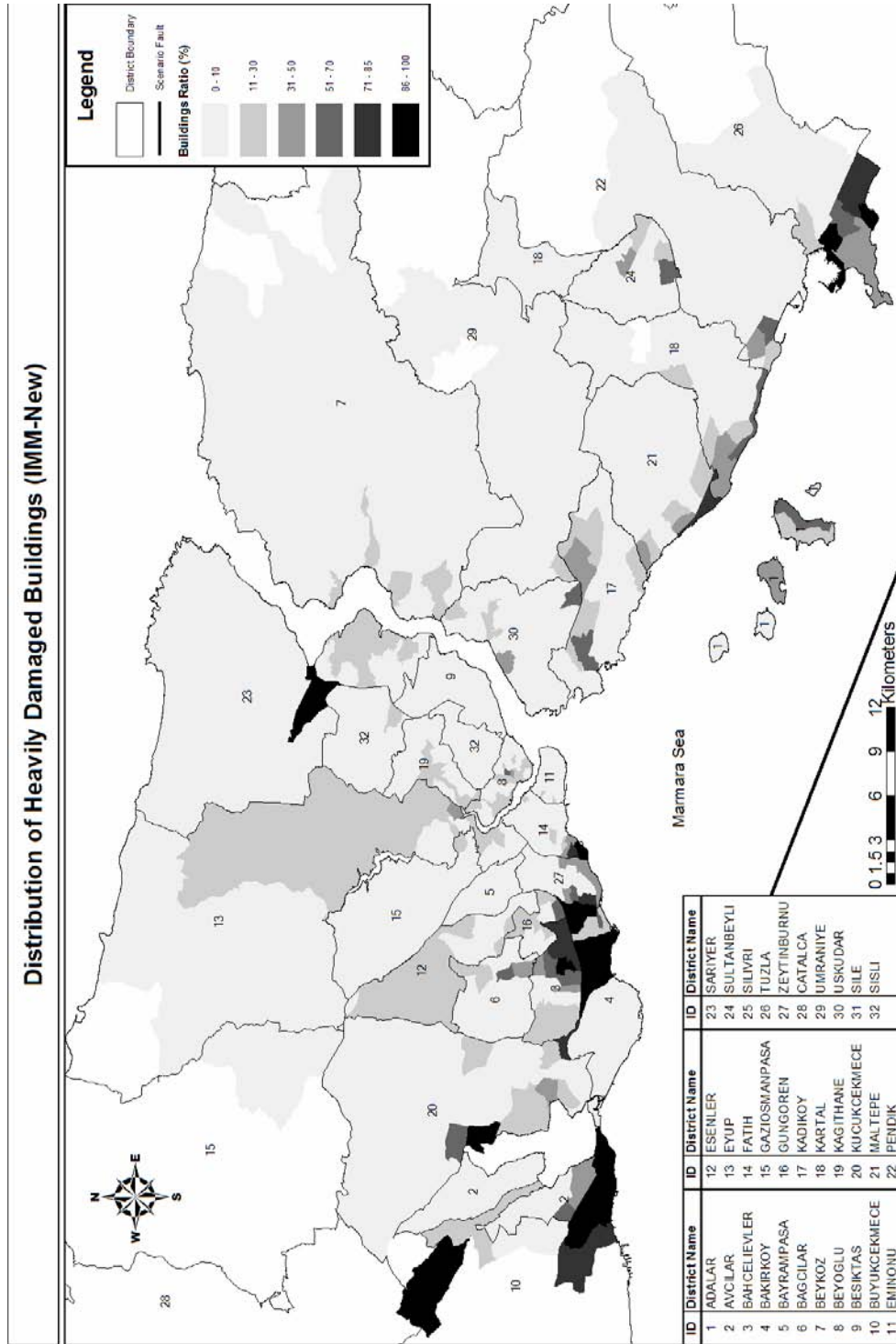


Figure 5.7 Distribution of heavily damaged buildings ratio (IMM-New)

Table 5.7 Summary of results obtained for JICA-Check

District Name	Total Building Number	Lightly Damaged		Moderately Damaged		Heavily Damaged	
		Number	(%)	Number	(%)	Number	(%)
ADALAR	6522	0	0.00	6039	92.59	483	7.41
AVCILAR	14033	160	1.14	6889	49.09	6984	49.77
BAGCILAR	36055	31	0.09	35153	97.50	871	2.42
BAHCELIEVLER	19687	1	0.01	4629	23.51	15057	76.48
BAKIRKOY	10068	0	0.00	2289	22.74	7779	77.26
BAYRAMPASA	20194	22	0.11	18559	91.90	1613	7.99
BESIKTAS	14398	2535	17.61	11863	82.39	0	0.00
BEYKOZ	28282	15019	53.10	13263	46.90	0	0.00
BEYOGLU	26463	2707	10.23	22648	85.58	1108	4.19
BUYUKCEKMECE	3348	2	0.06	3250	97.07	96	2.87
CATALCA	2573	515	20.02	1955	75.98	103	4.00
EMINONU	14145	594	4.20	11976	84.67	1575	11.13
ESENLER	22697	317	1.40	21719	95.69	661	2.91
EYUP	25715	4822	18.75	17791	69.19	3102	12.06
FATIH	31940	556	1.74	25077	78.51	6307	19.75
GAZIOSMANPASA	56485	11023	19.51	45462	80.49	0	0.00
GUNGOREN	10654	2	0.02	8096	75.99	2556	23.99
KADIKOY	38599	1877	4.86	36363	94.21	359	0.93
KAGITHANE	28737	4728	16.45	24009	83.55	0	0.00
KARTAL	24285	407	1.68	23735	97.74	143	0.59
KUCUKCEKMECE	45813	1610	3.51	35385	77.24	8818	19.25
MALTEPE	25312	111	0.44	24959	98.61	242	0.96
PENDIK	39874	1063	2.67	38565	96.72	246	0.62
SARIYER	30779	13685	44.46	17094	55.54	0	0.00
SILIVRI	8531	664	7.78	7754	90.89	113	1.32
SISLI	22570	3097	13.72	19473	86.28	0	0.00
TUZLA	14731	22	0.15	14231	96.61	478	3.24
UMRANIYE	43473	8323	19.15	35150	80.85	0	0.00
USKUDAR	43022	4983	11.58	38039	88.42	0	0.00
ZEYTINBURNU	15576	0	0.00	2788	17.90	12788	82.10
<i>Total</i>	724561	78876	10.89	574203	79.25	71482	9.86

Table 5.8 Summary of results obtained for JICA-New

District Name	Total Building Number	Lightly Damaged		Moderately Damaged		Heavily Damaged	
		Number	(%)	Number	(%)	Number	(%)
ADALAR	7534	0	0.00	6015	79.84	1519	20.16
AVCILAR	30795	0	0.00	8740	28.38	22055	71.62
BAGCILAR	64259	3	0.00	41466	64.53	22790	35.47
BAHCELIEVLER	38468	0	0.00	7153	18.59	31315	81.41
BAKIRKOY	17719	0	0.00	255	1.44	17464	98.56
BAYRAMPASA	37550	1	0.00	23366	62.23	14183	37.77
BESIKTAS	19282	5	0.03	16906	87.68	2371	12.30
BEYKOZ	37349	7010	18.77	30316	81.17	23	0.06
BEYOGLU	41342	348	0.84	34219	82.77	6775	16.39
EMINONU	24256	189	0.78	19948	82.24	4119	16.98
ESENLER	46520	454	0.98	26493	56.95	19573	42.07
EYUP	41180	498	1.21	34168	82.97	6514	15.82
FATIH	51188	208	0.41	17620	34.42	33360	65.17
GAZIOSMANPASA	95654	4365	4.56	91098	95.24	191	0.20
GUNGOREN	21722	0	0.00	6734	31.00	14988	69.00
KADIKOY	67595	265	0.39	63750	94.31	3580	5.30
KAGITHANE	52232	2091	4.00	47389	90.73	2752	5.27
KARTAL	43622	43	0.10	40881	93.72	2698	6.18
KUCUKCEKMECE	95174	512	0.54	58168	61.12	36494	38.34
MALTEPE	42596	28	0.07	41357	97.09	1211	2.84
PENDIK	55879	82	0.15	54056	96.74	1741	3.12
SARIYER	38009	4713	12.40	33284	87.57	12	0.03
SISLI	40371	856	2.12	39453	97.73	62	0.15
TUZLA	14825	3	0.02	11266	75.99	3556	23.99
UMRANIYE	76516	8549	11.17	67827	88.64	140	0.18
USKUDAR	63644	2850	4.48	60789	95.51	5	0.01
ZEYTINBURNU	30430	0	0.00	1087	3.57	29343	96.43
<i>Total</i>	1195711	33073	2.77	883804	73.91	278834	23.32

Table 5.9 Summary of results obtained for IMM-New

District Name	Total Building Number	Lightly Damaged		Moderately Damaged		Heavily Damaged	
		Number	(%)	Number	(%)	Number	(%)
ADALAR	7534	0	0.00	5218	69.26	2316	30.74
AVCILAR	30757	0	0.00	12720	41.36	18037	58.64
BAGCILAR	64017	22	0.03	58398	91.22	5597	8.74
BAHCELIEVLER	38596	0	0.00	23769	61.58	14827	38.42
BAKIRKOY	17647	0	0.00	10305	58.40	7342	41.60
BAYRAMPASA	37518	1	0.00	37293	99.40	224	0.60
BESIKTAS	19195	0	0.00	19187	99.96	8	0.04
BEYKOZ	43263	8886	20.54	31452	72.70	2925	6.76
BEYOGLU	41262	0	0.00	37535	90.97	3727	9.03
BUYUKCEKMECE	7513	1	0.01	6708	89.29	804	10.70
EMINONU	24256	0	0.00	23751	97.92	505	2.08
ESENLER	46492	1	0.00	44700	96.15	1791	3.85
EYUP	43526	115	0.26	39023	89.65	4388	10.08
FATIH	51200	93	0.18	47998	93.75	3109	6.07
GAZIOSMANPASA	93580	67	0.07	91932	98.24	1581	1.69
GUNGOREN	21742	2	0.01	18712	86.06	3028	13.93
KADIKOY	67656	97	0.14	59069	87.31	8490	12.55
KAGITHANE	52382	26	0.05	49759	94.99	2597	4.96
KARTAL	57580	1002	1.74	52401	91.01	4177	7.25
KUCUKCEKMECE	95253	223	0.23	85196	89.44	9834	10.32
MALTEPE	42845	31	0.07	38606	90.11	4208	9.82
PENDIK	63021	120	0.19	59557	94.50	3344	5.31
SARIYER	49454	4770	9.65	39561	80.00	5123	10.36
SISLI	40440	97	0.24	39862	98.57	481	1.19
SULTANBEYLI	40807	420	1.03	36645	89.80	3742	9.17
TUZLA	15351	3	0.02	9816	63.94	5532	36.04
UMRANIYE	106196	12459	11.73	92590	87.19	1147	1.08
USKUDAR	63693	2490	3.91	58296	91.53	2907	4.56
ZEYTINBURNU	30551	5	0.02	25292	82.79	5254	17.20
<i>Total</i>	1313327	30931	2.36	1155351	87.97	127045	9.67

Table 5.10 Summary of results obtained by JICA Study [11]

District Name	Total Building Number	Partly Damaged		Moderately Damaged		Heavily Damaged	
		Number	(%)	Number	(%)	Number	(%)
ADALAR	6522	1428	21.90	1089	16.70	1614	24.75
AVCILAR	14030	3609	25.72	2197	15.66	1975	14.08
BAGCILAR	36059	8438	23.40	3531	9.79	2384	6.61
BAHCELIEVLER	19690	5539	28.13	3171	16.10	2577	13.09
BAKIRKOY	10067	2748	27.30	1847	18.35	1839	18.27
BAYRAMPASA	20195	4559	22.57	2436	12.06	2493	12.34
BESIKTAS	14399	2334	16.21	826	5.74	584	4.06
BEYKOZ	28280	2957	10.46	792	2.80	476	1.68
BEYOGLU	26468	5257	19.86	2605	9.84	2335	8.82
BUYUKCEKMECE	3348	880	26.28	449	13.41	351	10.48
CATALCA	2573	353	13.72	109	4.24	67	2.60
EMINONU	14149	3104	21.94	1831	12.94	1967	13.90
ESENLER	22700	4904	21.60	1957	8.62	1355	5.97
EYUP	25718	4857	18.89	2232	8.68	1890	7.35
FATIH	31947	7781	24.36	4797	15.02	5111	16.00
GAZIOSMANPASA	56484	9181	16.25	3044	5.39	1888	3.34
GUNGOREN	10655	2967	27.85	1593	14.95	1253	11.76
KADIKOY	38615	7451	19.30	2811	7.28	1944	5.03
KAGITHANE	28737	4620	16.08	1640	5.71	1107	3.85
KARTAL	24295	5114	21.05	2365	9.73	1986	8.17
KUCUKCEKMECE	45817	10074	21.99	4920	10.74	4299	9.38
MALTEPE	25313	5070	20.03	2109	8.33	1600	6.32
PENDIK	39877	7978	20.01	3530	8.85	2835	7.11
SARIYER	30781	2965	9.63	707	2.30	410	1.33
SILIVRI	8534	1457	17.07	526	6.16	359	4.21
SISLI	22576	3512	15.56	1147	5.08	727	3.22
TUZLA	14727	3180	21.59	1513	10.27	1331	9.04
UMRANIYE	43473	5932	13.65	1725	3.97	1005	2.31
USKUDAR	43021	6357	14.78	1885	4.38	1093	2.54
ZEYTINBURNU	15573	4229	27.16	2704	17.36	2592	16.64
<i>Total</i>	724623	138835	19.16	62008	8.56	51447	7.10

CHAPTER 6

CONCLUSIONS AND RECOMMENDATIONS

6.1 SUMMARY

In this study, it is aimed to develop seismic damage estimation software, which is capable of handling buildings individually. The software developed, named as “Seismic Risk Analysis Software” (SRAS), uses the deterministic approach to predict the probable damage distribution for a specified region caused by a deterministic earthquake. SRAS is able to perform analysis using four attenuation relationships and three displacement demand computation methods. The software has been verified by using it for the estimation of damage distribution in Adapazarı due to August 17, 1999 Izmit Earthquake. By means of spot checks of intermediate steps, the modules of SRAS have been debugged. Then, considering unprecedented increase in the occurrence probability of a large magnitude earthquake in the proximity of Istanbul within 30 years, SRAS has been utilized for the estimation of probable damage distribution in Istanbul due to a scenario earthquake (model A of JICA Study [11]) of moment magnitude 7.5.

6.2 CONCLUSIONS

Considering the analysis performed and keeping in mind that SRAS is a computer program and it is the user responsibility to verify the reliability of the results produced by SRAS, the following conclusions can be derived:

- Reliability of regional seismic damage estimation strongly depends on the quality and accuracy of the data at hand. Dependable building inventory database is a must to obtain realistic damage distribution for the region under consideration.

Site classification maps affect the results considerably and need to be developed with special care. Capacity curve data are also crucial in performing the analysis and capacity curves specific to each building should be used when available.

- SRAS has proved to be a reliable tool for performing lengthy calculations of conventional regional assessment procedures. Provided that the input data are dependable, SRAS produces same results (even more accurate in the case of iterative methods) that should be obtained if hand calculation were preferred.
- SRAS has been developed to facilitate the usage of four attenuation relationships (Abrahamson and Silva [20], Boore et al. [12], Gülkan and Kalkan [21] and Sadigh et al. [16]) and three displacement demand computation procedures (Capacity Spectrum Method (ATC-40 [8]), Displacement Coefficient Method (FEMA-356 [19]) and Constant Ductility Method (Chopra and Goel [22])).
- Application of conventional regional damage estimation procedures to different districts for several scenario earthquakes is faster and simpler by using SRAS. Thus, researchers will have the opportunity of considering the effects of several parameters such as attenuation relationship, analysis method, etc. to the regional damage distribution pattern.
- SRAS has been developed as flexible as possible to make it handy not only for districts in Turkey but also for different regions of the world. The user defines capacity curve data peculiar to that region and a scenario earthquake fault. Then, SRAS takes care of the numerous computations and time consuming database operations.
- It should be noted that SRAS has been debugged by employing it just for two case studies. The reliability and serviceability of the software can be further improved if and only if SRAS is utilized by several users in different projects and feedback is conveyed to the developer. This is the common way of debugging and upgrading commercial software. Otherwise, SRAS will stay between the hard covers of this thesis waiting for the day to be discovered.

6.3 RECOMMENDATIONS FOR FUTURE STUDY

- Probabilistic seismic hazard component may be added to facilitate the usage of both seismic hazard assessment approaches under the same software structure. This requires preparation of earthquake catalog data and source zones.

- Communication with commercial GIS applications such as ArcGIS and MapInfo should be established for using powerful database operations provided by those programs. Thus, preparation of database queries could be faster and easier.
- Computation of casualties and monetary losses due to the scenario earthquake may also be integrated to the source code. As a consequence, an overall risk assessment studio tool could be developed and used effectively.
- Capabilities of the software should be improved by appending more attenuation relationships. Distance calculation algorithms may be revised for a better performance. Default databases for capacity curves, damage curves, scenario earthquake faults (including the past earthquakes) should be developed and installed with SRAS.
- The software should be upgraded and new versions should be distributed in order to track the most recent developments in seismic damage estimation area. Just as a reminder, although many improvements had been done, SRAS will remain as a computer program lacking of artificial intelligence. It is the user who leads SRAS.

REFERENCES

- [1] ATC-13, 1985, *Earthquake Damage Evaluation Data for California*, Applied Technology Council, Redwood City, California.

- [2] Whitman Robert V., Anagnos Thalia, Kircher Charles A., Lagorio Henry J., Lawson R. Scott, Schneider Philip, 1997, *Development of a National Earthquake Loss Estimation Methodology*, Earthquake Spectra, Vol. 13, No. 4, pp. 643-661, Oakland, CA: Earthquake Engineering Research Institute.

- [3] Kircher Charles A., Reitherman Robert K., Whitman Robert V. and Arnold Christopher, 1997, *Estimation of Earthquake Losses to Buildings*, Earthquake Spectra, Vol. 13, No. 4, pp. 703-720, Oakland, CA: Earthquake Engineering Research Institute.

- [4] Federal Emergency Management Agency (FEMA), 1992, *NEHRP Handbook for the Seismic Evaluation of Existing Buildings*, FEMA 178, Washington, D.C.

- [5] Frankel A., Mueller C., Barnhard T., Perkins D., Leyendecker E. V., Dickman N., Hanson S., and Hopper M., 1996, *National Seismic-Hazard Maps: Documentation June 1996*, USGS Open-File Report 96-532, Denver, CO, United States Geological Survey.

- [6] Building Seismic Safety Council (BSSC), 1997, *NEHRP Handbook for Seismic Rehabilitation of Existing Buildings*, Draft prepared for the Federal Emergency Management Agency, Washington, D.C.

- [7] Federal Emergency Management Agency (FEMA), 1997, *NEHRP Guidelines for the Seismic Rehabilitation of Existing Buildings*, FEMA 273, Washington, D.C.

- [8] Applied Technology Council (ATC), 1996, *Seismic Evaluation and Retrofit of Concrete Buildings Vol.1*. Report No. SSC 96-01 (ATC-40).

- [9] Kircher Charles A., Nassar Aladdin A., Kustu Onder and Holmes William T., 1997, *Development of Building Damage Functions for Earthquake Loss Estimation*, Earthquake Spectra, Vol. 13, No. 4, pp. 663-682, Oakland, California: Earthquake Engineering Research Institute.
- [10] National Institute of Building Science (NIBS), 1997, *Earthquake Loss Estimation Methodology, HAZUS97: Technical Manual*, Report prepared for the Federal Emergency Management Agency, Washington, D.C.
- [11] Japan International Cooperation Agency (JICA) and Istanbul Metropolitan Municipality (IMM), 2002, *The Study on A Disaster Prevention / Mitigation Basic Plan in Istanbul including Seismic Microzonation in the Republic of Turkey*, Final Report, December.
- [12] Boore D.M., Joyner W.B., Fumal T.F., 1997, *Equations For Estimating Horizontal Response Spectra and Peak Acceleration From Western North American Earthquakes: A Summary of Recent Work*, Seismological Research Letters, Vol. 68, No. 1, pp. 128-153, January/February.
- [13] Boğaziçi University, Department of Earthquake Engineering, 2002, *Earthquake Risk Assessment for Istanbul Metropolitan Area*, Final Report, KOERI (Kandilli Observatory and Earthquake Research Center), May.
- [14] NEHRP, 1997, *Recommended Provisions For Seismic Regulations For New Buildings and Other Structures, FEMA-303*, Prepared by the Building Seismic Safety Council for the Federal Emergency Management Agency, Washington, D.C.
- [15] Federal Emergency Management Agency (FEMA), 1999, *Earthquake Loss Estimation Methodology, HAZUS99 Technical Manual*, National Institute of Building Science, Washington, D. C.
- [16] Sadigh K., Chang C.-Y., Egan J.A., Makdisi F., Youngs R.R., 1997, *Attenuation Relationships for Shallow Crustal Earthquakes Based on California Strong Motion Data*, Seismological Research Letters Vol. 68(1), pp. 180-189, January/February
- [17] Campbell, K. W., 1997, *Empirical Near-Source Attenuation Relationships for Horizontal and Vertical Components of Peak Ground Acceleration, Peak Ground Velocity, and Pseudo Absolute Acceleration Response Spectra*, Seismological Research Letters Vol. 68(1), pp. 154-180, January/February

- [18] Spudich, P., Joyner W.B., Lindh A.G., Boore D.M., Magraris B.M. and Fletcher J.B., 1999, *SEA99: A Revised Ground Motion Prediction Relation for Use in Extensional Tectonic Regimes*, Bull. Seism. Soc. Am., Vol. 89, No. 5.
- [19] Federal Emergency Management Agency (FEMA), 2000, *Prestandard and Commentary for the Seismic Rehabilitation of Buildings*, Report FEMA 356, Washington, D.C
- [20] Abrahamson N. A. and Silva W. J., 1997, *Empirical Response Spectral Attenuation Relations for Shallow Crustal Earthquakes*, Seismological Research Letters, Vol. 68, No. 1, pp. 94-127, January/February.
- [21] Gülkan P. and Kalkan E., 2002, *Attenuation Modeling of Recent Earthquakes in Turkey*, Journal of Seismology, Vol. 6, pp. 397-409.
- [22] Chopra A. K. and Goel Rakesh K., 1999, *Capacity-Demand-Diagram Methods for Estimating Seismic Deformation of Inelastic Structures: SDF Systems*, Report No. PEER-1999/02, Pacific Earthquake Engineering Research Center, College of Engineering, University of California, Berkeley.
- [23] Newmark N. M. and Hall W. J., 1982, *Earthquake Spectra and Design*, Berkeley, California, Earthquake Engineering Research Institute.
- [24] Krawinkler H. and Nassar A. A., 1992, *Seismic design based on ductility and cumulative damage demands and capacities*. Nonlinear Seismic Analysis and Design of Reinforced Concrete Buildings, eds. P. Fajfar and H. Krawinkler. New York: Elsevier Applied Science.
- [25] Vidic T., Fajfar P. and Fischinger N. M., 1994, Consistent inelastic design spectra: strength and displacement, *Earthquake Engineering and Structural Dynamics* 23(5), pp.507-521
- [26] Chopra A. K., 1995, *Dynamics of Structures: Theory and Applications to Earthquake Engineering*, Chapters 3, 6, 7 and 19. Englewood Cliffs, N. J.: Prentice Hall.
- [27] NEHRP, 2000, *NEHRP Recommended Provisions For Seismic Regulations for New Buildings And Other Structures*, FEMA 368, Federal Emergency Management Agency (FEMA), Washington, D.C

- [28] Turkish Ministry of Public Works and Settlement, 1997, *Requirements for the Structures to be built in disaster areas*, Ankara, Turkey.
- [29] Yakut A., Ozturk, N. Y. and Bayili S., 2003, *Analytical Assessment of Seismic Capacity of RC Frame Buildings*, Proceedings of the International Conference on Earthquake Engineering to Mark 40 Years from Catastrophic 1963 Skopje Earthquake and Successful City Reconstruction, Macedonia, Skopje, 26-29 August.
- [30] Yakut A., Gülkan P., Bakır B. S. and Yılmaz M. T., *Reexamination of Damage Distribution in Adapazarı: Structural Considerations, (In Review)*, Engineering Structures.
- [31] Parsons T., Toda S., Stein R.S., Barka A.A., and Dieterich J.H., 2000, *Influence of the 17 August 1999 Izmit Earthquake on Seismic Hazards in Istanbul*, Manuscript accepted by JGR 2001.

APPENDIX A

SRAS MANUAL

INTRODUCTION

SRAS has been developed by Sezgin KUCUKCOBAN under supervision of Asst. Prof. Dr. Ahmet YAKUT as a part of thesis study performed in Civil Engineering Department of Middle East Technical University. The software is free of charge and can be distributed freely for educational purposes. It is the responsibility of user to verify the results generated by the software. This manual briefly describes the software interface, details of creating and analyzing a project, output operations, general options and limitations of the software. The information provided here is tried to be kept as concise as possible in order to facilitate rapid screening of the manual. Just as a reminder, SRAS is nothing but an ordinary computer program. It performs tiresome calculations for the user and presents the results. It is the user who will criticize the reliability of these results. Check for the updates from Internet or contact to ksezgin@metu.edu.tr.

INSTALLATION

To install SRAS:

1. Insert the CD into the CD-ROM drive. To start the installation process, from the Start menu, choose Run. Enter the CD-ROM drive letter, and “SRAS\setup.exe”. For example, enter “D:\SRAS\setup.exe”.
2. When “Welcome” page is displayed, choose OK.
3. Select an existing directory by clicking to “Change Directory” command button or accept default directory.

4. Click install button to start the installation
5. After finishing installation, copy the files under “CD Drive:\SRAS\SRAS_folder” to SRAS program folder created in your computer. If default directory has not been changed, “SRAS” folder will be under “Program Files” folder.
6. Restart your computer after you complete Setup process.

WARNING If you do not restart your computer, you may have problems running SRAS.

USER INTERFACE

SRAS has been developed in Visual Basic 6.0 Environment. It has a graphical user interface composed of a menu bar, toolbar, status bar and workspace. The interface is shown in Figure A.1.

SRAS has six menu items each of which is explained briefly in the subsequent paragraphs. Figure A.2 shows all menus that can be used in SRAS.

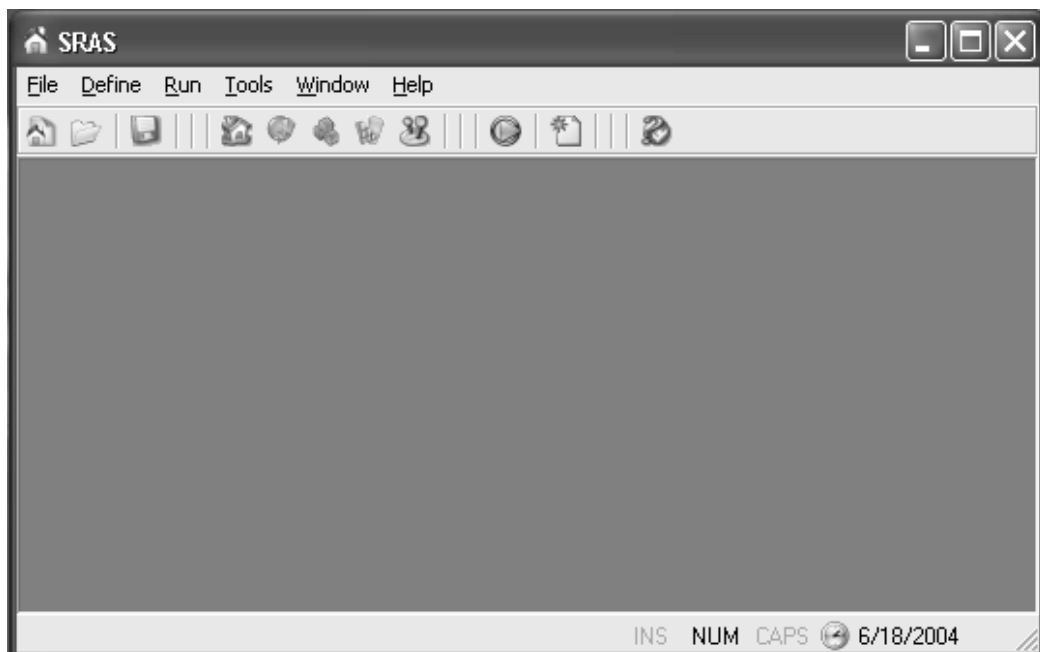


Figure A.1 SRAS user interface

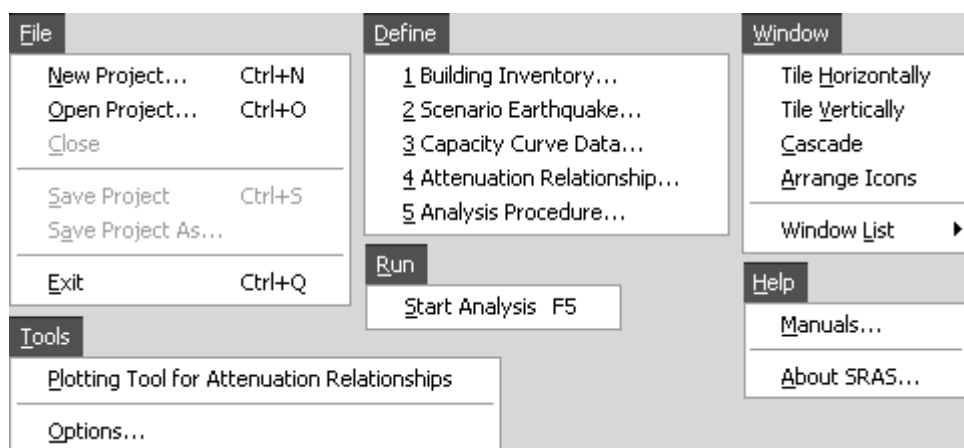


Figure A.2 SRAS menu items

File:

New Project: Creates a new project file (*.sra).

Open Project: Opens a project file (*.sra) from the hard disk.

Close: Closes an open project file without saving.

Save Project: Saves the new project file using the user-provided file name or updates preliminarily saved project file. Building inventory data will not be attached to the project file.

Save Project As: Saves the project file with a new name and location provided by the user.

Exit: Ends running SRAS.

Define:

Building Inventory...: Runs “Building Data Wizard”

Scenario Earthquake...: Runs “Scenario Earthquake Wizard”

Capacity Curve Data...: Runs “Capacity Curve Wizard”

Attenuation Relationship...: Runs “Attenuation Wizard”

Analysis Procedure...: Runs “Analysis Method Wizard”

Run:

Start Analysis: After completion of input files, clicking this menu item starts the damage estimation process.

Tools:

Plotting Tool for Attenuation Relationships: Runs a tool which takes moment magnitude, distance (km) and average shear wave velocity (m/s) in order to compute spectral acceleration values for the selected attenuation relationships.

Window:

Tile Horizontally: Arranges child windows horizontally.

Tile Vertically: Arranges child windows vertically.

Cascade: Arranges child forms in a stepwise manner.

Arrange Icons: Arranges minimized window icons.

Window List: Shows the list of open windows.

Help:

Manuals...: Runs windows explorer and opens manuals folder under software root directory.

About SRAS...: Provides information about the software.

CREATING A NEW PROJECT

Using one of the following methods, you can create a new project.

1. Click “New Project...” menu item.
2. Click  icon on the toolbar
3. Use “Ctrl + N” key combination

The screen, shown in Figure A.3, will appear and it will be labeled as “New Project”.

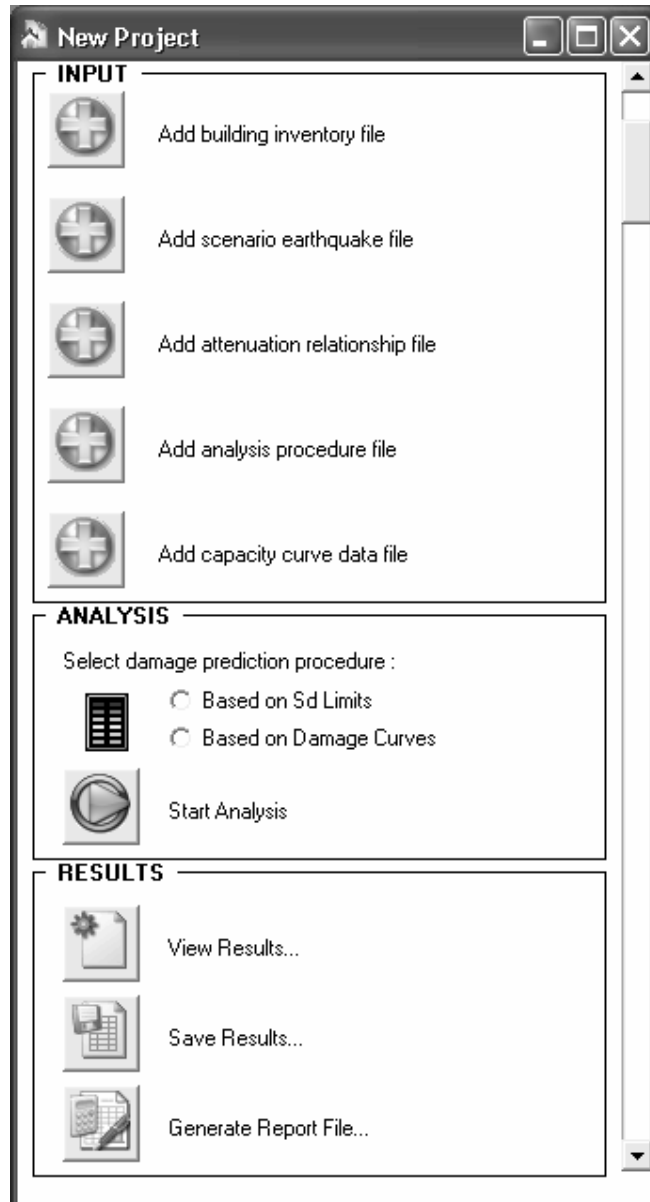


Figure A.3 New project file

The project window is separated into three frames as *INPUT*, *ANALYSIS* and *RESULTS*. *INPUT* frame collects required data for SRAS. *ANALYSIS* frame smoothes the process of damage criteria selection and performs the analysis. *RESULT* frame presents, exports and reports the computed results. Each part is discussed in the following sections.

***INPUT* frame:** It contains five command buttons that are used for adding data files to the current project. When the first button is clicked, the following screen will appear.

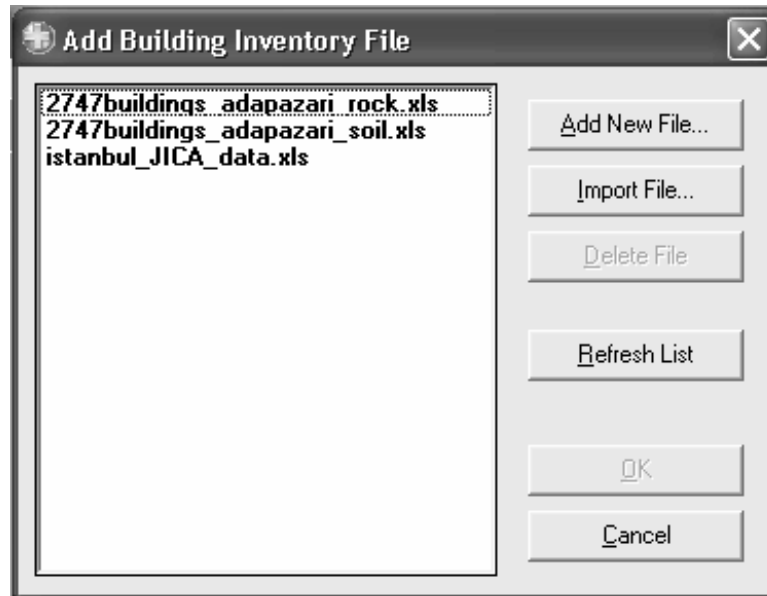


Figure A.4 Add building inventory file window

The file list, located on the right, shows the content of “building_files” folder under the root directory of SRAS. Building inventory files should have extensions of (*.xls) and (*.mdb).

Add New File...: You may create a new building inventory file by using the associated wizard. Clicking on this command button will activate the wizard. Detailed information is provided in part describing “Wizards”.

Import File...: You may import a building inventory file, created in Excel or Access, from a specified location. SRAS will create a copy of the selected file under “building_files” folder. If you want to import several files simultaneously, open “building_files” folder using windows explorer and paste here the copies of files to be imported. Preparation of a new building inventory file is explained as a separate part.

Delete File: You can delete selected file from the disk. Please, be careful while using this command, because undo is not available and the file will not be moved to recycle bin.

Refresh List: After some file operations, the list should be refreshed to view the changes in “building_files” folder.

OK: After selecting one of the files from the list, click this command button to close the window and use the selected file in the analysis.

Cancel: Terminates the file adding process.

All buttons in the *INPUT* frame activates the same window by just changing caption names and file filtering properties. Process, explained for the first button, is also valid for the others. Interface differences are provided in the table below.

Table A.1 Interface differences between “Add ... File” windows

Add ... File	Default File Folder	File List Filter	Associated Wizard
Building inventory	Root\building_files	*.xls or *.mdb	Building Data Wizard
Scenario earthquake	Root\scenario_files	*.sef	Scenario Earthquake Wizard
Attenuation relationship	Root\atten_files	*.att	Attenuation Wizard
Analysis procedure	Root\method_files	*.apf	Analysis Method Wizard
Capacity curve data	Root\capa_files	*.ccf	Capacity Curve Wizard

After adding each file, a new command button will appear on the right. This button is used for screening the data in the added file. It is also a verification showing that SRAS has read the added file correctly and will run properly. Before passing to the analysis stage, all data files must be added to the current project.

ANALYSIS

Prior to the analysis phase, all input data must be complete. Under *ANALYSIS* frame, there are two damage estimation procedures available.

If “Based on Sd limits” is selected, the following window will appear.

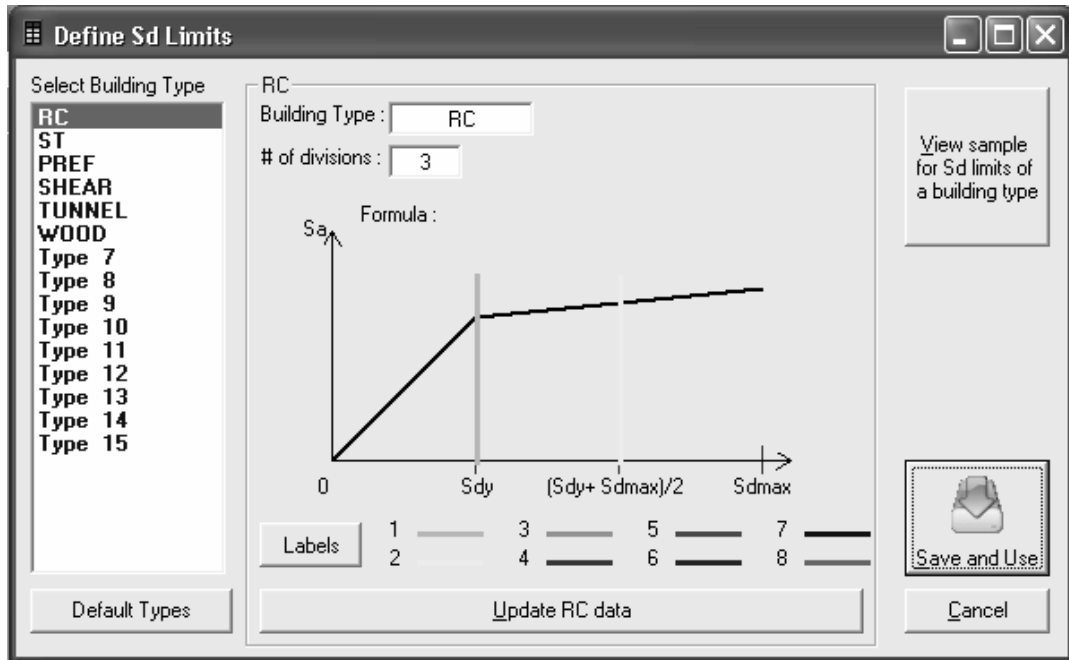


Figure A.5 “Define Sd Limits” window

For each building type,

1. Enter a building type name. Building type names must be same (case sensitive) with the ones defined in capacity curve file. Otherwise, damage level assignment process can not be performed.
2. Enter number of damage levels (divisions). It can be any number between 3 and 9. For example, if damage levels of “Light”, “Moderate_1”, “Moderate_2” and “Heavy” will be used, then 4 must be entered as number of divisions. SRAS automatically creates a damage level named as “Collapse/No Intersection” for those buildings fall beyond Sdmax.
3. Set damage limits by shifting those colorful bars to the left or right and checking the formula provided. You may hold left mouse button pressed on the bar and move the mouse left or right. Another way is to use arrow keys in the keyboard after clicking on the bar. Do not change the given order of bars. Use provided number-color twins not to mix up the sequence.

- Click “Labels” button. Text boxes will appear in order to define the damage level names that should be given to each division. An example is shown below.

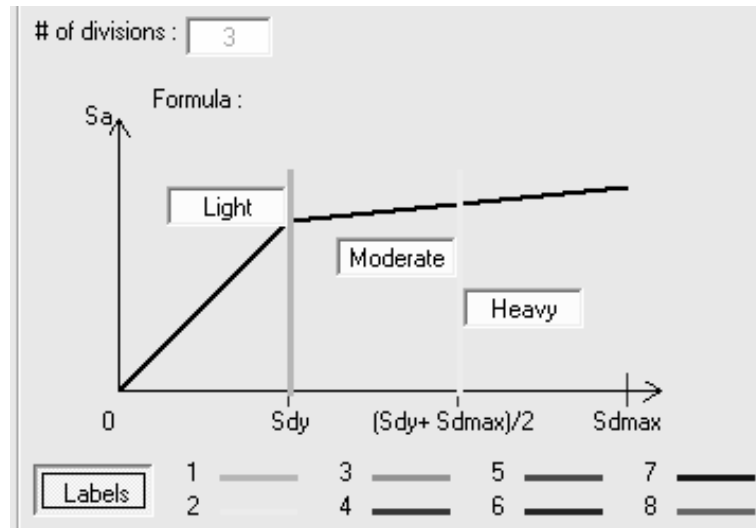


Figure A.6 Building type frame showing damage state labels

- Click “Update ... Data” button to save the modifications made.

After defining damage levels for all building types, click “Save and Use” button in order to return back to the project window.

If “Based on Damage Curves” is selected, the window shown in Figure A.7 will appear.

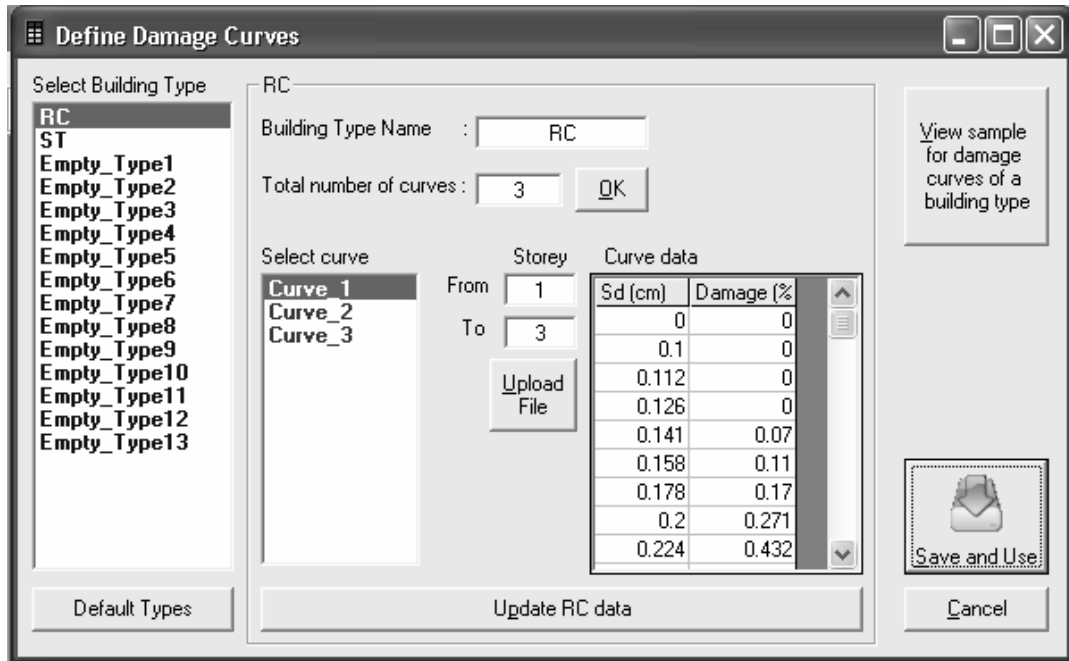


Figure A.7 “Define Damage Curves” window

For each building type,

1. Enter a building type name. Building type names must be same (case sensitive) with the ones defined in capacity curve file. Otherwise, damage level assignment process can not be performed.
2. Enter total number of damage curves. It can be any number between 1 and 9. For example, if damage curves are available for story intervals of “1-4”, “4-7”, “8-11” and “11-15”, then 4 must be entered as total number of curves. Click OK.
3. SRAS automatically creates damage curve list depending on the provided number. Select one of these curves. Enter for which interval the curve is valid and upload text file including damage curve data.
4. Press “Update ... data” button to save changes. Repeat steps 3 and 4 for other curves and do not forget to update after changes made for each curve.

After defining damage curves for all building types, click “Save and Use” button in order to return back to the project window.

Now you are ready to start analysis. The screen should look like as Figure A.8 before starting the analysis.

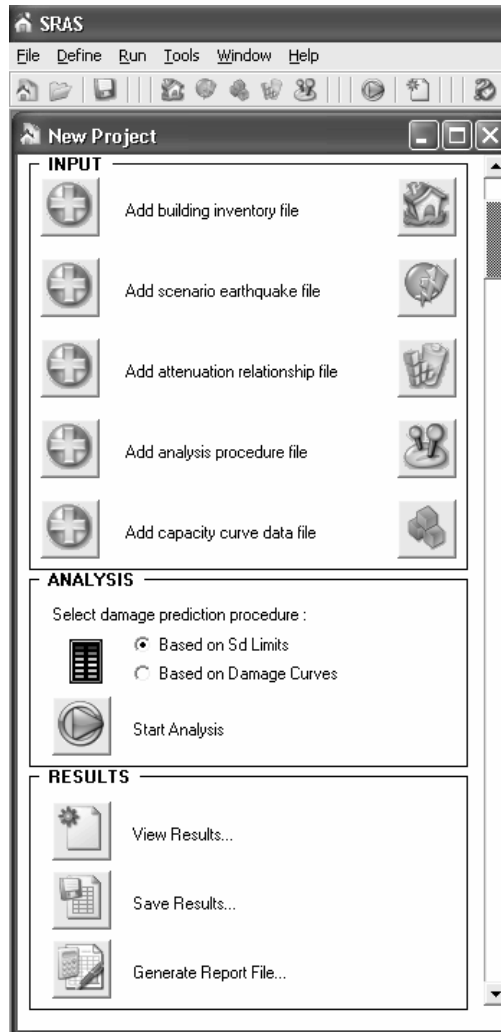


Figure A.8 The appearance of project file before starting the analysis

After clicking “Start Analysis” button, a window will be opened to show the progress. An example screenshot is shown below subsequent to completion of analysis.

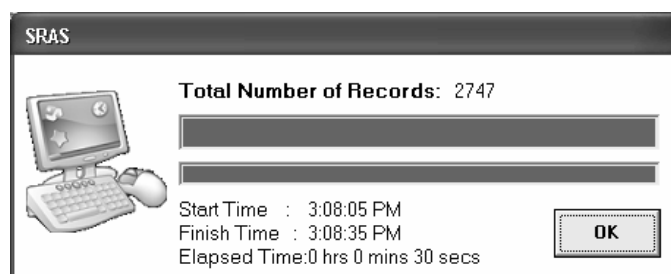


Figure A.9 Run window subsequent to completion of analysis

OUTPUT GENERATION

After completion of analysis, the command buttons in the “RESULTS” frame will be enabled.

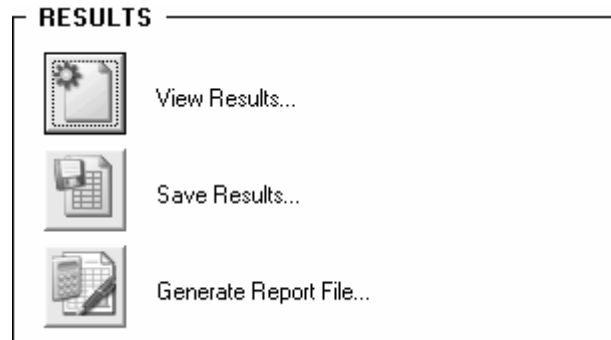


Figure A.10 “Results” frame after analysis has been completed

There are three things to do with the results.

- You can view tabular results in a window
- You can save results in a tabular format
- You can generate a report file for the project

Screen Display

This is the best way of rapid screening of results. Input-read errors can be easily observed if there are any. An example of this tabular data view window is shown in Figure A.11. You can use  button to go to the previous record,  button to go to the first record,  button to move to the next record,  button to go to the final record in the database. You may change the column widths. *Editing the results is not allowed.*

Export Results

It is possible to export the results tabulated in “View Results” window. There are two different database formats that can be used while exporting the results. These are Microsoft Excel and Access database formats. The exported files include everything shown in “View Results” window. These exported files may be used for mapping or some other type of post processing events.

	Sdy (cm)	Samax (g)	Sdmax (cm)	ppSd (cm)	ppSa (g)	ppT (sec)	Damage
▶	1.11	0.26	13.18	8.547721	0.205997	1.039623	Heavy
	1.11	0.26	13.18	8.547721	0.205997	1.039623	Heavy
	1.11	0.26	13.18	8.547721	0.205997	1.039623	Heavy
	1.11	0.26	13.18	8.547721	0.205997	1.039623	Heavy
	1.11	0.26	13.18	8.547721	0.205997	1.039623	Heavy
	1.11	0.26	13.18	8.547721	0.205997	1.039623	Heavy
	1.11	0.26	13.18	8.547721	0.205997	1.039623	Heavy
	1.11	0.26	13.18	8.547721	0.205997	1.039623	Heavy
	1.11	0.26	13.18	8.547721	0.205997	1.039623	Heavy
	1.11	0.26	13.18	8.547721	0.205997	1.039623	Heavy
	1.11	0.26	13.18	8.547721	0.205997	1.039623	Heavy
	1.11	0.26	13.18	8.547721	0.205997	1.039623	Heavy
	1.11	0.26	13.18	8.547721	0.205997	1.039623	Heavy
	1.11	0.26	13.18	8.547721	0.205997	1.039623	Heavy
	1.11	0.26	13.18	8.547721	0.205997	1.039623	Heavy
	1.11	0.26	13.18	8.547721	0.205997	1.039623	Heavy
	1.11	0.26	13.18	8.547721	0.205997	1.039623	Heavy
	1.11	0.26	13.18	8.547721	0.205997	1.039623	Heavy
	1.11	0.26	13.18	8.547721	0.205997	1.039623	Heavy
	1.11	0.26	13.18	8.547721	0.205997	1.039623	Heavy
	1.11	0.26	13.18	8.547721	0.205997	1.039623	Heavy
	1.11	0.26	13.18	8.547721	0.205997	1.039623	Heavy

Figure A.11 Tabular view of results

Generate Report

This extension prepares a report for the study performed. It includes every detail regarding to the project except building inventory data. Instead of building database, a table summarizing statistical distribution of buildings with respect to building type and number of stories was presented. Scenario earthquake fault model, attenuation relationship, analysis method and capacity curve data used in the project are added to the report. Finally, “SiteLabel” based summary of results are written for each type o building separately. For example, if “SiteLabel” was entered as district name, then the results will be summarized in district level. You may use “_” character while combining district name and sub-district names in order to perform a more refined analysis. For instance, “ISTANBUL_KADIKOY” can be used as “SiteLabel” to facilitate the generation of summary in sub-district level.

The report includes some other parameters such as report title and user information (this is explained in **GENERAL OPTIONS**). Summary of results is only written to the report when SDL method is selected for damage estimation. If DC method is preferred, report file will not give any information regarding to the results obtained. It will be a collection of input parameters used for that project.

There are two formats that are supported by SRAS: “Text File” and “Microsoft Word Document” having extensions of (*.txt) and (*.doc), respectively. Creation of word document may sometimes lead errors, so it is better to prefer text file format. Word document file generation takes longer time due to formatting such as insertion of tables and pictures. On the other hand text files are created almost instantaneously for small databases and require comparatively less time than word documents for large databases.

GENERAL OPTIONS

SRAS has a few general options that should be modified or kept as they were before starting to use the application. Select “Tools” menu and click on “Options...” menu item. Options window will be shown. There are two tabs: “User Details” and “Modification Factors”. In order to make changes in the user profile, select “User Details” tab and enter any valid data to the textboxes. A screenshot is provided in Figure A.12. Then click “Apply” command button to make changes permanent.

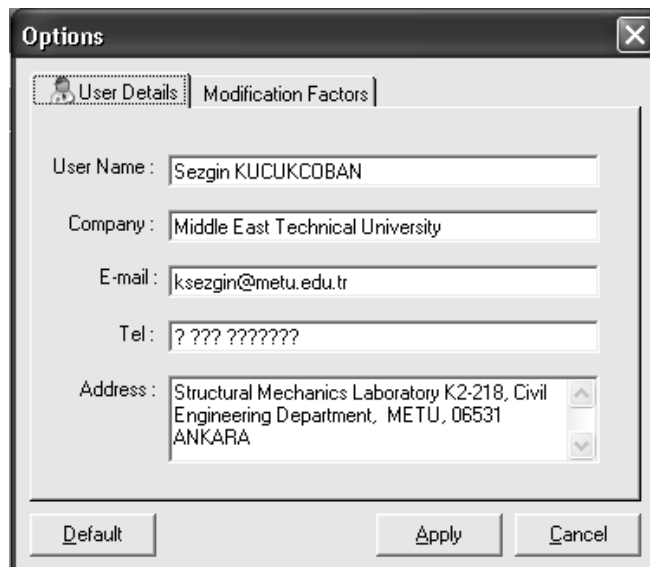


Figure A.12 “User Details” tab in “Options” windows

The process is also valid for modification factor changes. Click on “Modification Factors” tab. You may change default coefficients that are used to modify calculated spectral displacement values considering apparent condition and construction date. Do not forget to click “Apply” if you have made any edits.

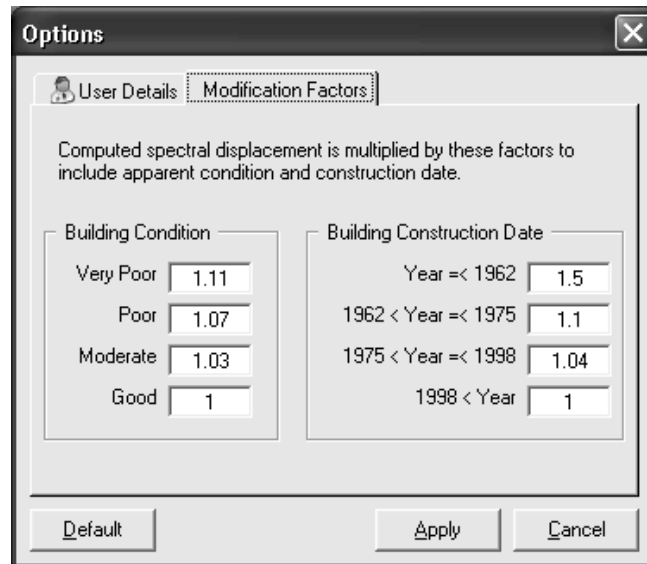


Figure A.13 “Modification Factors” tab in “Options” menu

TOOLS

A plotting tool for attenuation relationships is attached to the software for rapid visualization of spectral acceleration curve. Select “Tools” menu and click “Plotting Tool for Attenuation Relationships” menu item. The screen shown in Figure A.14 will appear.

Enter values for distance, shear wave velocity and moment magnitude. Select attenuation relationship and fault type. Then click “Plot” command button. You may plot all four graphs on the same plot. If you want to find out the values click on a point on the graphs and read the values from the right-bottom part having light yellow background. In order to save the coordinates of spectral acceleration curves, click “Save” command button and export results as a text file.

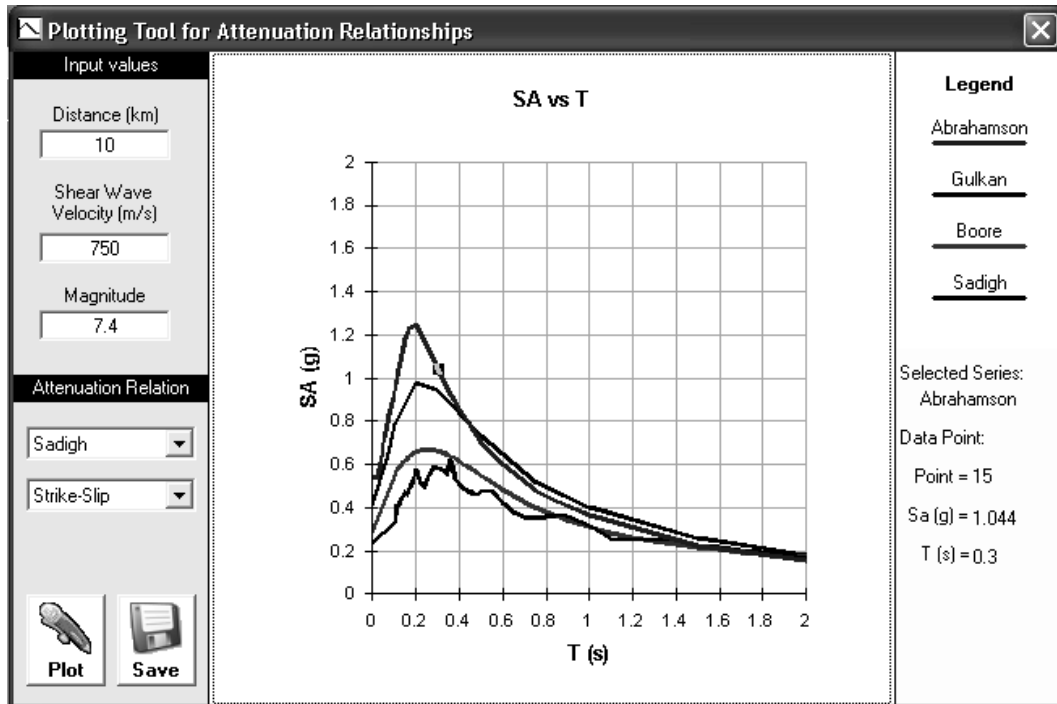


Figure A.14 “Plotting Tool for Attenuation Relationships” window

SRAS LIMITATIONS

SRAS is capable of handling large databases but the running time mostly depends on the hardware configuration details of the computer. SRAS has been developed only for four attenuation relationships and three demand displacement computation methods. These are:

Attenuation Relationships:

1. Abrahamson and Silva [20]
2. Boore et al. [12]
3. Gülkan and Kalkan [21]
4. Sadigh et al. [16]

Analysis Methods:

1. Capacity spectrum method of ATC-40 [8]
2. Displacement coefficient method of FEMA-356 [19]
3. Constant ductility method proposed by Chopra and Goel [22]

Limitations that are inherit in attenuation relationships and analysis methods are also valid for SRAS. Be careful to select the proper attenuation relationship and analysis method. Regarding to the capacity curve data, SRAS supports up to 15 building types. This limit can be easily increased in the next versions.

SRAS WIZARDS

1. Define New Building Inventory Data File

- a. On the Define menu, click Building Inventory.
- b. Select program type for which this data will be used and file type in which format this data will be saved, then click Next.
- c. Enter required information for the first building.
- d. Repeat step c until data for all buildings that are going to be analyzed are written to the table. After finishing, click Next.
- e. Enter a name for generated building inventory file considering file-naming limitations of Windows.

2. Define New Scenario Earthquake File

- a. On the Define menu, click Scenario Earthquake.
- b. Select the fault model to be used in the calculations. Click Next.
- c. If you have selected “linear fault”, enter spatial coordinates of each node. Nodes must be in numerical order as 1, 2, 3....
- d. If you have selected “meshed fault”, besides spatial coordinates of nodes, a mesh size should be entered for each segment. Click a mesh size cell. An input box will appear. Enter mesh size for that segment and repeat this procedure for all other segments. Then, click Next.
- e. The tabulated information about all segments is displayed. Enter a moment magnitude for the scenario earthquake. Click Next.
- f. Enter a name for generated fault model considering file-naming limitations of Windows.

3. Define New Capacity Curve Data File

- a. On the Define menu, click Capacity Curve Data.
- b. Enter building type names for database creation. Click Next.

c. Select building type. Add capacity curve data for buildings having number of stories “From” ... “To” Capacity curve data for interior number of stories will be generated automatically from the boundary values.

d. After finishing addition, do not forget to assign! Repeat step 3 and 4, until capacity curve data for all defined building types are defined. Click Next.

e. Enter a name for generated capacity curve data file considering file-naming limitations of Windows.

4. Define New Attenuation Relationship File

a. On the Define menu, click Attenuation Relationship.

b. Select an attenuation relationship. Read the provided information carefully in order to select the most appropriate relationship for analysis. Click Next.

c. Select faulting style. Click Next.

d. Select site classification scheme. There are two schemes available in this version. Site class definitions are provided below. You should use default “ID” values while entering site classes in the building data input file. Be sure that you have selected the correct scheme which is used during the preparation of input file. Click Next.

e. Enter a name for generated attenuation model considering file-naming limitations of Windows.

5. Define New Analysis Method File

a. On the Define menu, click Analysis Procedure.

b. Select an analysis method. There are three methods available in this version. Click Next.

c. Enter required information for that model. Click Next.

d. Enter a name for generated analysis model considering file-naming limitations of Windows.

PREPARING A BUILDING INVENTORY FILE

SRAS is capable of handling database files that have extensions *.xls and *.mdb. Although it supports Microsoft Excel files created in XP and previous versions, it gives support only for Access database files created in or exported to 97 format. While

preparing building inventory files, the procedure differs slightly. Please, read and apply the procedures very carefully to facilitate error-free analysis by SRAS.

Using Microsoft Excel:

1. Open a new Excel Worksheet.
2. Rename one of the sheets as “BD” (referring to building database) and delete the other sheets. (It is crucial to rename the sheet as “BD”. Other names will lead errors.)
3. Starting from cell “A1” write the field names for the following fields. Any name can be used for the fields provided that it is free of special characters such as “+ , . / \ [] ? ! & % () ’ = < > | ~ : ; £ # \$ { }”. Underscore “_” should be used instead of spacing character. The order of fields must not be changed. If a field is empty, write field name and leave that column blank.

Table A.2 List of field types for building input file (Excel)

Order	Field Name	Field Type
1	SiteID	Long Integer
2	SiteLabel	String * 100
3	BuildingLabel	String * 100
4	Latitude	Double
5	Longitude	Double
6	SiteClass	Single
7	NumberOfStories	Integer
8	BuildingType	String * 15
9	NumberOfBuildings	Single
10	ConstructionYear	Integer
11	Condition	Integer (!!!)
12	Information	String * 100

!!! : (1=Very Poor, 2=Poor, 3=Moderate or 4=Good)

4. Write data for each building or building group and save your building inventory file.

NOTE: If there is an available building inventory database, modify the field characteristics and sequence in order to satisfy the requirements specified above for the use in SRAS.

Using Microsoft Access:

1. Open a new access database file.
2. Insert a new table named as “BD”. (It is crucial to rename the database table as “BD”. Other names will lead errors.)
3. Starting from first field, create the following fields using “Table Designer tool of Access. Provide specific information about field types. The order of fields must not be changed. If a field is empty, write field name and leave that column blank. (Please, be careful that Access takes “0” as the default value of generated number fields. Clear “0” from the default value textbox before proceeding to the next field.)

Table A.3 List of field types for building input file (Access)

Order	Field Name	Field Type
1	SiteID	Long Integer
2	SiteLabel	String * 100
3	BuildingLabel	String * 100
4	Latitude	Double
5	Longitude	Double
6	SiteClass	Single
7	NumberOfStories	Integer
8	BuildingType	String * 15
9	NumberOfBuildings	Single
10	ConstructionYear	Integer
11	Condition	Integer (!!!)
12	Information	String * 100

!!!: (1=Very Poor, 2=Poor, 3=Moderate or 4=Good)

4. Write data for each building or building group and save your building inventory file.

5. Then using “Convert Database” tool of Microsoft Access, convert the generated database table to Access 97 format. Microsoft Access will give you a message saying that you will lose some properties of the database. Click OK to proceed.

NOTE: If there is an available building inventory database, modify the field characteristics and sequence in order to satisfy the requirements specified above for the use in SRAS.

APPENDIX B

CASE STUDY: ADAPAZARI

Table B.1 GDDA database damage statistics [30]

ID	District	Collapsed and Heavily Damaged		Moderately and Lightly Damaged		Total
		Number	%	Number	%	
1	Maltepe	0	0	42	100	42
2	Hızırtepe	0	0	12	100	12
3	Şirinevler	9	35	17	65	26
4	Güllük	4	36	7	64	11
5	Mithatpaşa	23	14	139	86	162
6	Yenidoğan	101	57	75	43	176
7	Papuçcular	53	38	87	62	140
8	Akıncılar	13	33	27	68	40
9	Yenicami	26	48	28	52	54
10	Çukurahmediye	3	19	13	81	16
11	Semerciler	55	29	135	71	190
12	Tığcılar	19	10	163	90	182
13	Yenigün	78	19	336	81	414
14	Tepekum	5	8	60	92	65
15	Şeker	111	40	168	60	279
16	Cumhuriyet	31	22	111	78	142
17	Orta Mahalle	17	13	117	87	134
18	Yahyalar	14	16	72	84	86
19	Yağcılar	9	6	142	94	151
20	Kurtuluş	5	13	33	87	38
21	İstiklal	8	13	55	87	63
22	Karaosman	29	38	47	62	76
23	Ozanlar	12	15	69	85	81
24	Sakarya	4	11	33	89	37
25	Tekeler	7	7	87	93	94
26	Tuzla	2	13	13	87	15
	Total	638		2088		2726

Table B.2 Predicted damage for the GDDA dataset based on soft soil type and Gülkan and Kalkan [21] attenuation relationship

ID	District	Damage Distribution(%)								
		ATC-40			FEMA-273			Chopra & Goel		
		L	M	H	L	M	H	L	M	H
1	Maltepe	0	0	100	0	0	100	0	100	0
2	Hızırtepe	0	0	100	0	0	100	0	100	0
3	Şirinevler	0	0	100	0	0	100	0	100	0
4	Güllük	0	0	100	0	0	100	0	100	0
5	Mithatpaşa	0	100	0	0	0	100	0	100	0
6	Yenidoğan	0	100	0	0	0	100	0	100	0
7	Papuçcular	0	100	0	0	0	100	0	100	0
8	Akıncılar	0	100	0	0	0	100	0	100	0
9	Yenicami	0	100	0	0	0	100	0	100	0
10	Çukurahmediye	0	100	0	0	0	100	0	100	0
11	Semerciler	0	100	0	0	30	70	0	100	0
12	Tığcılar	0	100	0	0	58	42	0	100	0
13	Yenigün	0	100	0	0	0	100	0	100	0
14	Tepekum	0	100	0	0	51	49	0	100	0
15	Şeker	0	100	0	0	78	22	0	100	0
16	Cumhuriyet	0	100	0	0	43	57	0	100	0
17	Orta Mahalle	0	100	0	0	36	64	0	100	0
18	Yahyalar	0	100	0	0	42	58	0	100	0
19	Yağcılar	0	100	0	0	100	0	0	100	0
20	Kurtuluş	0	100	0	0	11	89	0	100	0
21	İstiklal	0	100	0	0	95	5	0	100	0
22	Karaosman	0	100	0	0	92	8	0	100	0
23	Ozanlar	0	100	0	0	100	0	0	100	0
24	Sakarya	0	100	0	0	100	0	0	100	0
25	Tekeler	0	100	0	0	100	0	0	100	0
26	Tuzla	0	100	0	0	100	0	0	100	0

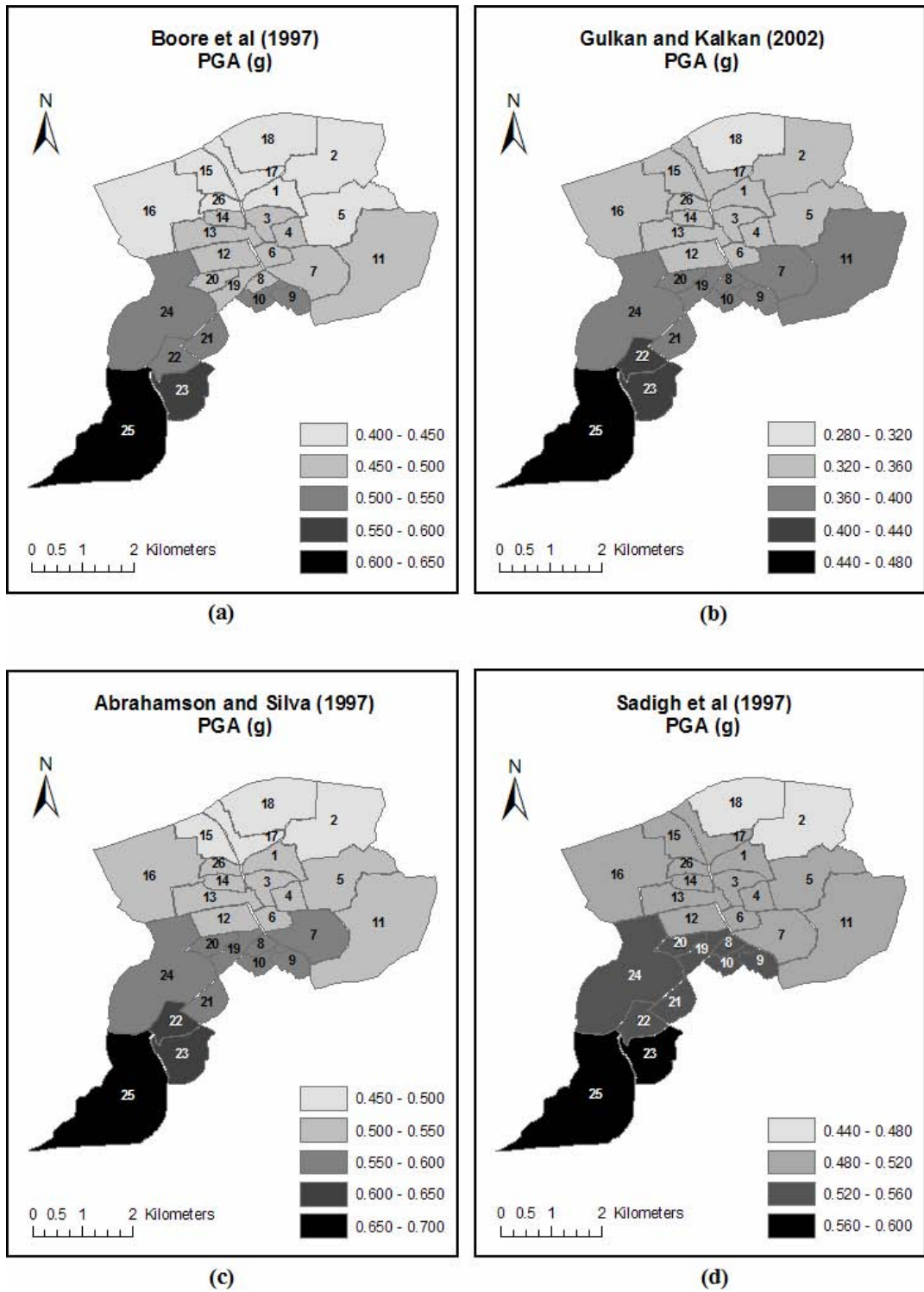


Figure B.1 PGA distribution obtained for different attenuation relationships

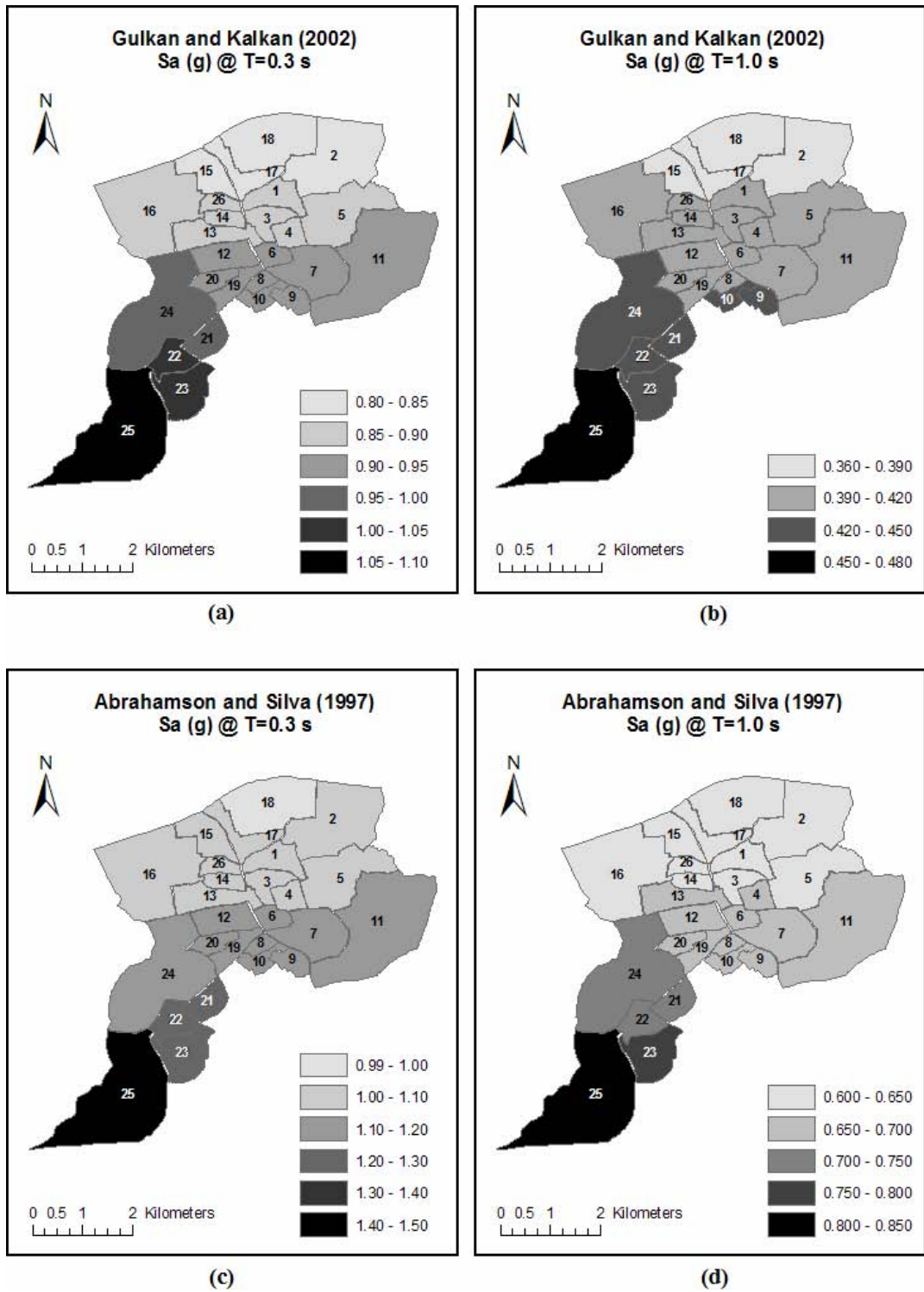
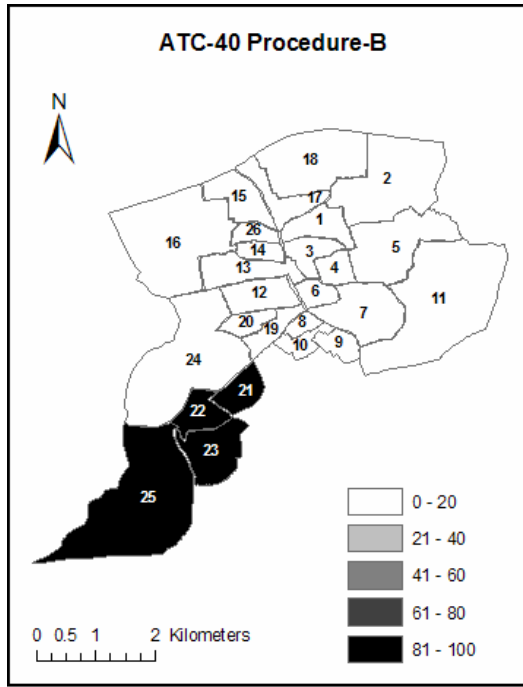
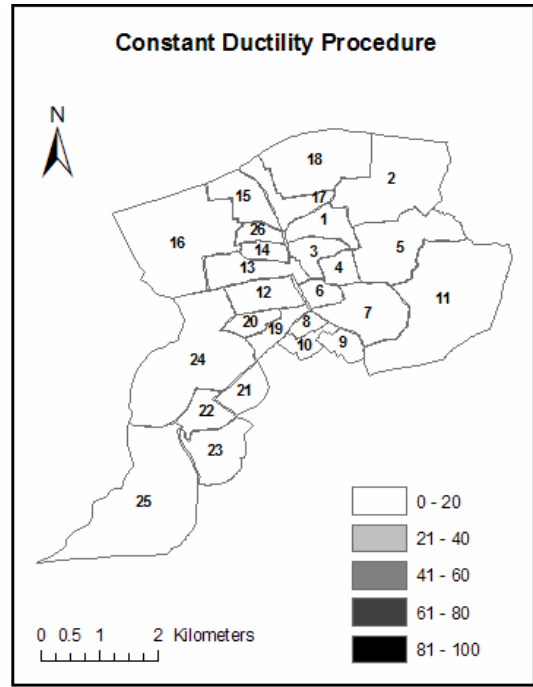


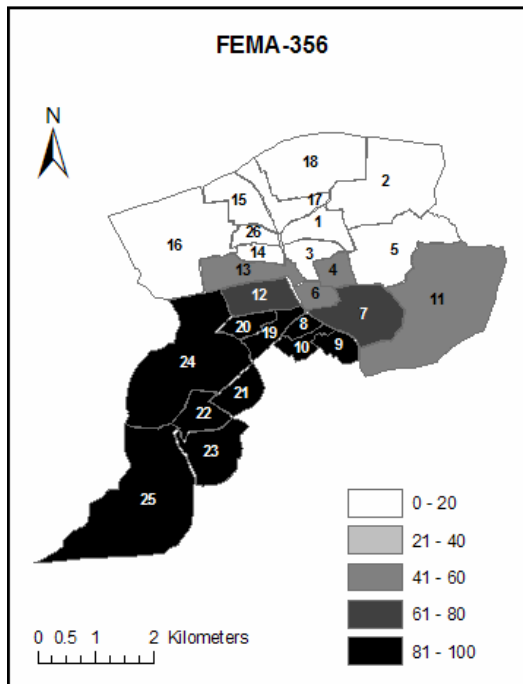
Figure B.2 Distribution of S_a values at T = 0.3 s and 1.0 s for two attenuation relations



(a)



(b)

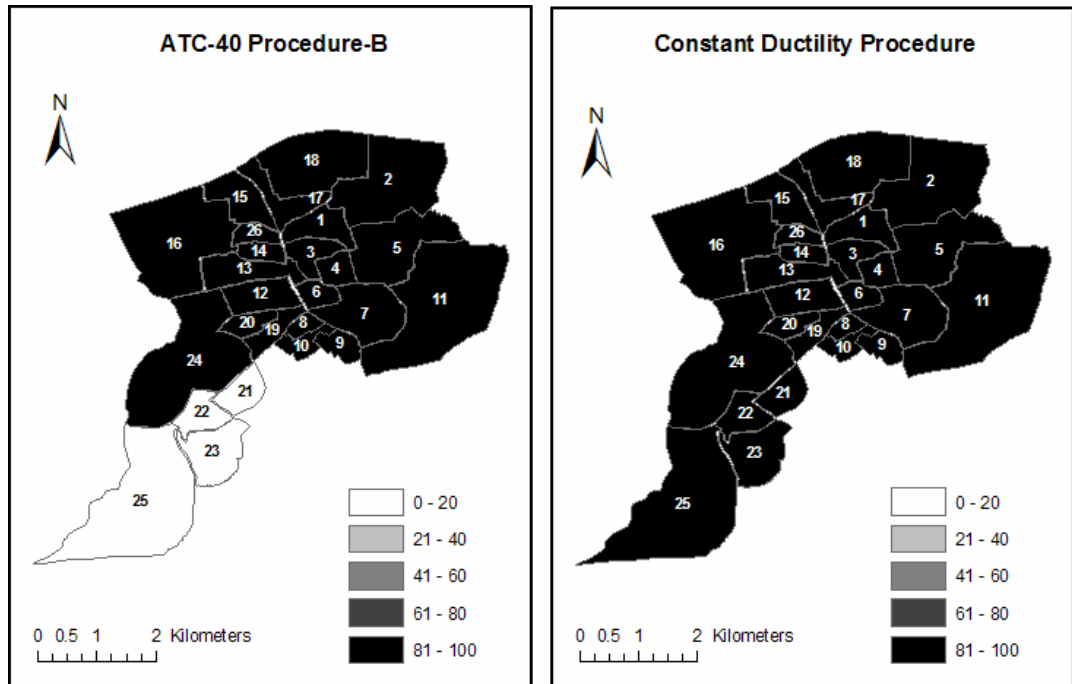


(c)

Sub-District Names	
1 KARAOSMAN	14 KURTULUS
2 TUZLA	15 OZANLAR
3 ORTAMAHALLE	16 SEKER
4 YAHYALAR	17 SAKARYA
5 YAGCILAR	18 TEKELER
6 TIGCILAR	19 PAPUCCULAR
7 YENIGUN	20 YENIDOGAN
8 YENICAMI	21 GULLUK
9 CUKURAHMEDIYE	22 SIRINEVLER
10 AKINCILAR	23 HIZIRTEPE
11 TEPEKUM	24 MITHATPASA
12 SEMERCILER	25 MALTEPE
13 CUMHURIYET	26 ISTIKLAL

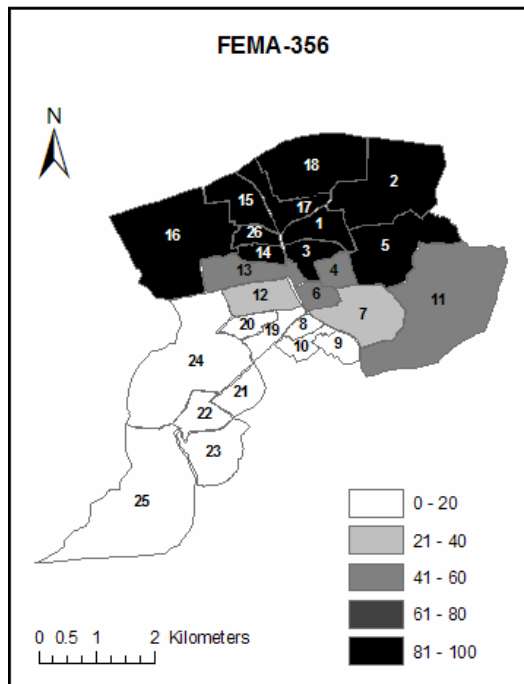
(d)

Figure B.3 Estimated percentage distribution of heavy damage/collapse using Gülkan and Kalkan [21] (GDDA set)



(a)

(b)

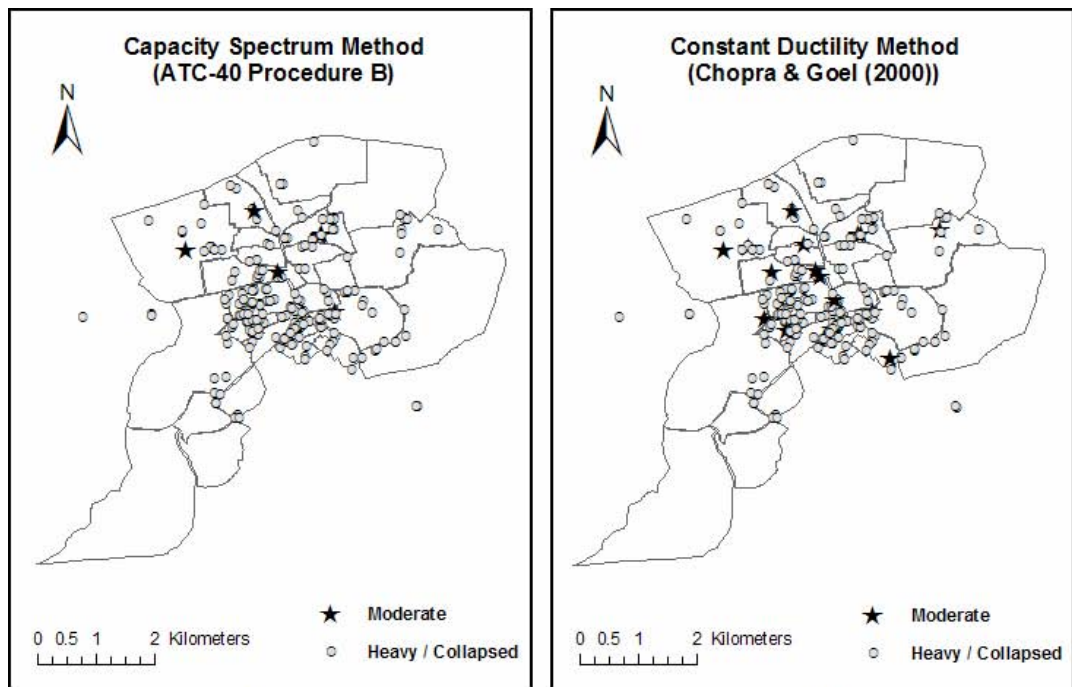


(c)

Sub-District Names	
1 KARAOSMAN	14 KURTULUS
2 TUZLA	15 OZANLAR
3 ORTAMAHALLE	16 SEKER
4 YAHYALAR	17 SAKARYA
5 YAGCILAR	18 TEKELER
6 TIGCILAR	19 PAPUCCULAR
7 YENIGUN	20 YENIDOGAN
8 YENICAMI	21 GULLUK
9 CUKURAHMEDIYE	22 SIRINEVLER
10 AKINCILAR	23 HIZIRTEPE
11 TEPEKUM	24 MITHATPASA
12 SEMERCILER	25 MALTEPE
13 CUMHURIYET	26 ISTIKLAL

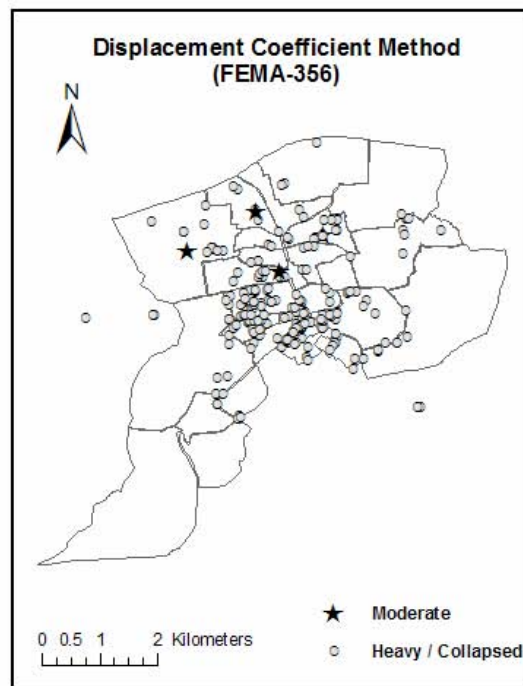
(d)

Figure B.4 Estimated percentage distribution of moderate damage using Gülkan and Kalkan [21] (GDDA set)



(a)

(b)



(c)

Figure B.5 Estimated damage for SU database based on soft soil using Boore et al. [12]

APPENDIX C

CASE STUDY: ISTANBUL

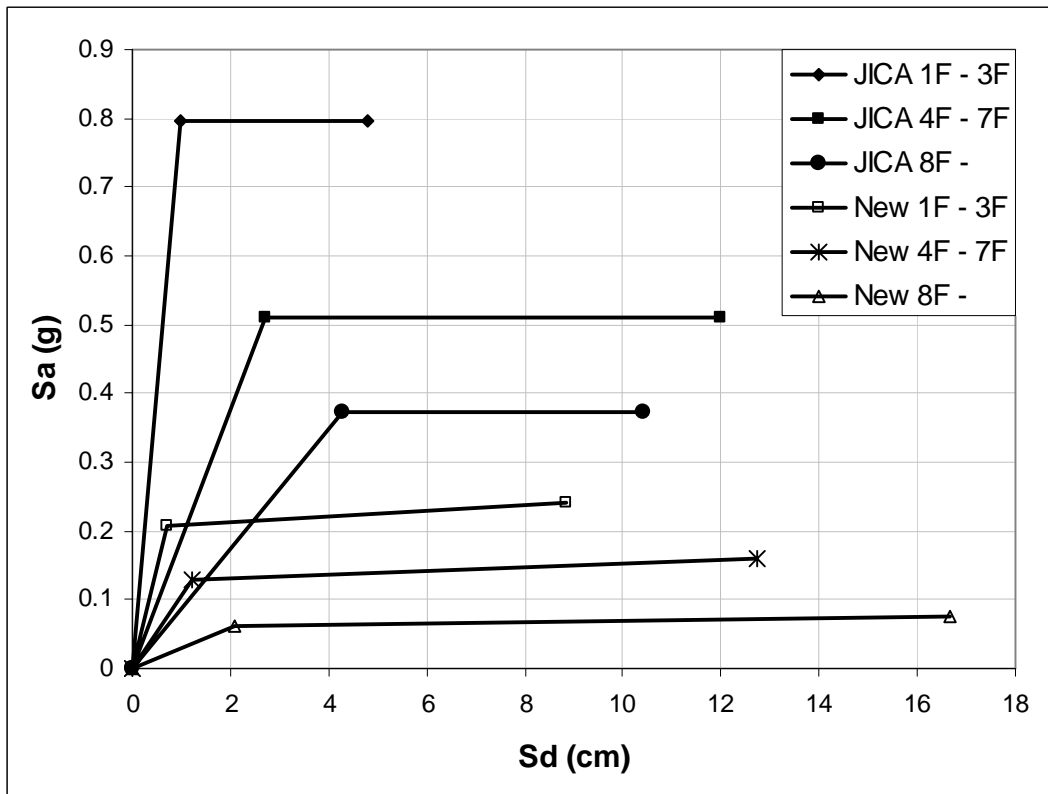


Figure C.1 A sample group of capacity curves for RC buildings

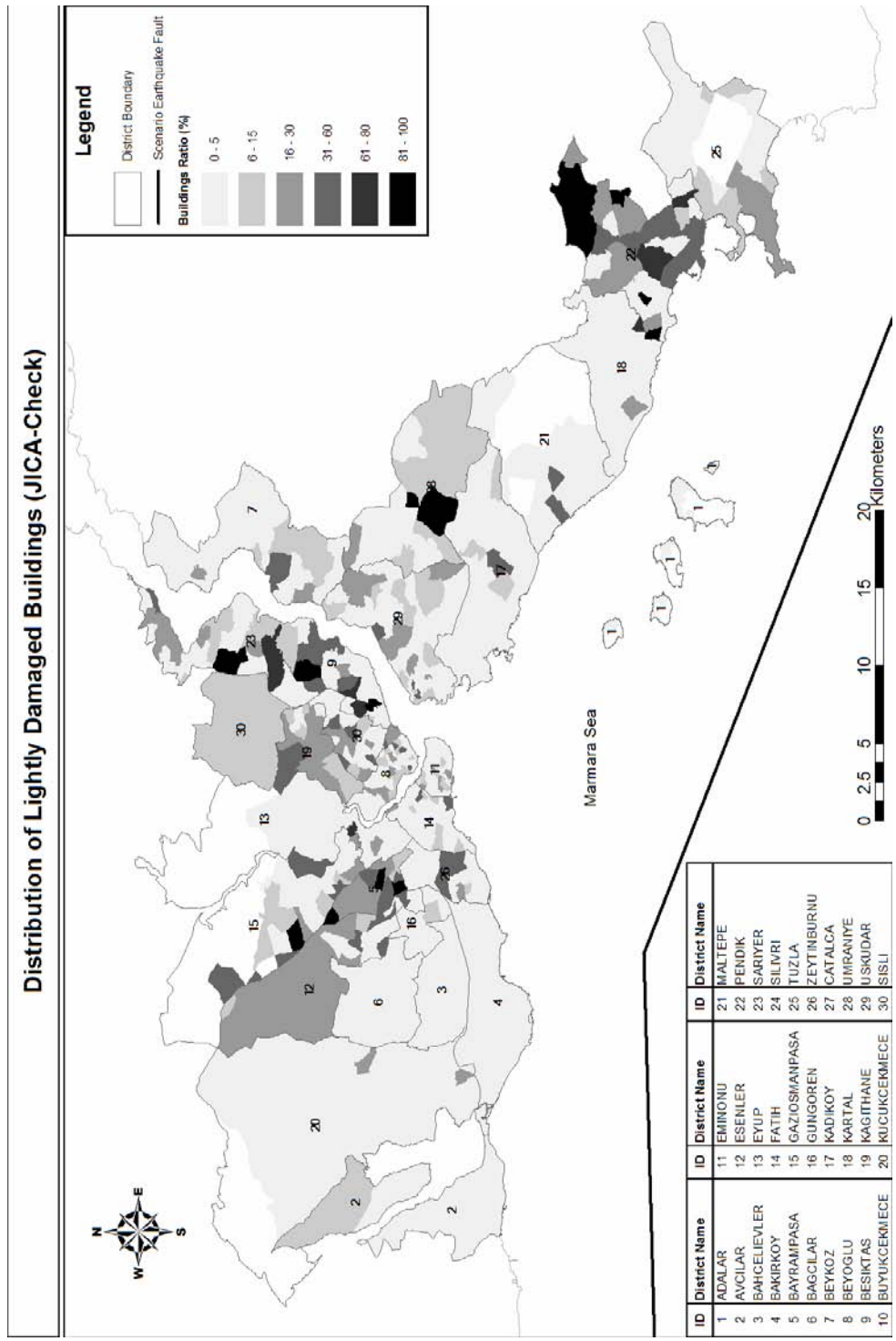


Figure C.2 Distribution of lightly damaged buildings ratio (JICA-Check)

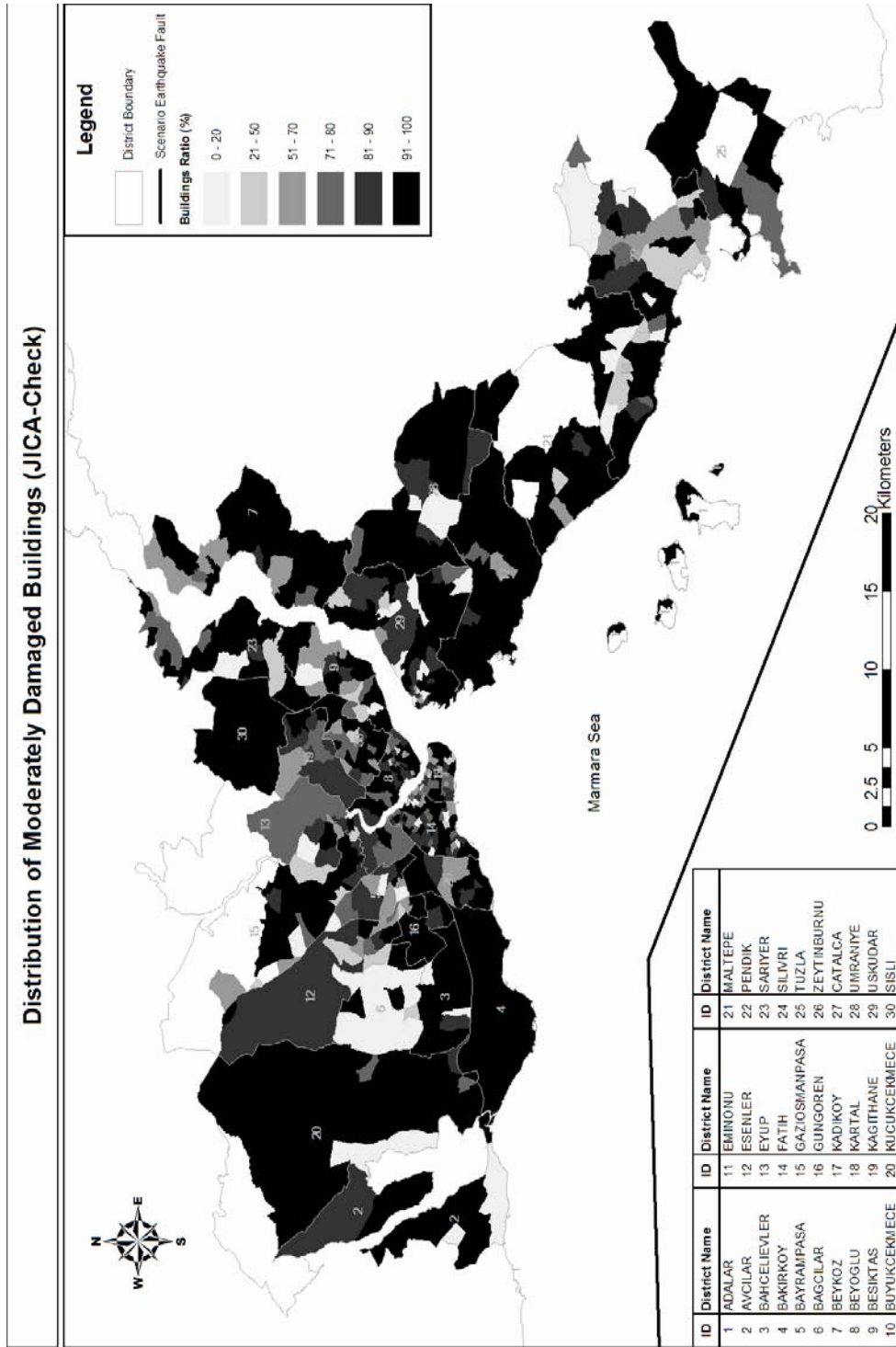


Figure C.3 Distribution of moderately damaged buildings ratio (JICA-Check)

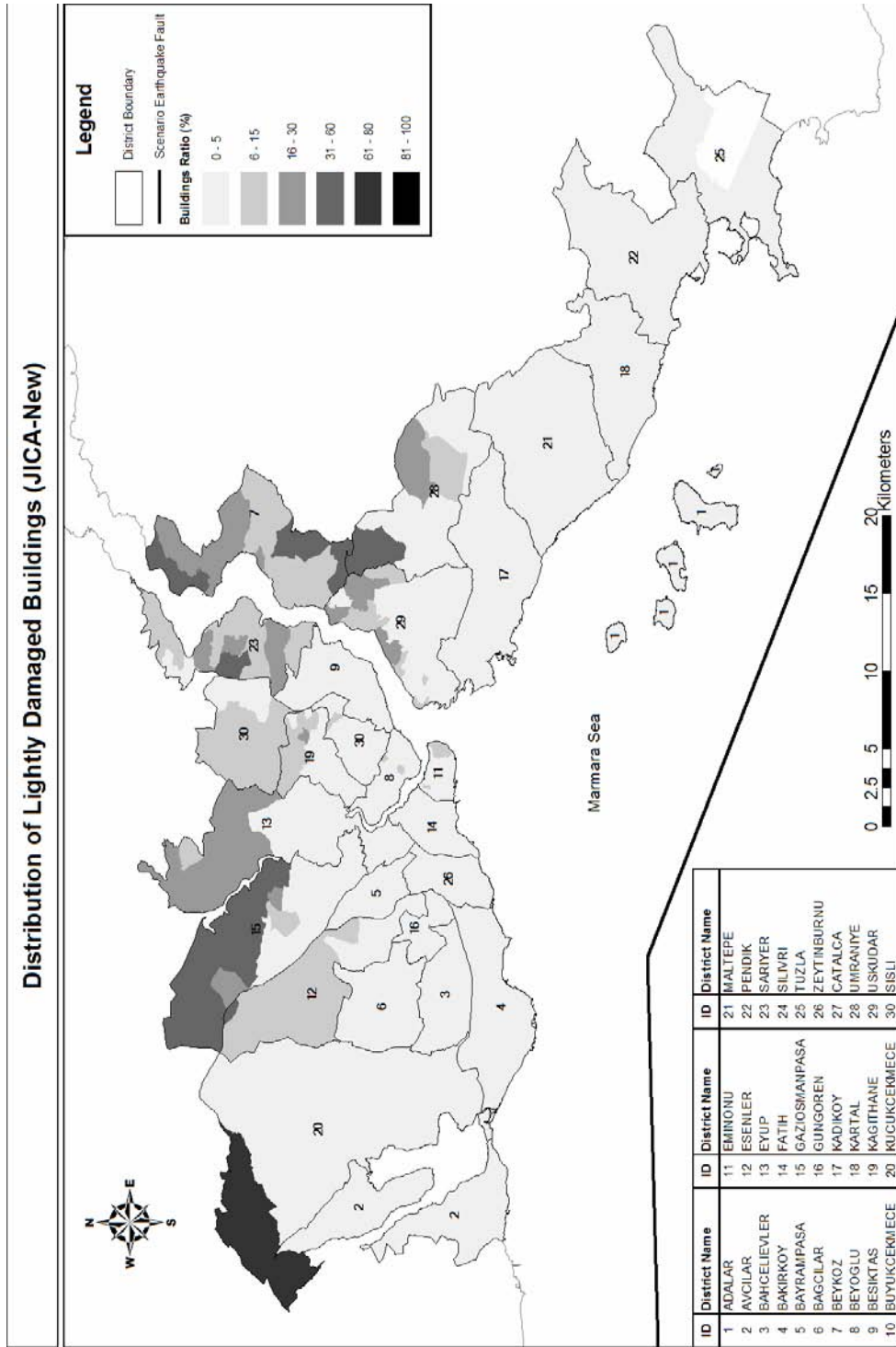


Figure C.4 Distribution of lightly damaged buildings ratio (JICA-New)

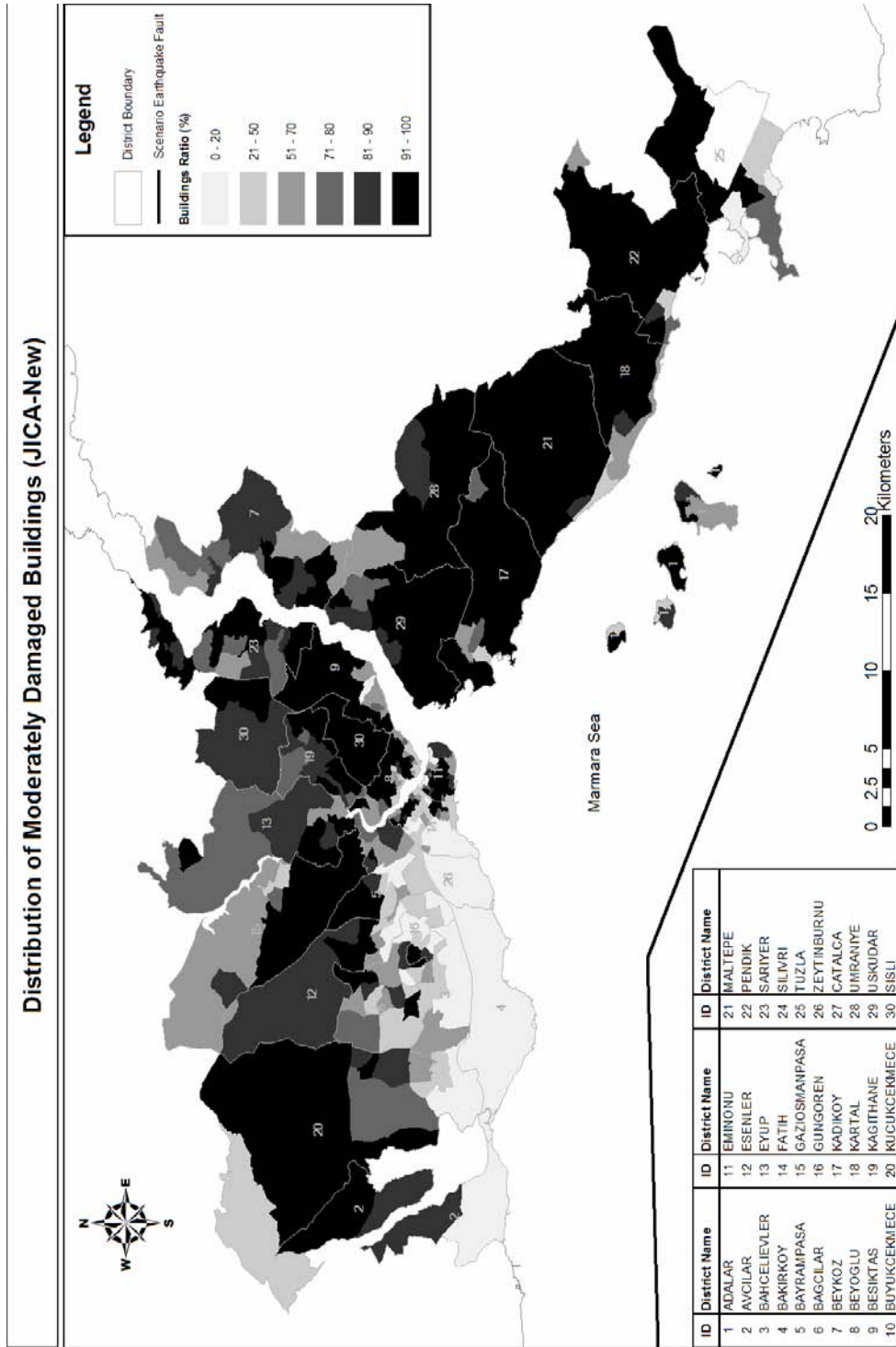


Figure C.5 Distribution of moderately damaged buildings ratio (JICA-New)

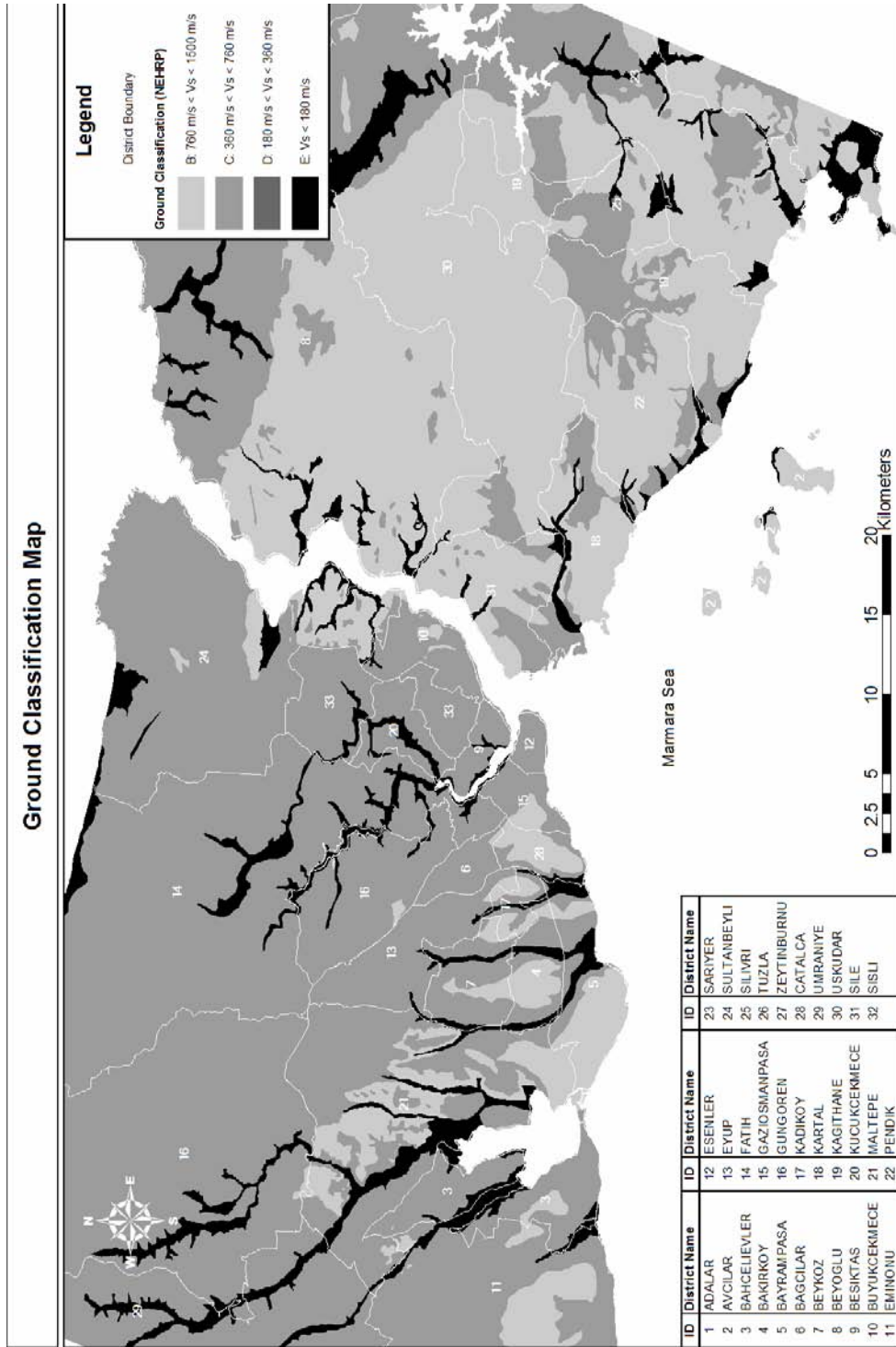


Figure C.6 New ground classification map proposed by this study

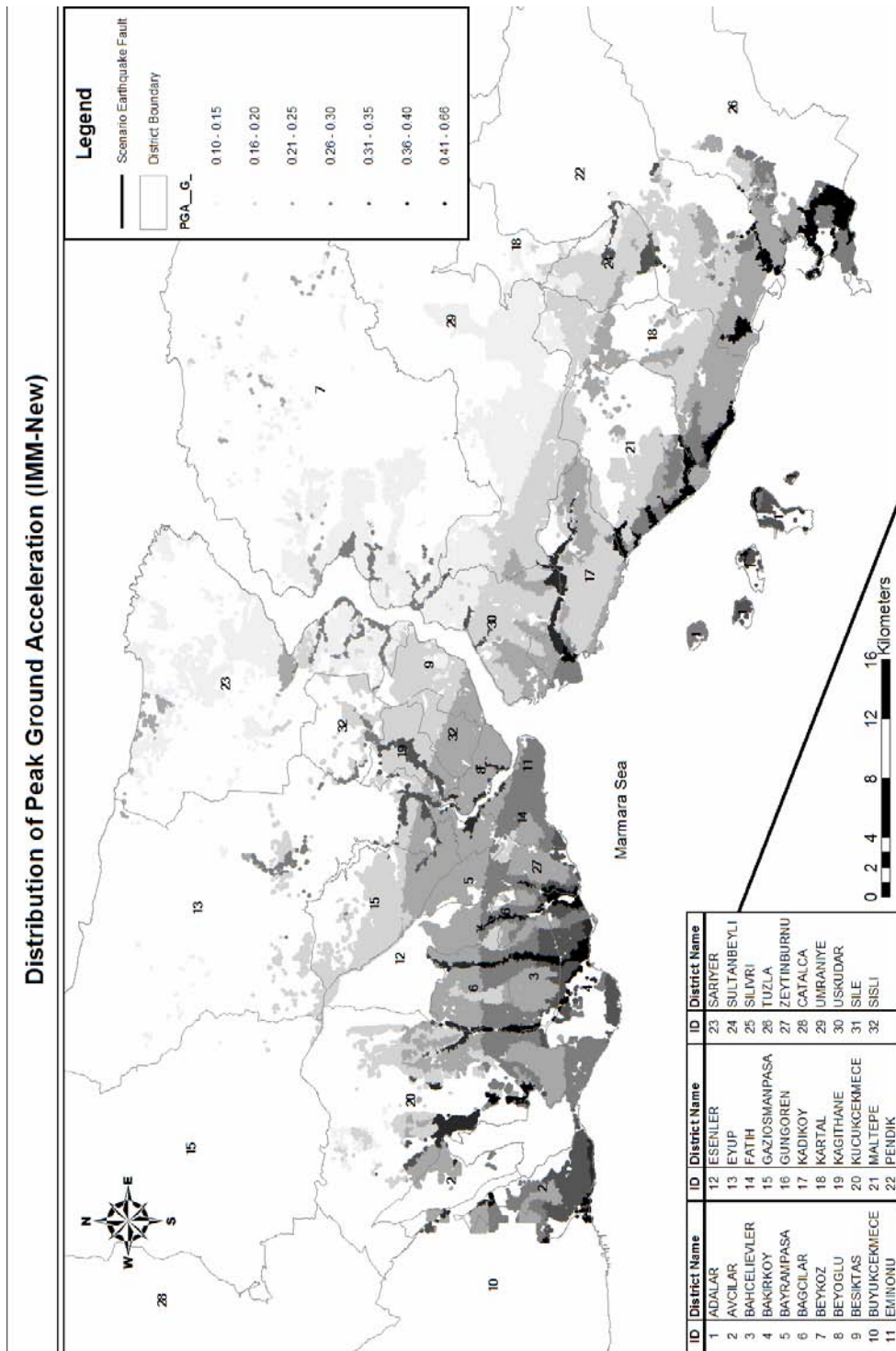


Figure C.7 Distribution of peak ground acceleration (IMM-New)

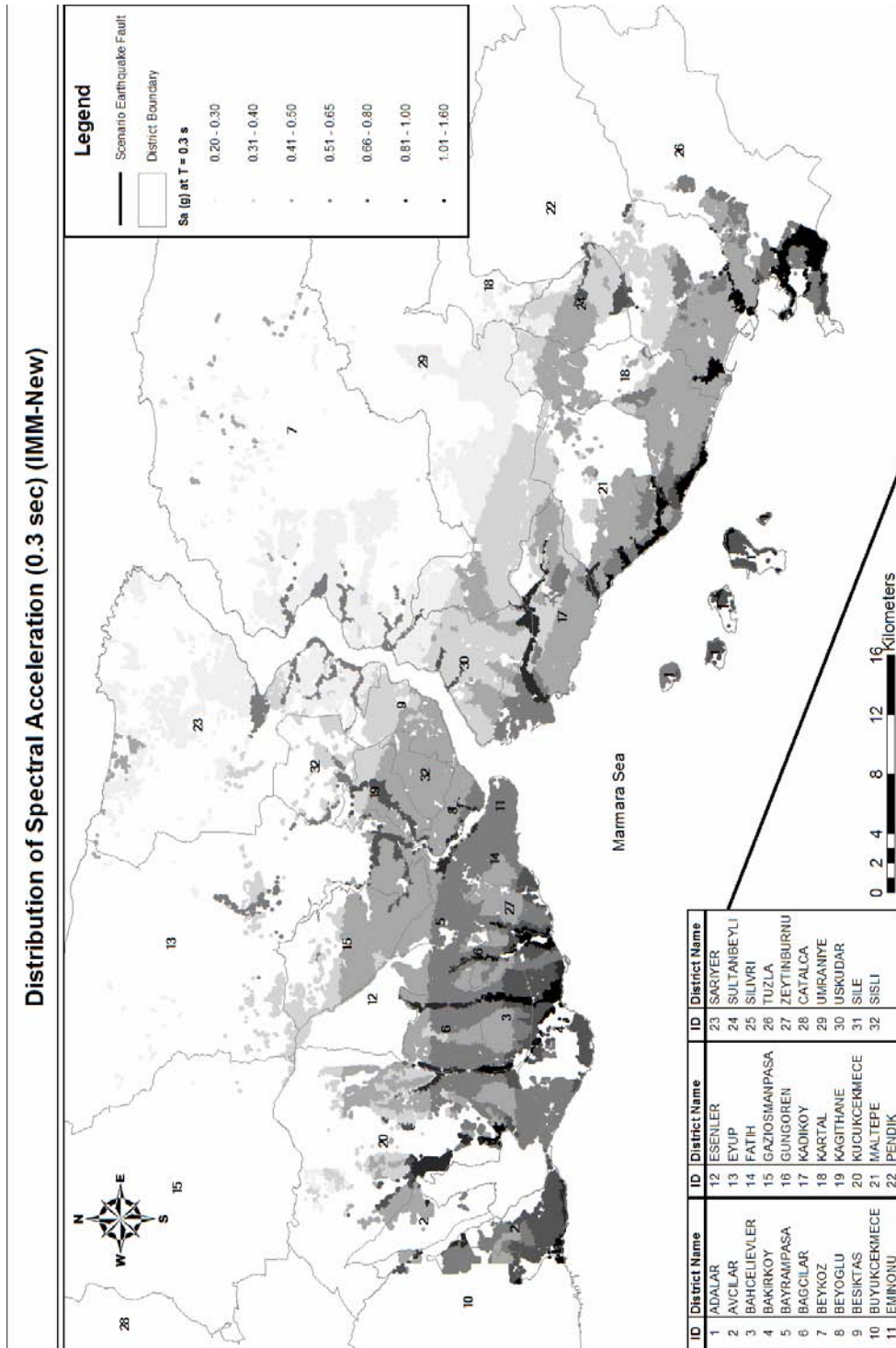


Figure C.8 Distribution of S_a values at the period of 0.3 sec (IMM-New)

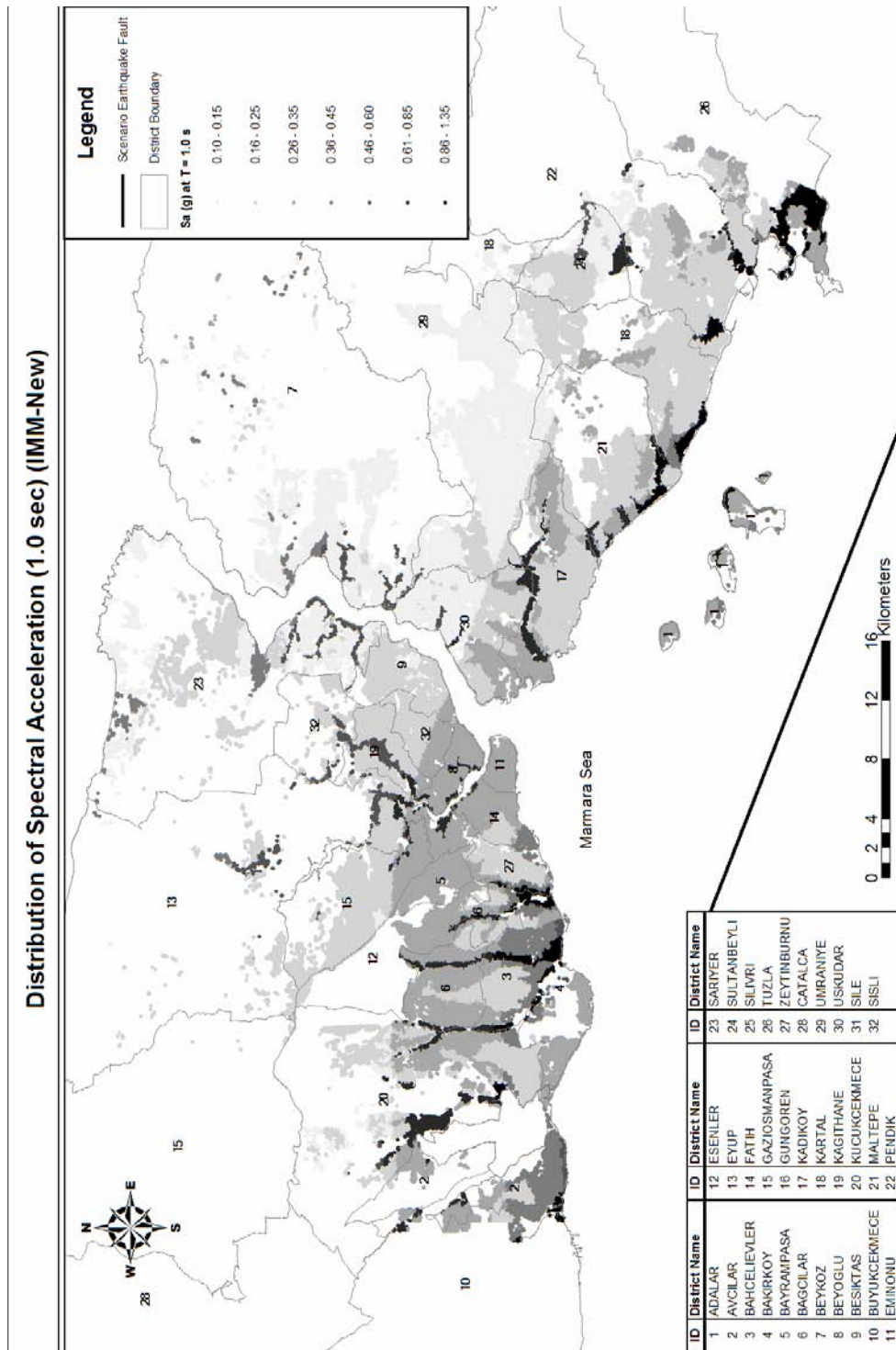


Figure C.9 Distribution of S_a values at the period of 1.0 sec (IMM-New)

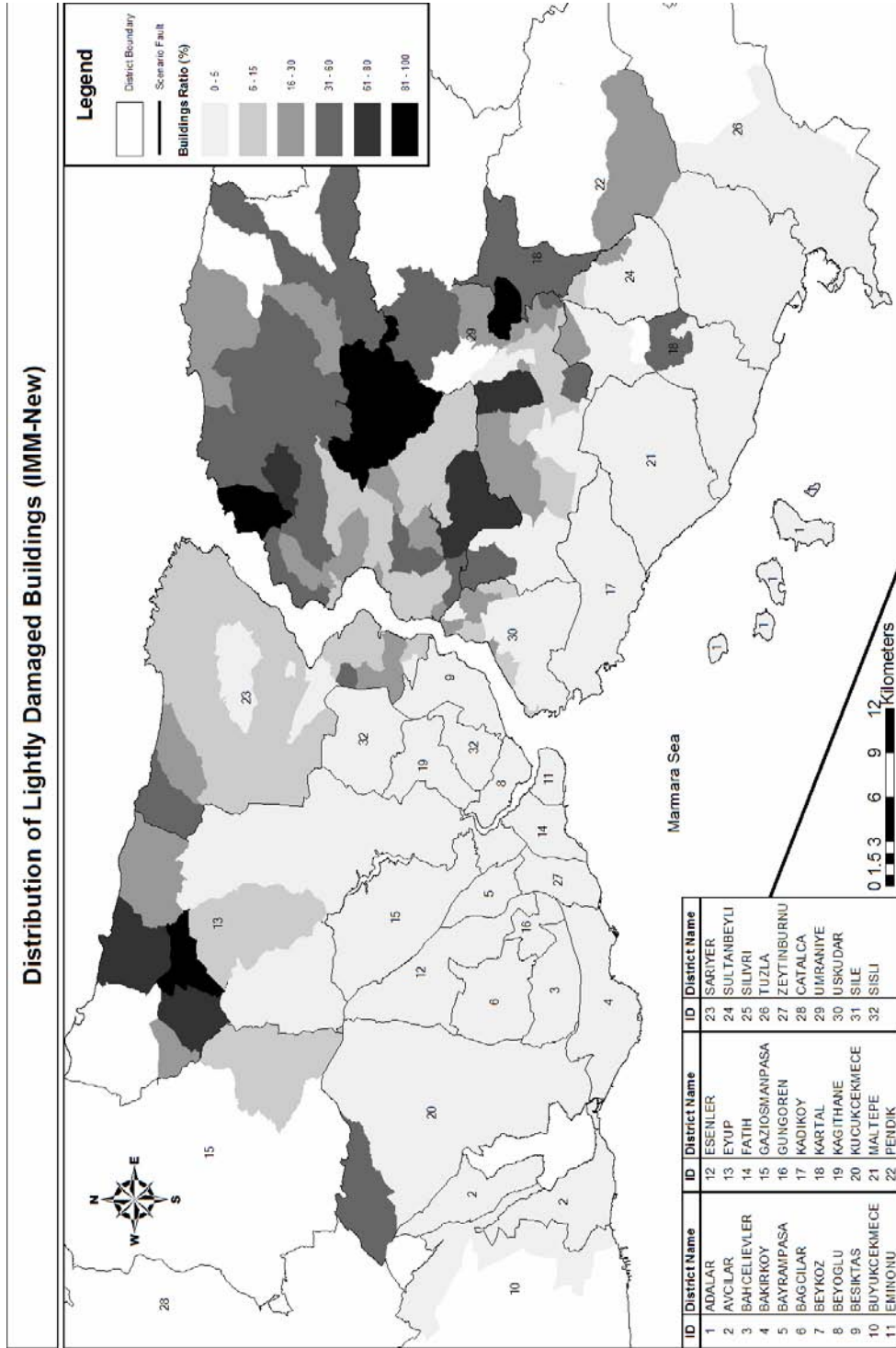


Figure C.10 Distribution of lightly damaged buildings ratio (IMM-New)

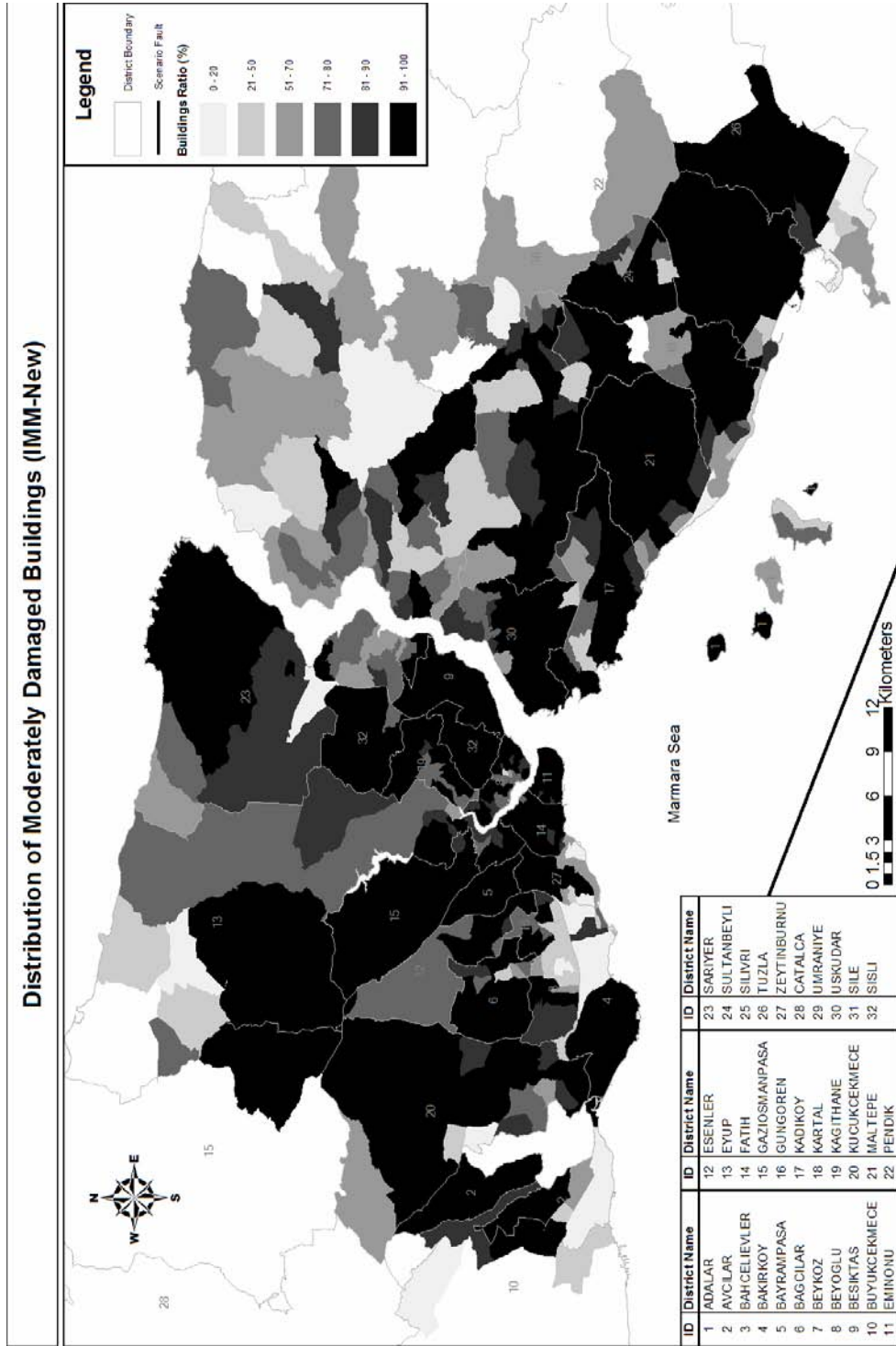


Figure C.11 Distribution of moderately damaged buildings ratio (IMM-New)

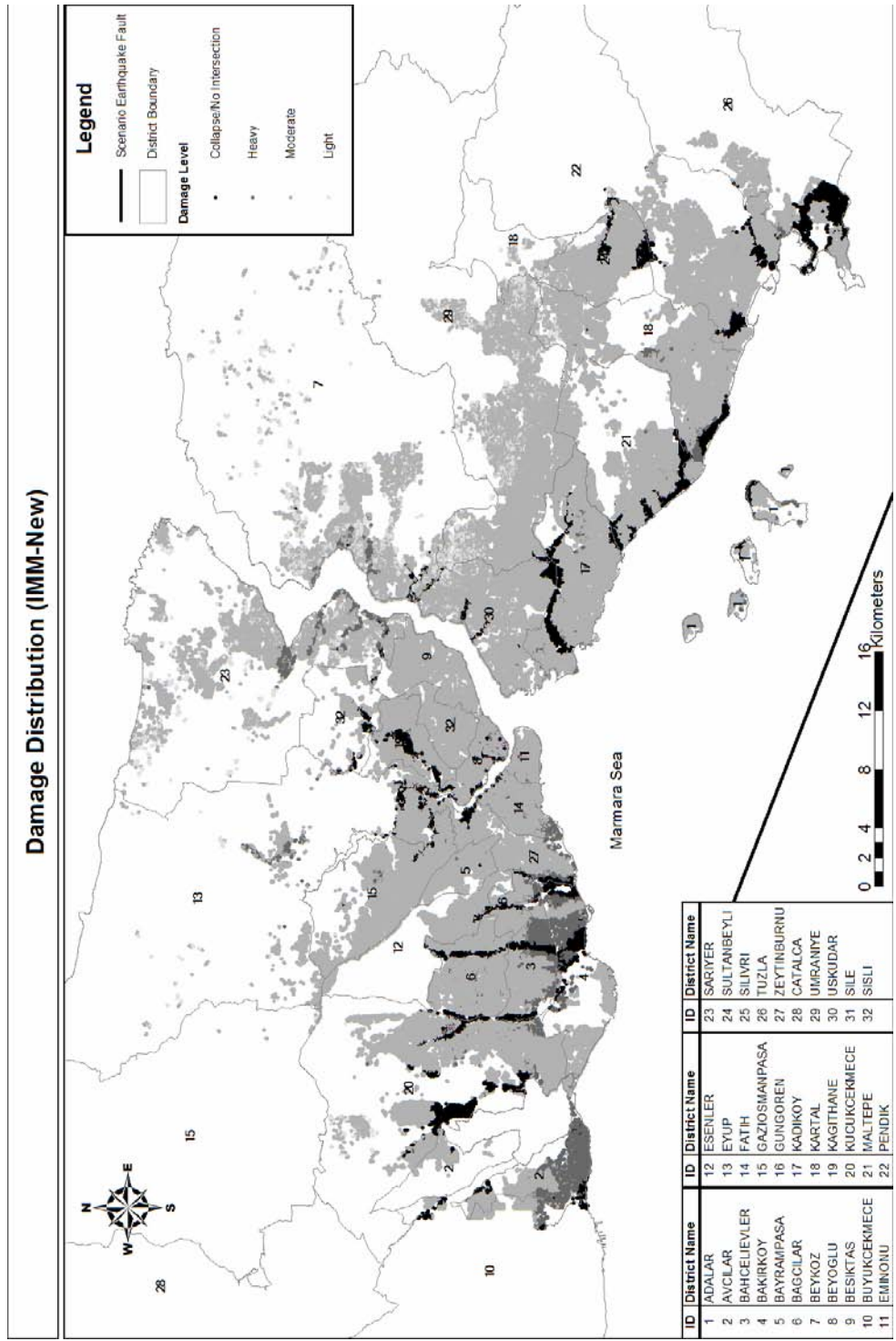


Figure C.12 Damage distribution obtained in IMM-New part (all-in-one)